Investigating the Influence of Loss Models Associated with 2D Flood Modelling Applications

May 2010

Ben Caddis (M Eng (Civil))

Supervisor: James Ball
University of Technology Sydney

18 Credit Point Graduate Project (49183 and 49184)

Submitted in partial fulfilment for the Master of Engineering Science Degree in Hydrology and Water Resources University of New South Wales

DOCUMENT CONTROL SHEET

Title :	Investigating the Influence of Losses Associated with 2D Flood Modelling Applications
Document:	R.Masters.01.002.doc
Author:	Ben Caddis
Supervisor:	James Ball
Institution:	University of Technology Sydney

REVISION/CHECKING HISTORY

REVISION NUMBER	DATE OF ISSUE	CHECKED BY		ISSUED BY	
0	8-Jan-10	BMC		BMC	
1	19-May-10	BMC		BMC	

DISTRIBUTION

DESTINATION	REVISION			
	0	1	2	3
University of Technology Sydney, NSW	1	1		
BMC	1	1		

CONTENTS

LIST OF FIGURES

LIST OF TABLES

1 INTRODUCTION

1.1 Background

For over a century, scientists have studied the interaction between surface and sub-surface flow. This component of the hydrological cycle is of interest to a range of disciplines including engineers, agricultural scientists and hydrogeologists. Essentially, there are four key fields of interest amongst these disciplines:

> ➢ surface runoff – typically for water resource, water quality or flood investigations;

> ➢ soil moisture variability – typically for agricultural research;

> ➢ groundwater recharge – typically for water resource, water quality or groundwater dependant ecological investigations; and

> ➢ water balance modelling – typically for water resource investigations.

Quantification of surface runoff is the prime focus of this study, particularly in the context of computer based flood modelling. However, due to the synergies between the fields of interest, the concepts and processes discussed in this report are applicable amongst the different disciplines.

Traditionally, flood modelling has involved two distinct stages. Firstly, hydrologic analysis enables the analyst to quantify the flow of water within a watercourse during any particular rainfall event. Such events may be historical storms typically used for calibration purposes, or design events used for a range of catchment management purposes. Once the flow has been determined, hydraulic analysis is performed to define the mechanisms of flow along watercourses and across floodplains.

Hydrologic analysis used in this two-step process is commonly performed using lumped runoff-routing models. In this process the catchment is divided into sub-catchments, and average values are assigned to each catchment variable as model inputs. Thus, each sub-catchment is treated uniformly. Spatial variability is limited to the degree the parent catchment is sub-divided. The numerical models used in practice have been extensively verified and applied against gauged catchments and are, therefore, generally considered appropriate tools for hydrological modelling.

The second step in the process is the hydraulic analysis where the watercourse and floodplain can be represented in either one, two or three dimensions. For most flood modelling applications, one or two dimensional hydrodynamic schemes are used.

As computer processing time reduces with improving technology, the opportunity arises to improve the functionality of hydraulic models. A method of applying rainfall directly to the 2D domain of a hydraulic model is one such area that is currently under development. This direct rainfall approach eliminates the need for a separate hydrological model. More importantly, the combined approach enables the spatial variability of a catchment to be represented on a much finer scale. Thus, the lumped model is replaced by a distributed one. Spatial variability then becomes a function of the 2D grid element sizes.

1.2 Defining the Problem

Although the direct rainfall approach has been a feature of many of the commercially available hydraulic models for some years, its use remains limited. This can be attributed to some of the following reasons:

- ➢ increased computational time;

- ➢ limited testing and validation, and the validity of the shallow water equations at very shallow depths;

- ➢ reluctance for the analyst to discard traditional lumped models;

- ➢ limited literature available on this type of application; and

- ➢ robustness of the software.

The first of these reasons is becoming less of a concern as access to computers with increased processing power is improving. With further testing and potential improvement to the robustness of software, literature will often follow and, hence, user confidence will broaden.

As the need for separate hydrologic and hydraulic models is potentially replaced by direct rainfall modelling, a range of opportunities arise for further enhancement of the scheme. Limitations or assumptions associated with the lumped hydrologic schemes can now be resolved. The key limitations pertinent to this study are associated with the loss mechanisms applied to the model.

Horton (1933) described surface runoff as:

> *'neglecting interception by vegetation, surface runoff is that part of the rainfall which is not absorbed by the soil by infiltration…'.*

Based on this definition, surface runoff is also described as rainfall excess. The traditional two stage flood modelling approach applies the rainfall excess concept, where infiltration losses are applied to the rainfall hyetograph. As the resulting hydrologic flows are applied to the hydraulic model, no further consideration is given to losses.

A significant opportunity with direct rainfall modelling is to apply the loss model to the ground surface, rather than the rainfall hyetograph. Therefore, infiltration beyond the temporal and spatial extent of the rainfall can be accounted for. Additionally, the depth of surface water can potentially increase the rate of infiltration. Since water depth is calculated in the hydraulic modelling, this influence can also be quantified.

1.3 Study Objectives

1.3.1 Objectives

Whilst attempting to address some of the issues described in the previous section, this study has involved a broader look at the influence of losses on two-dimensional (2D) hydrodynamic flood modelling applications.

The study objectives are summarised as:

1. Investigate depression storage inherent in digital topographic data and its influence on modelled losses;

2. Assess of the influence that application of loss models to the ground surface rather than the rainfall hyetograph can have on surface runoff;

3. Assess the influence that varying soil types have on surface runoff; and

4. Assess the influence that ponding depth has on infiltration, and the subsequent affect on surface runoff.

1.3.2 Hypothesis

1.3.2.1 Depression Storage

In the physical environment, in particular urban environments, large depressions are usually drained by a sub-surface drainage system. In all, but the most detailed urban flood models, not all sub-surface drainage infrastructure is represented. Hence, water entering the depressions in the model has no mechanism for release.

It is expected that the influence of depression storage will be more pronounced in:

➢ **urban environments** where the depressions represented in the DEM are likely to be directly connected to a sub-surface drainage system; and

➢ **steep catchments** where the two-dimensional grid representation and sampling process generates artificial depressions within the model.

Elimination of these depressions from the DEM prior to modelling is expected to improve modelling results by:

➢ minimising the water lost to depression storage; and

➢ improving the continuity of water flow.

1.3.2.2 Runoff Rate and Volume

The presence of ponding at the soil surface is expected to have an influence on the calculated infiltration. Thus, ponding will have a greater influence on discharge volume in rural catchments with expansive floodplains.

A simple comparison between the infiltration capacity curves for the 11 United States Department of Agriculture (USDA) soil texture classifications and typically used initial and continuing loss estimates reveals that it is likely infiltration is being underestimated when using typical values for initial and continuing losses.

Furthermore, abstracting the losses from the ground surface, rather than the rainfall hyetograph, will result in higher cumulative infiltration. This is due to the continuing losses as the flood wave is routed

through the catchment. Naturally, this effect will be more pronounced in larger catchments with a slower response.

1.4 Report Outline

The following list is a summary of the scope of this study, as presented in the associated chapters:

Chapter 2.   Runoff Processes

For background information, the major processes influencing catchment runoff are discussed.

Chapter 3.   Existing Loss Models

A range of existing loss models are investigated and discussed, many of which are commonly used in practice.

Chapter 4.   Available Software

The currently available software for hydrologic and hydraulic modelling is investigated, with a particular emphasis on the loss modelling methods used in each.

Chapter 5.   Selecting a Loss Model for Analysis

The factors considered during selection of a loss model for the subsequent analysis are described in this chapter.

Chapter 6.   Loss Module Development

Due to the limitations with existing software, an infiltration module has been developed for the TUFLOW flood modelling software. The module development is discussed in this chapter.

Chapter 7.   Model Testing

Following development of the module, a validation process is followed to ensure model output is theoretically sound. Two test models have been developed for validation. These models are used to highlight some of the key infiltration processes.

Chapter 8.   Case Studies

Three catchments are used to highlight the issues associated with digital elevation data. One catchment is modelled to investigate the influence of the losses on flood behaviour.

Chapter 9.   Conclusions

Key findings from the investigation are summarised and discussed. The implications of the study findings for practitioners are also presented and areas where further research is required are identified.

2 RUNOFF PROCESSES

2.1 Precipitation

Precipitation, or rainfall, is the primary cause of runoff. Flooding can occur from a range of different rainfall events, ranging from low intensity, long duration events to high intensity, short duration events. The magnitude of the flood is a function of the intensity and duration of the rainfall, and the size and characteristics of the receiving catchment. Generally, short duration events are localised and are unlikely to cause major flooding in large catchments. However, that same storm event could lead to flash flooding within a small and highly responsive catchment.

2.2 Runoff

Surface runoff is typically described as the horizontal flow of water across the ground surface which occurs once the storage requirements of depressions have been satisfied and the soil is saturated. This is commonly referred to as Hortonian overland flow, after Robert E. Horton.

USACE(1994) discuss how Hortonian overland flow rarely occurs in forested environments due to the significant ground surface cover and extensive tree root structure. USACE (1994) continue to describe the hillslope runoff process where direct runoff is a combination of surface runoff and seepage.

2.3 Losses

2.3.1 Interception

Interception is the term used to describe the precipitation that is intercepted by vegetation before it reaches the ground. This water eventually evaporates. The amount of water subject to interception is a function of vegetation cover. Naturally, large trees with dense foliage have a considerably larger surface area than small plants.

Due to the minimal proportion of intercepted rainfall, interception is normally neglected for flood modelling purposes.

2.3.2 Evapotranspiration

Evapotranspiration is the collective term used to describe evaporation and transpiration. Quantification of evapotranspiration is more applicable to long duration water balance modelling, rather than event based flood modelling. For most flood modelling purposes, evapotranspiration is neglected.

2.3.3 Infiltration

Infiltration is the process where rainfall and surface water soaks into the ground. Infiltrated water will usually either:

> ➢ Recharge the groundwater storage;

➢ Become seepage;

➢ Evaporate from the surface soil layer; or

➢ Be used by vegetation.

There are many factors that influence the infiltration process, including:

➢ Ground cover and land use;

➢ Ground composition; and

➢ Soil moisture deficit.

2.3.4 Depression Storage

Depression storage is the term used for topographical depressions which have to be filled prior to runoff commencing. The water used to fill depressions will not become runoff. Rather, it will eventually be evaporated or infiltrated.

2.4 Seepage

Seepage occurs when sub-surface flow reaches the surface and becomes overland flow. Seepage typically occurs at the base of hills, or along hillslopes where a rock layer meets the surface. A perched aquifer flowing on top of the rock layer becomes runoff.

2.5 Ground Cover and Land Use

The ground cover can influence runoff processes in many ways. The two fundamental characteristics being:

➢ **Surface roughness** normally represented using the Manning's 'n' coefficient; and

➢ **Imperviousness of the surface** represented as a fraction of the total surface area.

Caddis et al (2008) discuss the results of an urban flood study where the Manning's 'n' values were lowered at shallow depths from initial estimates to decrease the response time of the catchment. This accounted for roofs and hardstand surfaces that are directly connected to surface and sub-surface drainage paths. Once depths increase, the effects of obstructions due to buildings, fences and landscaping are accounted for with a higher roughness. Conversely, across homogenous surfaces such as roads and open space, the surface roughness generally decreases with depth as the surface composition has a lesser effect on flow.

Particularly in the urban environment, impervious surfaces can significantly influence runoff. Faster response times due to smoother surfaces and greater volumes due to limited infiltration are the key influences. Ground cover can also influence infiltration losses by slowing down surface runoff, thus, enabling more time for infiltration to occur.

3 EXISTING LOSS MODELS

3.1 Summary

This chapter contains a summary of the most commonly used infiltration models in practice. The different models have been categorised as empirical, theoretical or conceptual as described below.

Empirical Models are typically simplistic equations with parameters derived by curve fitting to field observations. The empirical equations generally do not have any physical basis (US EPA, 1998), although some are widely used due to their simplicity and ease of fitting to field observations (Mein and Larson, 1973).

Theoretically Based Models are typically based on the conservation of mass. The three commonly used models are the Richards, Phillips and Green-Ampt equations. All three models have been shown to give similar results (Maidment, 1998).

Conceptual Models are simplistic models generally associated with the rainfall excess concept. Assumed losses are extracted from the rainfall hyetograph, with the remaining rainfall translated to runoff.

3.2 Empirical Models

3.2.1 Horton's Model

The equation proposed by Horton in 1940 is the most commonly used empirical infiltration model. Horton observed that the initially high infiltration rate reduced with time to a constant rate.

Horton's equation is expressed as:

$$f_p = f_c + \left(f_o - f_c\right)e^{-\beta t}$$
3-1

where

f_p is the infiltration capacity;

f_c is the ultimate infiltration rate;

f_o is the maximum initial infiltration rate; and

β is the decay coefficient.

Although the parameters of the equation have no physical significance (Mein and Larson, 1973), they can be related to the theoretically based Green-Ampt model (Maidment, 1998).

Equation 3-1 is conditional to a constant supply of water being available at the ground surface. Bauer extended the work of Horton (CRCCH, 1994) to account for unsteady rainfall. Bauer proposed a

simulation starting time based on soil moisture content and a drainage rate. Thus, during periods of rainfall hiatus, the infiltration capacity curve exhibits recovery.

3.2.2 Holtan's Model

In 1961 Holton proposed an infiltration model based on soil porosity. Holton suggested that the dominant factors influencing infiltration rate are the macropores within the soil horizon, such as from worm holes and decaying tree roots.

Holton's equation, modified by Holton and Lopez (Maidment, 1998), is expressed as:

$$f = GIAS_a^{1.4} + f_c \qquad \qquad 3\text{-}2$$

where

f is the infiltration rate;

GI is the growth index of the surface crop;

A is the infiltration capacity of available storage;

S_a is the available storage in the surface layer; and

f_c is the ultimate infiltration rate.

3.2.3 Soil Conservation Service

In 1957, the United States Department of Agriculture's (USDA) Soil Conservation Service (SCS) developed the following equation for the relationship between rainfall and runoff:

$$Q = \frac{(P - I_a)^2}{(P - I_a) + S} \qquad \qquad 3\text{-}3$$

where

Q is the runoff rate;

P is the rainfall;

I_a is the initial abstraction; and

S is the potential maximum retention after runoff begins.

The empirical equation

$$I_a = 0.2S \qquad \qquad 3\text{-}4$$

can be substituted into equation 3-3 to eliminate I_a. S can then be derived from the SCS curves for different land cover (Maidment, 1998).

3.2.4 Boughton's Equation

In 1957 Boughton (US EPA, 1998) modified the SCS equation 3-3 to:

$$Q = P - F_r \tanh\left(\frac{P}{F_r}\right)$$

3-5

where

F_r is an empirical parameter.

3.2.5 Kostiakov's Model

In 1932 Kostiakov presented the following empirical model:

$$f_p = K_k t^{-\alpha}$$

3-6

where

f_p is the infiltration rate;

K_k is a constant; and

α is a constant.

The constants in Kostiakov's model need evaluating based on observed field data. Kostiakov's model is considered to describe infiltration well during the early period (US EPA, 1998). As $t \to \infty$, $f_p \to 0$, thus, highlighting the inadequacy of Kostiakov's model at large values of t.

3.2.6 Mezencev's Equation

Recognising the limitations of Kostiakov's model for large values of t, Mezencev modified the Kostiakov model to (US EPA, 1998):

$$f_p = f_c + K_k t^{-\alpha}$$

3-7

where

f_c is the ultimate infiltration rate.

3.3 Theoretical Based Models

3.3.1 Richards Equation

Vertical unsaturated flow can be well described using Richards equation, which combines Darcy's equation with the equation of continuity (Gowdish 2009). The partial differential equation is the most complex infiltration model in use.

$$\frac{\partial \theta}{\partial t} = \nabla\big(K(\theta)\nabla h(\theta)\big) - \frac{\partial K(\theta)}{\partial z}$$

3-8

where

t is time;

K is the unsaturated hydraulic conductivity;

θ is the soil moisture content

z is the elevation head; and

h is the capillary head.

Application of Richard's equation requires the assumptions that the soil profile is homogenous, of infinite depth, and has constant initial soil moisture content.

3.3.2 Green-Ampt Model

In 1911 Green and Ampt (Green & Ampt, 1911) proposed a simplistic theoretical infiltration model, the solution of which, being a simplified version of Richards equation. The model conceptualised the infiltration process as a 'piston' type with a well defined wetting front. As the infiltrated water moves in a vertical direction through the soil profile, soil moisture changes instantly from the initial content to a saturated state.

The Green-Ampt method has received widespread use and further development due to its simplicity and proven performance against field measurements. In practice, solution of the Green-Ampt method is simpler than the complex numerical methods required to solve Richards equation.

In the basic form of the Green-Ampt equation, the infiltration rate, f(t) is expressed as:

$$f(t) = K\left(1 + \frac{\Delta\theta(\psi + h_0)}{F(t)}\right)$$

3-9

where

t is time;

K is the saturated hydraulic conductivity;

$\Delta\theta$ is defined as the available space within the soil profile for water to occupy;

ψ is the soil suction head;

h_0 is the depth of ponded water; and

F(t) is the cumulative infiltration, calculated from:

$$F(t) - \Delta\theta(\psi + h_0)ln\left(1 + \frac{F(t)}{\Delta\theta(\psi + h_0)}\right) = Kt \qquad\qquad 3\text{-}10$$

The Green-Ampt infiltration is illustrated in Figure 3-1. Refer to Section 5.1 for a full derivation of the equations. The key assumptions in the Green-Ampt model are soil homogeneity, uniform antecedent soil moisture conditions and a constant supply of water is available at the surface.
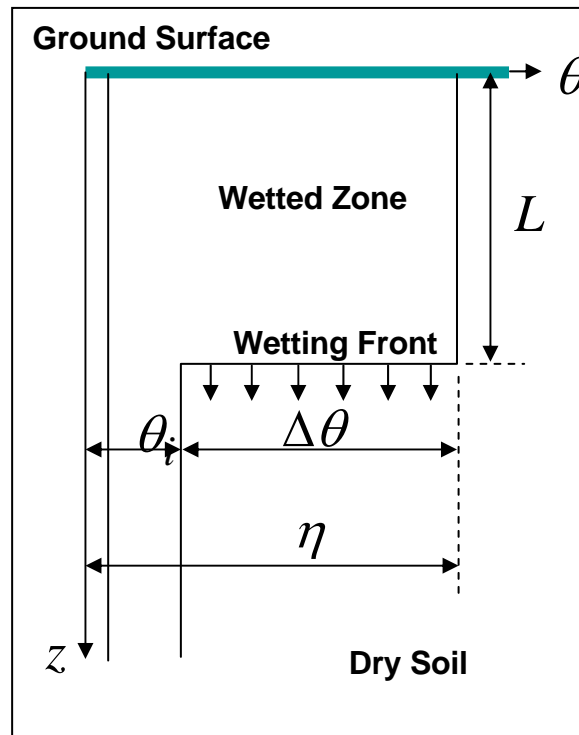
Figure 3-1   Green-Ampt Model Concept (University of Texas, 2007)

Mein and Larson (1973) developed a modified form of the Green-Ampt model to account for the infiltration prior to surface ponding. Their study focussed on the application of steady rainfall at the soil surface, highlighting that once surface ponding occurs, a quantity of water has already infiltrated into the soil profile.

During steady rainfall, the soil moisture increases until surface saturation occurs. At this point the rainfall intensity equals the infiltration capacity of the soil and ponding commences. Ponding continues until rainfall ceases; the infiltration rate being equal to the infiltration capacity. It is, therefore, important to note that during steady rainfall, there is only one period where ponding occurs.

Chu (1978) extended the work of Mein and Larson (1973) to account for unsteady rainfall. In the case of unsteady rainfall, the conditions leading up to the time of ponding are the same as in the steady rainfall case. Again, once the rainfall intensity equals the infiltration capacity of the soil, ponding commences. As the rainfall intensity reduces, there will again be a point where the rainfall intensity equals the infiltration rate. If the rainfall intensity continues to reduce, ponding no longer occurs and the infiltration rate equals the rainfall intensity.

It is common that rainfall events comprise more than one rainfall burst. In this situation, the rainfall intensity may again increase to, and beyond, the infiltration capacity of the soil. Ponding will then

occur in the same manner as described above. This process can repeat numerous times. Hence, in comparison to the steady rainfall case, during unsteady rainfall there can be any number of ponding periods.

The method developed by Chu (1978), can be extended to consider not only rainfall as the source of surface water, but also overland flow. Since the source of the surface water is irrelevant to the scheme, this extension is valid. Obviously, during overland flow, the surface is considered to be ponded and the infiltration rate equals the infiltration capacity. This is particularly relevant to this study, especially in the case of rising and receding floodwaters.

Ogden and Saghafian (1997) extended the Green-Ampt model to account for the redistribution of soil moisture. With an emphasis placed on multi-storm time series, the Green-Ampt with Redistribution (GAR) approach showed good agreement with a solution of Richards equation.

The GAR method is essentially the same as the traditional Green Ampt approach for the first period of surface saturation. A single wetting front passes down through the soil profile. However, during rainfall hiatus when the rainfall is less than the saturated hydraulic conductivity, the soil moisture content reduces and a period of soil moisture deficit recovery occurs. Losses due to evapotranspiration and seepage are neglected, and the piston wetting front is elongated as the soil moisture is subject to capillary and gravitational forces. As rainfall again exceeds the saturated hydraulic conductivity, a second 'wave' occurs in the wetting front. Conceptually, this can be represented by multiple wetting fronts.

Recognising the limitations of the GAR approach when applied to soils with relatively large saturated hydraulic conductivity values, Gowdish and Munoz-Carpena (2009) developed the Modified Green-Ampt with Redistribution (MGAR) approach.

3.3.3 Phillips Model

Phillip proposed calculation of the cumulative potential infiltration using a form of the following equation:

$$F(t) = St^{\frac{1}{2}} + Kt \qquad\qquad\qquad 3\text{-}11$$

where

t is time;

S is the sorptivity of the soil, being a function of soil water diffusivity; and

K is the saturated hydraulic conductivity.

The same limitations of soil homogeneity, uniform antecedent soil moisture content and availability of water at the surface apply, as per the Green-Ampt model.

3.4 Conceptual Models

3.4.1 Initial Loss / Continuing Loss

The IL/CL model is the most commonly applied loss model throughout Australia for flood estimation. The initial loss accounts for interception, depression storage and infiltration prior to surface saturation. Once the initial loss is satisfied, then runoff commences. The continuing loss is specified in depth over time, accounting for the constant infiltration rate for the remainder of the rainfall duration.

The IL/CL concept is easy to apply, with suggested design loss rates listed in Australian Rainfall and Runoff (IEAust, 1987) (ARR87). Mean and median continuing loss values from 54 Australian catchments are listed in ARR87.

3.4.2 Proportionate Loss

Sometimes used in conjunction with an initial loss, the proportionate loss is a fraction of the rainfall, considered to be lost to interception, depression storage and infiltration.

4 AVAILABLE SOFTWARE

4.1 Hydrologic Software

4.1.1 Overview

Hydrologic modelling for storm flow estimation is usually performed using lumped rainfall-runoff routing techniques. Simplistic models, based on the mass balance equation, are used to determine the outflow hydrograph from the catchment. Although these models can be applied using a spreadsheet, there are numerous software packages available. Such software provides a convenient way to integrate other features that influence runoff, such as storages.

The input required for the model depends upon the numerical model used and its underlying assumptions. Usually a combination of catchment area, channel slope, channel length, catchment roughness, loss parameters and fraction impervious are required for each sub-catchment. Model inputs are lumped for each sub-catchment to provide an average value. Different models use different parameters. For example, Boyd et al (2007) argue that channel slope and length are closely correlated to the catchment area, thus do not add any significant value to the solution.

There is also a range of distributed runoff-routing packages that use a two-dimensional (2D) grid in much the same manner as 2D hydraulic models. Models such as the System Hydrologique Europeen (Abbott et al, 1986) and CASC2D (Julien et al, 1995) use a 2D grid approach. These models solve a diffusive wave approximation to the dynamic wave equations where local and convective acceleration terms are neglected. Of key interest with these models is the interaction between surface and sub-surface flow. However, for flood modelling purposes, once rainfall has infiltrated into the surface, it is no longer of interest. The approximations applied to the numerical models in these packages make them unsuitable for most hydraulic flood modelling applications.

The following sections contain a summary of the key hydrologic modelling software used in Australian flood modelling practice.

4.1.2 WBNM

The Watershed Network Bounded Model (WBNM) was originally developed by Boyd, Pilgrim and Cordery between 1975 and 1979. WBNM is currently available from the University of Wollongong, NSW.

WBNM is a simplistic lumped runoff-routing model used for estimation of runoff from natural and urban catchments. The model is widely used throughout Australia, having been extensively tested on gauged catchments.

Catchment area and impervious fraction are the only variables used to describe the catchment. Slope is considered to have a minimal impact on runoff, and stream length has been shown to be proportionate to catchment area (Boyd and Bodhinayake, 2006). Independent verification by the author on two catchments comprising approximately 100 sub-catchments has confirmed the area to stream length relationship described by Boyd and Bodhinayake.

Four options are available for loss accounting:

> ➢ Initial loss and continuing loss;

> ➢ Initial loss and proportionate loss;

> ➢ Horton infiltration; and

> ➢ User defined time varying loss.

The rainfall excess concept is adopted in WBNM.

4.1.3 RORB

RORB has been developed by Monash University and Sinclair Knight Merz, originally released in 1975. Similar to WBNM, RORB is a simplistic lumped runoff-routing model used for estimation of runoff from natural and urban catchments. RORB has also been extensively tested and verified using gauged catchments.

Input variables for RORB include catchment area, flowpath length and impervious fraction.

Two options are available for loss accounting:

> ➢ Initial loss and continuing loss; and

> ➢ Initial loss and proportionate loss.

The rainfall excess concept is adopted in RORB.

4.1.4 XP-RAFTS

Distributed by XP Software, XP-RAFTS is a simplistic lumped runoff-routing model, similar to WBNM and RORB. XP-RAFTS has also received widespread use throughout Australia as well as extensive benchmarking against gauged catchments.

Input variables for XP-RAFTS are catchment area, slope, roughness and impervious fraction.

Three options are available for loss accounting:

> ➢ Initial loss and continuing loss;

> ➢ Initial loss and proportionate loss; and

> ➢ ARBM loss method using Phillip's equation.

The rainfall excess concept is adopted in XP-RAFTS.

4.1.5 MIKE SHE

The Systeme Hydrologique Europeen (SHE) was developed jointly by the Danish Hydraulic Institute (DHI), the British Institute of Hydrology and SOGREAH from 1977 and throughout the early 1980's

(Abbott et al, 1986). SHE is a physically based, distributed hydrological model incorporating surface and sub-surface flow and the interactions between the two. MIKE SHE is the current version of the model, marketed by DHI Water and Environment since the mid 1980's.

In MIKE SHE, surface flow is simulated using the diffusive wave approximations of the Saint-Venant equations, across a two-dimensional (2D) grid.

The sub-surface flow module of MIKE SHE includes unsaturated infiltration and saturated groundwater flow zones. For unsaturated infiltration, three methods are available:

➢ One-dimensional (1D) vertical flow using Richards equation;

➢ Gravity flow method neglecting capillarity; and

➢ Unsaturated water balance method for long term water balance applications.

Infiltration losses are extracted at the ground surface, rather than the runoff source.

4.1.6 HEC-HMS

Developed by the US Hydraulic Engineering Corps (HEC), the Hydrologic Modelling System (HMS) is a rainfall-routing model used for continuous and event based simulations.

HEC-HMS offers 10 different methods for loss accounting:

➢ Soil moisture deficit and continuing losses;

➢ Exponential loss;

➢ Green-Ampt model;

➢ Distributed initial and continuing losses;

➢ Distributed SCS curve number;

➢ Distributed soil moisture accounting;

➢ Initial and continuing losses;

➢ SCS curve number;

➢ Smith Parlange approximation of Richard's equation; and

➢ Soil moisture accounting.

The rainfall excess concept is adopted in HEC-HMS.

4.1.7 CASC2D / GSSHA / WMS

CASC2D was originally a 2D overland flow routing program developed at the Colorado State University. The model was further developed by Julien and Ogden (Julien et al. 1995). The model has since been reformulated by the US Army Corps of Engineers (USACE) into the Gridded Surface

Subsurface Hydrologic Analysis (GSSHA) model (EMSI, 2009). The model is now available through EMSI's WMS software.

Unlike the original CASC2D model, GSSHA enables simulation of non-Hortonian basins. Thus, surface and sub-surface flows are modelled including the interaction between the two zones.

WMS incorporates the GSSHA engine, together with many other engines, such as HEC-HMS and MODRAT (Modified Rational Method). The options available for loss accounting are, therefore, similar to those of HEC-HMS, although include runoff coefficients for the rational method calculations.

4.2 Hydraulic Software

4.2.1 Overview

Flood modelling is generally approached as either one-dimensional (1D), two-dimensional (2D), or a combination of 1D and 2D. One-dimensional flow is described by the Saint-Venant equations developed by Barre de Saint-Venant in 1871 (Chow, 1988). These partial differential equations are based upon continuity and conservation of momentum. Two-dimensional flood flows are well described by the shallow water equations, and include the additional effects of 2D inertia, sub-grid scale turbulence and less influential terms such as Coriolis force and atmospheric pressure variant.

The Saint-Venant and shallow water equations, referred to as the dynamic wave equations in their full form, have often been used in simplified form for various applications. Two such simplified forms are the diffusive and kinematic wave approximations. There is no direct solution to the dynamic wave equations, therefore, various numerical and analytical schemes have been developed to enable them to be used in practice.

Described in this section are the three most commonly used integrated one-dimensional (1D) and two-dimensional (2D) hydraulic modelling software systems in Australia. These are TUFLOW, Sobek and MIKE FLOOD.

4.2.2 TUFLOW

Developed by BMT WBM, TUFLOW is a one-dimensional (1D) and two-dimensional (2D) flood and tide simulation engine. It solves the 1D Saint-Venant equations and the full 2D free-surface shallow water equations using an alternating direction implicit scheme. TUFLOW uses grid of square elements.

TUFLOW offers two methods for application of rainfall to the 2D grid:

> ➢ Surface Area (SA) – the rainfall hyetograph, or routed hydrograph, for each sub-catchment is applied directly to the 2D grid. Initially, when the grid is dry, water is applied to the lowest grid cells within each sub-catchment area. Subsequently, water is distributed across all wet cells within each sub-catchment area; and

> ➢ Direct Rainfall (DR) – the rainfall hyetograph for each sub-catchment is applied uniformly across every grid cell within each sub-catchment area.

Losses are typically extracted from the rainfall hyetograph as initial and continuing losses. Alternatively, negative rainfall can be assigned to the grid to account for time varying losses.

4.2.3 Sobek

Developed by Delft Hydraulics, Sobek is a 1D and 2D flood modelling package, based on a solution of the 2D Saint-Venant equations. Sobek uses grid of square elements.

Application of rainfall to the Sobek model can only be achieved using the direct rainfall approach. The rainfall hyetograph is applied uniformly across every grid cell within each sub-catchment area.

Losses are typically extracted from the rainfall hyetograph as initial and continuing losses.

4.2.4 MIKE FLOOD

Developed by the DHI Software, MIKE FLOOD is the combination of three separate models:

- ➢ MIKE 11 – 1D network model;

- ➢ MIKE 21 – 2D model; and

- ➢ MIKE Urban – Sub-surface drainage model.

The 2D engine of MIKE 21 solves the hydrodynamic Saint-Venant equations on either a rectangular, flexible or curvilinear grid.

Application of rainfall to the MIKE FLOOD model can only be achieved using the direct rainfall approach. MIKE FLOOD's 'precipitation mode' allows the rainfall hyetograph to be applied uniformly across every grid cell within each sub-catchment area.

Losses are typically extracted from the rainfall hyetograph as initial and continuing losses.

4.3 Software Performance Comparisons

As direct rainfall modelling is increasingly applied, it is important that the practitioner has an understanding of:

- ➢ how the results compare with traditional approaches; and

- ➢ whether modelling variables are directly transferable between the different approaches.

Clark (2008) compared the output from direct rainfall modelling in TUFLOW and Sobek, to the output from WBNM. The research identified that the results from each model were inconsistent when using the same variables. Clark (2008) concluded that further testing should be conducted, preferably on a gauged catchment.

Britton and Subasing (2004) compared the direct rainfall output of MIKE 21 to recorded flows. The timing of the peaks was generally reproduced, although the magnitude of flows was inconsistent. For a different catchment, they also compared MIKE 21 results to those from XP-RAFTS. Although the general form of the hydrographs were similar, the timing and magnitude were not in good agreement.

Caddis et al. (2008) reported on a study comparing the direct rainfall results to the traditional modelling approach results using TUFLOW. The study concluded that the same variables for

roughness and losses used in the two different approaches would lead to significantly different results. Thus, to reproduce the traditional method output, variables needed to be different.

4.4 Adopted Software

All three of hydraulic models discussed above have an option for applying rainfall directly onto the 2D grid. However, all three only have the simplistic initial and continuing loss options, applied using the rainfall excess concept.

Due to ease of customisation, TUFLOW has been used for investigating the influence of losses. The customisation of TUFLOW to include the two selected loss models discussed in Chapter 4 is discussed in Chapter 6.

For hydrological modelling, WBNM has been selected due to ease of GIS interfacing.

5 SELECTING LOSS MODELS FOR ANALYSIS

Due to the ease of application, widespread use and acceptance, and the availability of model parameters, the Green-Ampt model is used for this study. For application of the Green-Ampt infiltration equation on a catchment scale, to introduce spatial variability the Cooperative Research Centre suggested 3 possible approaches:

➢ sub-division of the catchments into a number of smaller homogenous sub-areas, and combining the calculated runoff from each;

➢ use of a contributing area related to rainfall intensity and antecedent conditions; or

➢ use of probability distributions of infiltration parameters.

Application of the Green-Ampt infiltration to a 2D hydraulic model grid is essentially a form of the first approach, with each 'sub-area' being equal to one grid cell element. The standard form of the equation is modified to account for intermittent wetting and drying, and surface ponding.

In addition to the Green-Ampt model, a modified form of the initial and continuing loss concept is used, where losses are extracted at the ground surface.

At this point the differentiation between 'rainfall excess' and 'surface loss' should be clarified.

➢ **Rainfall Excess** represents the traditional approach whereby losses are extracted from the rainfall hyetograph prior to application of the rainfall to the ground surface.

➢ **Surface Loss** is the term used in this report to describe losses being applied to the ground surface opposed to the rainfall hyetograph. This option allows rainfall losses to continue across all wetted cells, regardless of rainfall.

5.1 Application of the Green-Ampt Model

Derivation of the Green-Ampt infiltration equation is modified here from Chow (1988), and extended for the current purpose. Shown in Figure 5-1 is a conceptualised representation of the Green-Ampt infiltration process.
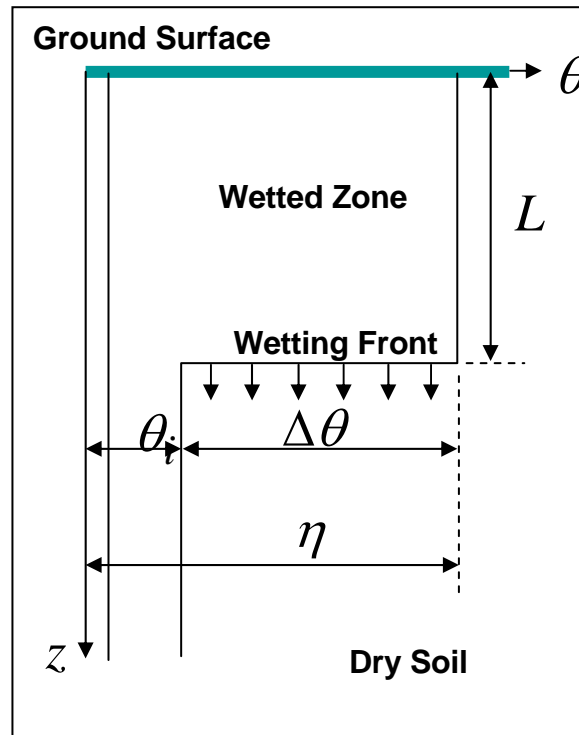
Figure 5-1   Green-Ampt Conceptualisation (University of Texas, 2007)

Examining the continuity of the infiltration process and inspection of Figure 5-1, the cumulative infiltration, *F*, at time, *t*, is

$$F(t) = L(\eta - \theta_i) \qquad\qquad\qquad 5\text{-}1$$

where

η is the soil porosity;

θ_i is the initial water content of the soil; and

L is the depth from the surface to the wetting front.

Let $\Delta\theta = \eta - \theta_i$ $\qquad\qquad\qquad 5\text{-}2$

where $\Delta\theta$ is defined as the available space within the soil profile for water to occupy.

Thus (1) can be written as

$$F(t) = L\Delta\theta \qquad\qquad\qquad 5\text{-}3$$

To examine the momentum of the infiltration process, we can use Darcy's law, expressed as

$$q = -K\frac{\partial h}{\partial z}$$
5-4

where K is the saturated hydraulic conductivity in units of L/T and q is the Darcy flux in units of L/T, which is the synonymous with the negative of the infiltration rate, f. This is due to the Darcy flux being positive in the upward direction and the infiltration rate being defined as positive in the downwards direction.

If the subscripts 1 and 2 refer to points at the surface and the wetting front respectively, then 5-4 can be written as

$$f = K\left[\frac{h_1 - h_2}{z_1 - z_2}\right]$$
5-5

The head at the surface, h_1, is equal to the depth of ponded water, which can be denoted as h_0. Additionally, the head at the wetting front equals $-\psi - L$, where ψ is the soil suction head in units of L.

Substituting into (4) gives

$$f = K\left[\frac{h_0 - (-\psi - L)}{L}\right]$$
5-6

or

$$f = K\left[\frac{h_0 + \psi + L}{L}\right]$$
5-7

At this point in the derivation, Chow (1988) assumes that the depth of ponded water at the surface is negligible, hence drops the h_0 term of 5-6. For this investigation, h_0 is important, thus, we will continue the derivation with h_0.

Noticing that the infiltration rate, f, is the derivative of the cumulative infiltration, F, 5-7 can be written as

$$\frac{dF}{dt} = K\left[\frac{h_0 + \psi + L}{L}\right]$$
5-8

Substituting 5-3 into 5-8 gives

$$\frac{dF}{dt} = K\left[\frac{\Delta\theta(\psi + h_0) + F}{F}\right]$$
5-9

Cross multiplying 5-9 gives

$$\left[\frac{F}{\Delta\theta(\psi + h_0) + F}\right]dF = Kdt$$
5-10

Split the left hand side into two parts gives

$$\left[\frac{\Delta\theta(\psi + h_0) + F}{\Delta\theta(\psi + h_0) + F} - \frac{\Delta\theta(\psi + h_0)}{\Delta\theta(\psi + h_0) + F} \right] dF = K dt$$

5-11

And integrating within the limits of 0 and F(t)

$$\int_0^{F(t)} \left(1 - \frac{\Delta\theta(\psi + h_0)}{\Delta\theta(\psi + h_0) + F} \right) dF = \int_0^t K dt$$

5-12

To obtain

$$F(t) - \Delta\theta(\psi + h_0)\{ln[F(t) + \Delta\theta(\psi + h_0)] - ln[\Delta\theta(\psi + h_0)]\} = Kt$$

5-13

which reduces to

$$F(t) - \Delta\theta(\psi + h_0)ln\left(1 + \frac{F(t)}{\Delta\theta(\psi + h_0)} \right) = Kt$$

5-14

Equation 5-14 is the Green-Ampt equation for cumulative infiltration under ponded conditions. The equation is implicit in F, thus must be solved by iterative methods. Once the cumulative infiltration, *F*, has been calculated, the infiltration rate, *f*, can be found from the integral of 5-14, which is

$$f(t) = K\left(1 + \frac{\Delta\theta(\psi + h_0)}{F(t)} \right)$$

5-15

We now introduce the work of Mein & Larson (1971, 1973) and Chu (1978), who investigated the use of the Green-Ampt equation under constant and variable rainfall respectively. The following derivation is a simplified version of that presented by Chu (1978), extended here to incorporate surface ponding depth. The same notation of Chow (1988) is adopted for continuity.

At the time the surface becomes saturated, the infiltration rate equals the rainfall intensity. At this point, ponding commences. This is referred to here as the ponding time, denoted by t_p.

Prior to the ponding time, all rainfall is infiltrated. Therefore, two simple but important relationships for the ponding time can be shown as

$$i(t_p) = f(t_p)$$

5-16

$$F(t_p) = P(t_p)$$

5-17

where

$i(t_p)$ is the rainfall intensity at the ponding time;

$f(t_p)$ is the infiltration rate at the ponding time

$F(t_p)$ is the cumulative infiltration at the ponding time; and

$P(t_p)$ is the cumulative rainfall at the ponding time

To calculate the infiltration during ponded conditions, say at time, t_n, it is important to realise that the infiltration rate curve must be shifted along the time axis so that the cumulative infiltration equals the cumulative rainfall. This accounts for the occurrence of rainfall under unsaturated conditions. This time shift is referred to by Chu (1978) as the pseudotime, and is denoted by t_s.

To calculate the cumulative infiltration at t_n, we must substitute $t = t_n - t_p + t_s$ into equation 14. Thus, (14) becomes

$$F(t_n) - \Delta\theta(\psi + h_0)ln\left(1 + \frac{F(t_n)}{\Delta\theta(\psi + h_0)}\right) = K(t_n - t_p + t_s)\, t_1 > t_p \qquad \text{5-18}$$

Equation 5-18 is the modified form of the Green-Ampt equation to describe infiltration under ponded conditions during a variable rainfall event (Chu 1978). Equation 5-18 also accounts for the ponding depth.

For practical use of Equation 5-18, the time to ponding, t_p, and the pseudotime, t_s, must be calculated.

At the ponding time, we can apply 5-16 and 5-17 to 5-15 to give

$$i(t_p) = K\left(1 + \frac{\Delta\theta(\psi + h_0)}{P(t_p)}\right) \qquad \text{5-19}$$

rearranging 5-19 gives

$$i(t_p) - K = K\frac{\Delta\theta(\psi + h_0)}{P(t_p)} \qquad \text{5-20}$$

then

$$P(t_p) = \frac{K\Delta\theta(\psi + h_0)}{i(t_p) - K} \qquad i(t_p) > K \qquad \text{5-21}$$

Equation 5-21 can be used to calculate the ponding time, t_p, although is implicit in t_p, therefore, requires iterative solution.

At the ponding time $t_n = t_p$, therefore, equation 5-18 becomes

$$F(t_n) - \Delta\theta(\psi + h_0)ln\left(1 + \frac{F(t_n)}{\Delta\theta(\psi + h_0)}\right) = K(t_s) \qquad \text{5-22}$$

Substituting (17) into (22) gives

$$P(t_p) - \Delta\theta(\psi + h_0)ln\left(1 + \frac{P(t_p)}{\Delta\theta(\psi + h_0)}\right) = K(t_s) \qquad \text{5-23}$$

Once t_p has been calculated, equation 5-23 can be directly solved for t_s. These two time parameters can be fed back into equation 5-18, to calculate the cumulative infiltration under ponded conditions at time, t_n.

Chu (1978) draws attention to a special case whereby the rainfall event is split into a series of short periods, where the rainfall intensity is approximated as constant. In this case,

$$i(t) = \frac{[P(t_n) - P(t_{n-1})]}{(t_n - t_{n-1})} = I = \text{constant}$$

5-24

The subscript, n, is to identify the time of the short period.

The cumulative rainfall is then described by

$$P(t) = P(t_{n-1}) + (t - t_{n-1})I$$

5-25

Applying 5-24 and 5-25 to the equation for ponding time, 5-21, results in

$$P(t_{n-1}) + (t - t_{n-1})I = \frac{K\Delta\theta(\psi + h_0)}{I - K}$$

5-26

If $t = t_p$ then

$$P(t_{n-1}) + (t_p - t_{n-1})I = \frac{K\Delta\theta(\psi + h_0)}{I - K}$$

5-27

and

$$It_p + P(t_{n-1}) - It_{n-1} = \frac{K\Delta\theta(\psi + h_0)}{I - K}$$

5-28

so

$$I(t_p - t_{n-1}) = \frac{K\Delta\theta(\psi + h_0)}{I - K} - P(t_{n-1})$$

5-29

finally

$$t_p = \frac{\left[\dfrac{K\Delta\theta(\psi + h_0)}{I - K} - P(t_{n-1})\right]}{I} + t_{n-1}$$

5-30

Equation 5-30 is explicit in t_p, therefore, is more convenient to apply than 5-21. For the purpose of this investigation, Equation 5-30 suits our needs since within each calculation timestep, the rainfall will be essentially constant.

Application of Equation 5-30 to ponded conditions, we can simply substitute

$$I = \frac{h}{\Delta t}$$

5-31

into 5-30, where the calculation timestep, Δt, is in the same time units as the saturated hydraulic conductivity, K. For large ponding depths, this substituted value for I can potentially be very large for small timesteps.

5.2 Process Parameters

Definition of appropriate parameters for use with the Green-Ampt model is not an objective of this study. Rather, based on the literature, parameters presented by Rawls et al (1993) have been adopted. Values for soil porosity, effective porosity, soil suction head and hydraulic conductivity are provided for the 11 United States Department of Agriculture (USDA) soil types as listed in Table 5-1. These parameters have been derived based on extensive testing of different soils, and are the most commonly used in practice.

Table 5-1   Green-Ampt Parameters for 11 USDA Soil Textures (after Rawls et al, 1993)

USDA Soil Texture	Porosity	Effective Porosity	Suction Head (mm)	Hydraulic Conductivity (mm/hr)
Sand	0.437	0.417	49.5	117.8
Loamy Sand	0.437	0.401	61.3	29.9
Sandy Loam	0.453	0.412	110.1	10.9
Loam	0.463	0.434	88.9	3.4
Silt Loam	0.501	0.486	166.8	6.5
Sandy Clay Loam	0.398	0.330	218.5	1.5
Clay Loam	0.464	0.309	208.8	1.0
Silty Clay Loam	0.471	0.432	273.0	1.0
Sandy Clay	0.430	0.321	239.0	0.6
Silty Clay	0.479	0.423	292.2	0.5
Clay	0.475	0.385	316.3	0.3

5.3 Assumptions

Three key assumptions of Hortonian overland flow pertinent to this study are:

➢ Losses due to interception from vegetation and evaporation are neglected. For event based modelling, such losses are minimal;

➢ Only rainfall contributes to surface runoff, hence, any sub-surface flow reaching the surface is neglected. During high intensity, short duration storms, this assumption can be considered reasonable. However, sub-surface flow can significantly contribute to surface runoff during low intensity, longer duration storms. The type of soil is a considerable factor; and

> ➢ Extractions due to infiltration are only applied to the rainfall, rather than the ground surface. Infiltration due to ponding and runoff outside the spatial or temporal extent of the rainfall are not considered.

The former two assumptions remain for this current study. However, investigating the influence of the latter is one of the objectives of this study.

The following assumptions are inherent in the Green-Ampt process to be applied here:

> ➢ Infiltration process is one-dimensional;

> ➢ Homogenous soil profile;

> ➢ Uniform antecedent soil moisture distribution;

> ➢ Movement of surface water flow does not alter infiltration capacity of the soil;

> ➢ Lateral sub-surface flow is neglected; and

> ➢ There is no soil moisture deficit recovery like the GAR / MGAR as presented in Section 3.3.2.

6 LOSS MODULE DEVELOPMENT

6.1 Summary

To test the performance and influence of different loss models on flood modelling applications, a module has been developed to operate within TUFLOW. The module is a dynamic link library (DLL) called from TUFLOW at the initialisation stage and every second half timestep. As described in Section 5, two infiltration models have been incorporated into the infiltration module:

1.   Initial surface loss and continuing surface loss; and

2.   Green-Ampt infiltration.

Variables common to both routines are:

  ➢   Impervious fraction (%) – for each grid element;

  ➢   Depth to Groundwater (m) – set globally;

  ➢   Groundwater Elevation (m AHD) – set globally; and

  ➢   Effective porosity for each soil type (dimensionless) – for each grid element.

Typical values for the 11 USDA soil textures as reproduced in Table 5-1 have been inbuilt in the module.

Development of the DLL is discussed in the following sections.

6.2 Surface Loss

Additional to the variables listed above, the following variables are specific to the surface loss routine:

  ➢   Initial Loss (mm) – for each grid element; and

  ➢   Continuing Loss (mm/hr) – for each grid element.

For each timestep, and each grid element, one of six conditions is established, and the appropriate abstraction applied.

  ➢   Condition 1 – Cell dry

  ➢   Condition 2a –Water depth < Initial surface loss

    o   Infiltrate all surface water provided capacity not reached

  ➢   Condition 2b –Water depth > Initial surface loss

    o   Infiltrate difference between cumulative infiltration and initial surface loss

  ➢   Condition 3a – Water depth < Continuing surface loss increment

o   Infiltrate all surface water provided capacity not reached

➢   Condition 3b – Water depth > Continuing surface loss increment

o   Infiltrate continuing surface loss increment

➢   Condition 4 – Soil capacity reached

6.3 Green-Ampt

6.3.1 General Process

A procedure for calculating the Green-Ampt infiltration as presented in Chow (1988) is shown in Figure 6-1. Interacting with TUFLOW enables the wet/dry checks to be omitted. For each timestep, the only information carried over from the previous timestep is the cumulative infiltration. From the cumulative infiltration, the time can be calculated.

Additional to the variables listed in Section 6.1, the following variables are specific to the Green-Ampt routine:

➢   Saturated Hydraulic Conductivity (mm/hr) – for each grid element; and

➢   Suction Head (mm) – for each grid element.

For each timestep, and each grid element, one of six conditions is established, and the appropriate abstraction applied.

➢   Condition 1 – Cell dry

➢   Condition 2a – Water depth < Infiltration capacity increment (F = 0)

o   Infiltrate all surface water provided capacity not reached

➢   Condition 2b – Water depth < Infiltration capacity increment (F > 0)

o   Infiltrate all surface water provided capacity not reached

➢   Condition 3a – Water depth > Infiltration capacity increment (F = 0)

o   Infiltrate Green-Ampt increment provided capacity not reached

➢   Condition 3b – Water depth > Infiltration capacity increment (F > 0)

o   Infiltrate Green-Ampt increment provided capacity not reached

➢   Condition 4 – Soil capacity reached

At time $t_0 = 0$,
Cumulative infiltration, $F_0 = 0$

At time t_n,
Cumulative Infiltration, F_{n-1} is known

Calculate f_{n-1} from F_{n-1} using (15)

Is $f_{n-1} > \dfrac{h_n}{\Delta t}$?

$f_{n-1} \leq \dfrac{h_n}{\Delta t}$

$f_{n-1} > \dfrac{h_n}{\Delta t}$

Ponding occurs throughout interval

No ponding at beginning of timestep

Time to ponding, $t_p = t_n$

Calculate time to ponding, t_p from (30)

Calculate pseudotime, t_s from (23)

Is $t_p \geq t_n$?

Calculate F_n and f_n from (14) and (15)

Ponding occurs during current timestep

No ponding throughout timestep
$$F_n = F_{n-1} + \frac{h_n}{\Delta t}$$

Calculate pseudotime, t_s from (23)

Calculate F_n and f_n from (14) and (15)

Figure 6-1   Green-Ampt Procedure

6.3.2 Iterative Calculations

The Green–Ampt function is implicit in F, thus, an iterative solution is required. Various iterative methods were investigated, and Newton's method chosen for its relative simplicity and favourable results. Shown in Figure 6-2 is a comparison of residuals for each iteration for calculations performed using the method of successive substitution and Newton's method.   The plot highlights the computational efficiency of Newton's method, where the convergence criterion of 0.001mm/hr is achieved after 6 iterations.
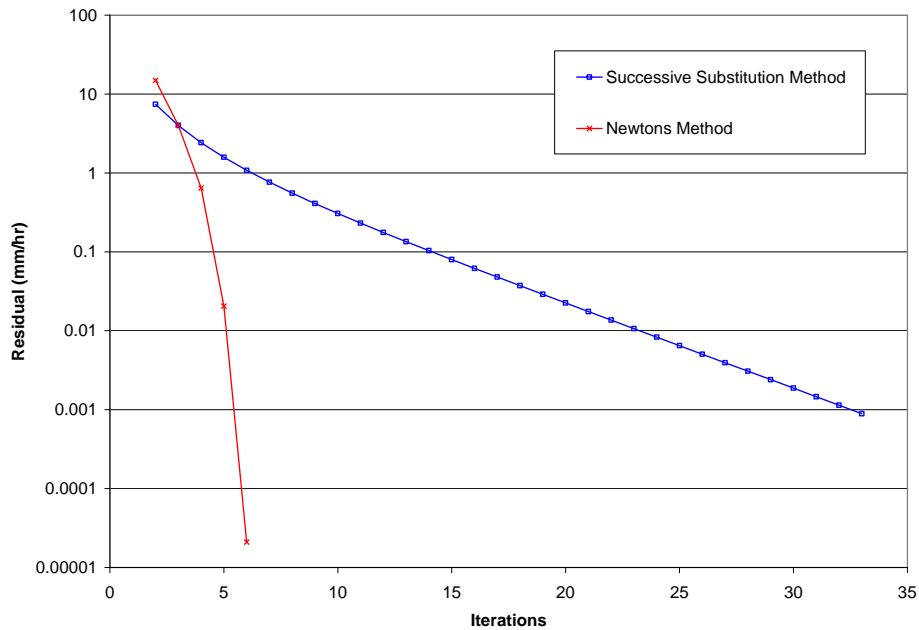
Figure 6-2   Comparison of Iterative Methods

For the case where the solution fails to converge, it is important to limit the number of iterations used. In the absence of a limiting number of iterations, this unstable case would cause the program to stall at this point while the program enters a continuous loop. Eventually a run time error may occur when the variables exceed pre-defined dimensions. A limit of 50 iterations was adopted.

7 MODEL TESTING

7.1.1 Recommended Procedure

To suitably reproduce recorded flood behaviour within an estuarine environment, a range of variables are used, with many requiring calibration. Such variables within a typical flood model are:

- ➢ Topography;

- ➢ Surface roughness;

- ➢ Spatial and temporal rainfall distribution;

- ➢ Streamflow data and rating curve;

- ➢ Recorded flood marks; and

- ➢ Infiltration parameters.

To gain a thorough understanding of the modelled system, a comprehensive parameter sensitivity analysis is required. This process will reduce the potential for compensatory errors in the calibration, or reproducing the natural flood behaviour by using inappropriate parameters. Therefore, since the temporal variability of a flood wave can be reproduced using a range of parameter sets, use of a complex flood model for assessing the performance of the infiltration module has limited value. Rather, use of a gauged catchment without tailwater influence is likely to result in a more reliable understanding of the model performance.

In essence, the volumetric output is of primary interest, since rainfall can be lumped into two categories; runoff and loss. In a gauged catchment the volumetric runoff is known, thus the focus can be applied to the loss mechanism, without undue attention being given to factors such as topography or roughness. Hence, the number of variables is greatly reduced. However, there still remains the uncertainty of rainfall and rating curve accuracy.

7.1.2 Adopted Procedure

Two test models have been developed for the following purposes:

- ➢ Verify the performance of the module and ensure input data is appropriately assigned and used; and

- ➢ Highlight the sensitivity of variables and processes.

Each test model is discussed in the following sections.

7.1.3 Test Model 1

The first test model (TM1) represents four grid cells in a square configuration. All cells are assigned an equal elevation of 10.0m above an arbitrary datum. This test model is designed for one-dimensional water movement, hence, water movement is static in x and y. As such, the size of the grid elements is irrelevant. Various scenarios have been tested as described in the following sections.

7.1.3.1 Scenario 1 – Initial and Continuing Losses

An initial water level of 10.2m is assigned to TM1 for Scenario 1, thus, representing 200mm of initial surface water. No other boundary conditions have been applied. Initial and continuing losses have been set to 100mm and 60mm/hour respectively.

With no restriction to the abstraction rate of the initial loss, 100mm is infiltrated within the first timestep (60 seconds). For each successive timestep, 1mm is infiltrated until the surface water is depleted after 101 minutes.

The cumulative infiltration plot for Scenario 1 is presented as Figure 7-1.
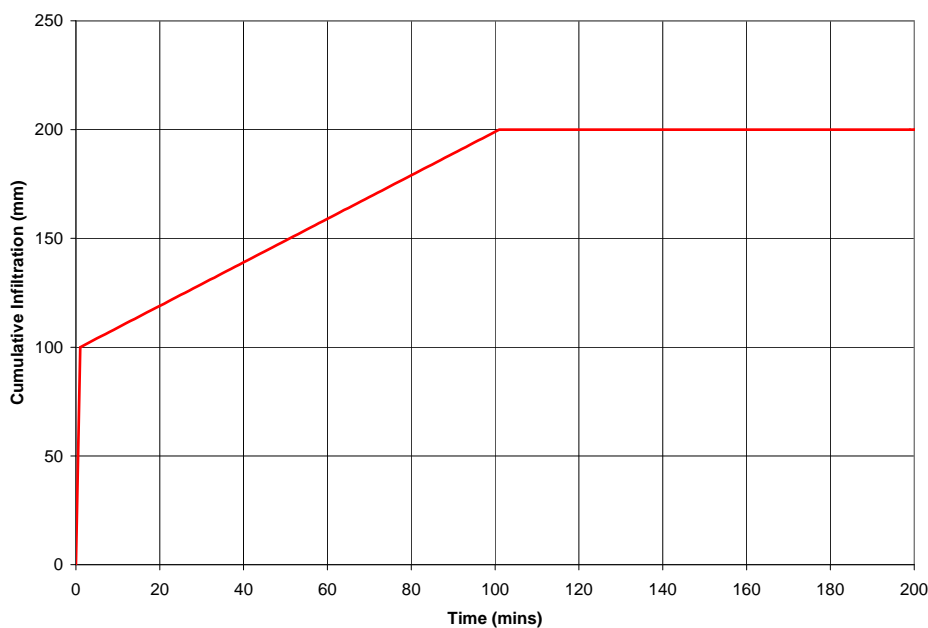
Figure 7-1   IL/CL Cumulative Infiltration

7.1.3.2 Scenario 2 - Initial and Continuing Losses with Upper Bound

Scenario 2 is a repeat of Scenario 1, however, the soil porosity is set equal to 0.4 and a groundwater elevation equal to 9.6m. Hence, only 160mm of water can infiltrate before the soil reaches saturation. The resulting cumulative infiltration plot is similar to Figure 7-1, although with a 160mm upper bound to the cumulative infiltration.

7.1.3.3 Scenario 3 – Green-Ampt Infiltration no Ponding

Infiltration rates for the 11 United States Department of Agriculture (USDA) soil textures are presented in Figure 7-2. The clear trend is the decreasing infiltration rate as the sand content reduces and clay content increases. As expected, the curve for each soil texture is asymptotic with the saturated hydraulic conductivity for that soil.
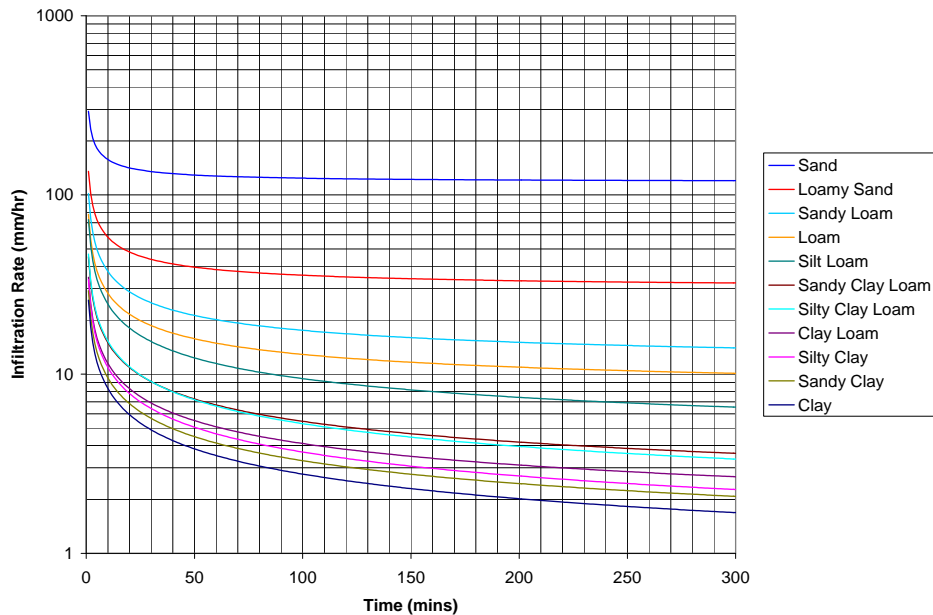
Figure 7-2   Infiltration Rate of 11 USDA Soil Textures

7.1.3.4 Scenario 4 – Green-Ampt Infiltration with Ponding

Presented in Figure 7-3 are the corresponding infiltration rates with 1,000mm of surface ponding. As expected, surface ponding significantly increases the infiltration rate. It is worth noting, however, that the infiltration rate curves presented in Figure 7-3 are also asymptotic with the saturated hydraulic conductivity.

A comparison between the ponding and no ponding cases is presented in Figure 7-4. This figure shows the percentage increase of infiltration rate with 1,000mm of ponding on the surface. From this figure we can see that:

➢ Surface ponding significantly influences the initial infiltration rate of soils with a high saturated hydraulic conductivity (sand, loamy sand and sandy loam);

➢ The influence of surface ponding is reduced for the same soils as time elapses, i.e. there is a faster decay rate;

➢ The infiltration rate associated with the soils with a low saturated hydraulic conductivity (clays) is approximately double the 'no ponding' case; and

➢ The decay rate of these same soils is less than the sandy soils.
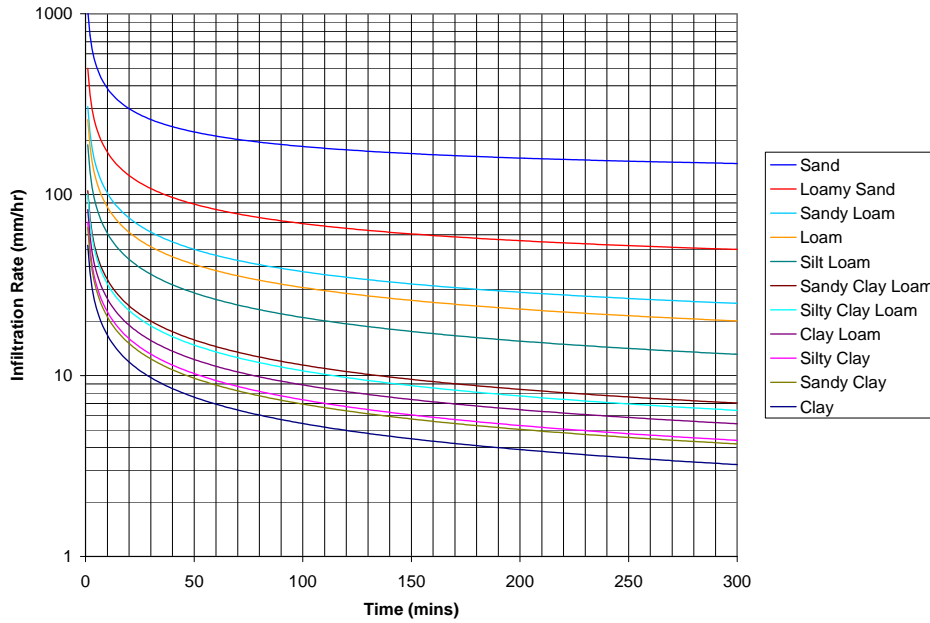
Figure 7-3   Infiltration Rate of 11 USDA Soil Textures with Surface Ponding
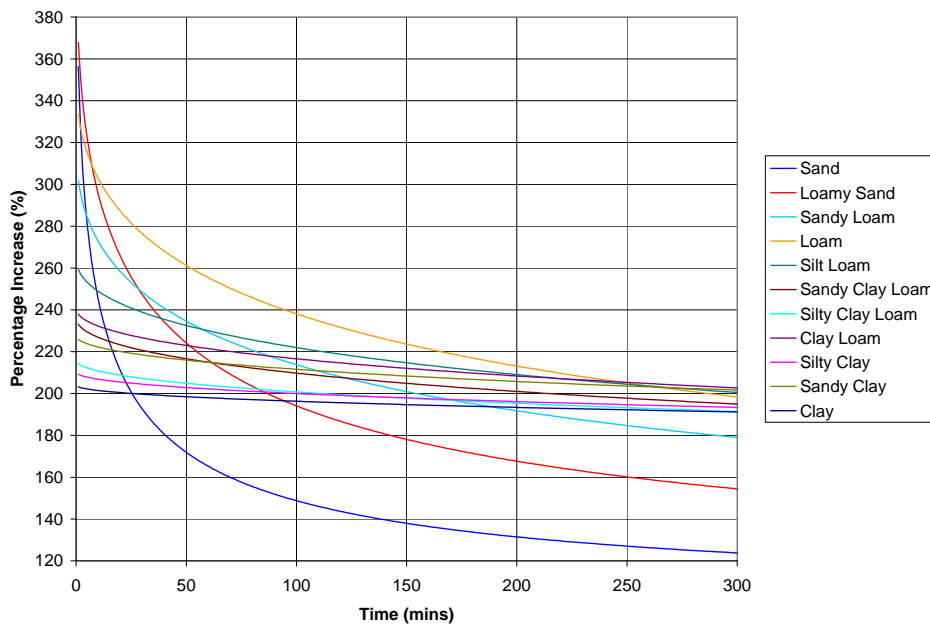
Figure 7-4   Percentage Increase in Infiltration Rate due to Surface Ponding

A comparison between the infiltration rate of a sandy loam for the ponding and no ponding cases is presented in Figure 7-5. We can clearly see from this plot that without surface ponding, there is a faster decay rate. Whilst the initial difference between infiltration rates is high, as time elapses, the difference reduces. As stated previously, both curves are asymptotic with the saturated hydraulic conductivity value of 10.9mm/hr. These trends are common to all 11 soil textures.
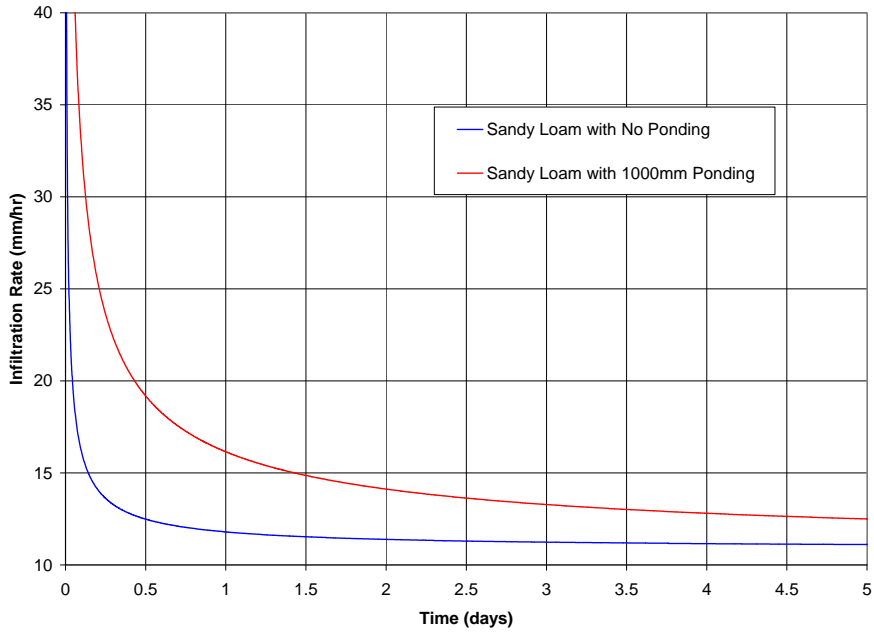
Figure 7-5   Infiltration Rate of Sandy Loam – Ponding Comparison

7.1.3.5 Scenario 5 – Green-Ampt Infiltration with Variable Ponding

Presented in Figure 7-6 is the infiltration rate of a Sandy Loam with variable ponding depth up to 1,000mm. This scenario shows how the typical decaying infiltration curve can be distorted by the influence of ponding head.
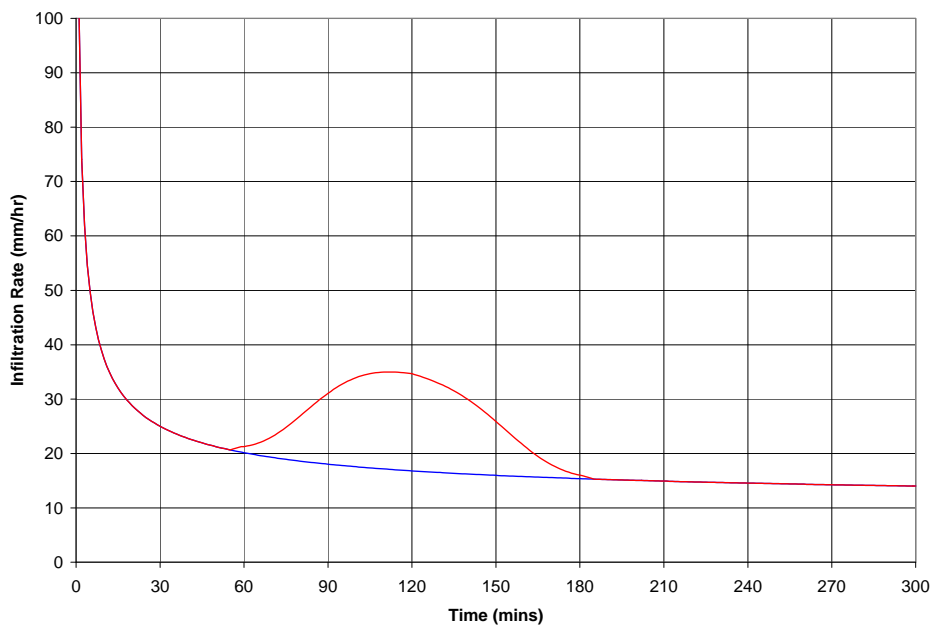
Figure 7-6   Infiltration Rate of Sandy Loam – Variable Ponding

7.1.4 Test Model 2

Test Model 2 represents a hypothetical catchment, with similar topographical characteristics to a desert wadi. Steep hills define the extent of a wide alluvial floodplain, and ephemeral riverbed. The longitudinal grade of the river is approximately 0.3%. Initial conditions are dry, and no tailwater influence is assumed. A homogenous sandy soil profile of infinite depth is assumed.

Refer to Figure 7-7 for digital elevation model of Test Model 2. Also shown on Figure 7-7 are the hydraulic model extents (red polygon), boundary conditions (tracked blue lines) and plot output locations (brown lines and red stars).
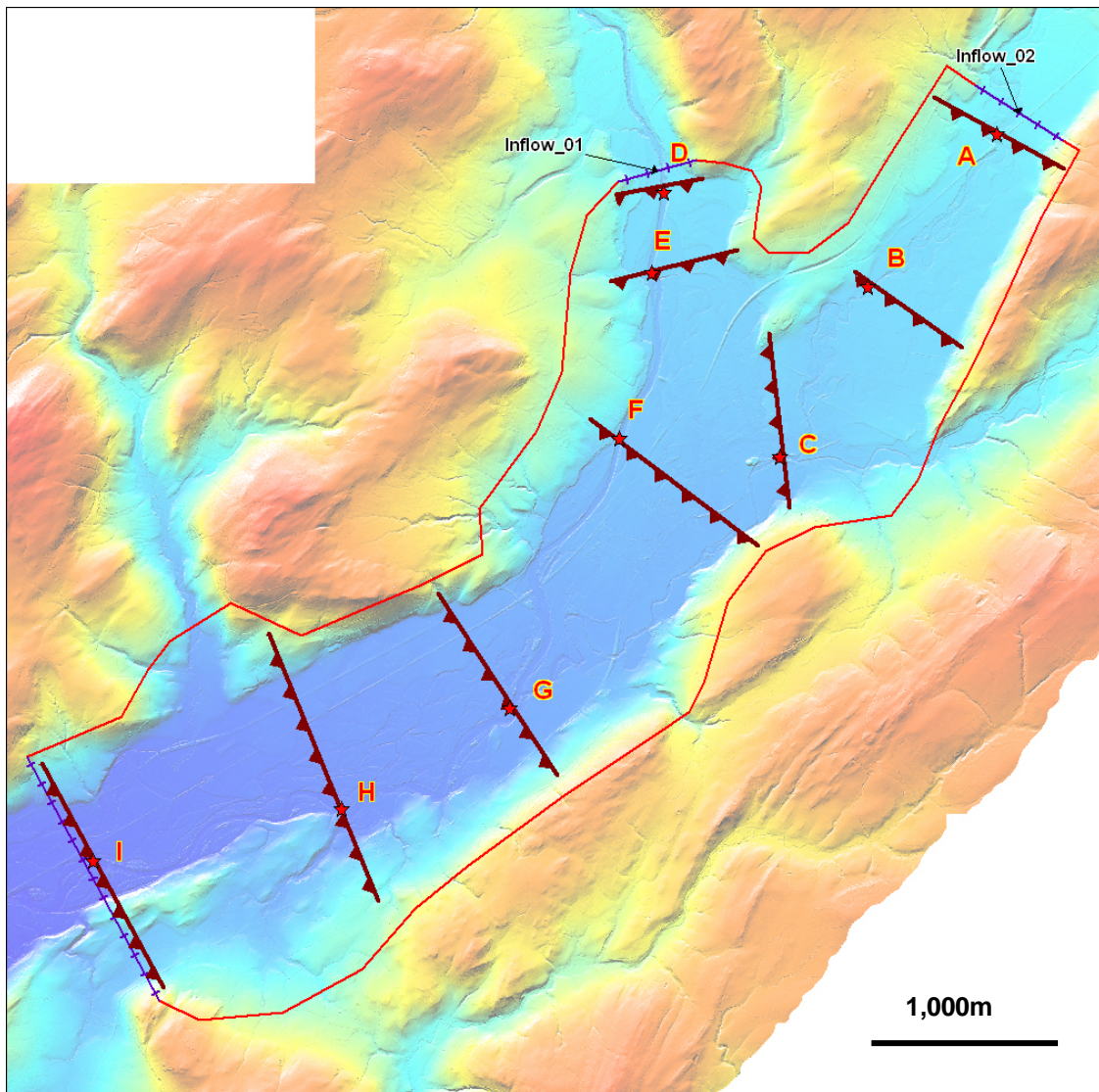
Figure 7-7   Test Model 2 Digital Elevation Model

Triangular inflow hydrographs with peaks flow rates of 200m3/s and 15m3/s have been applied to 'Inflow 01' and 'Inflow 02' respectively over a period of 48 hours. A head versus flow boundary is applied to the downstream boundary based on a hydraulic gradient of 0.3%. No rainfall is applied to the 2D grid. A 20m grid element size and uniform Manning's 'n' of 0.03 are used. All simulations are run until the catchment is mostly drained.

The scenarios listed in Table 7-1 have been modelled as presented in the following sections.

Table 7-1   Test Model Scenarios

Scenario	Initial Surface Loss	Continuing Surface Loss	Depth to Groundwater Table
1 – No Losses	-	-	unlimited
2 – Surface Losses	20mm/hr	2.5mm/hr	unlimited
3 – Green-Ampt without Ponding	-	-	unlimited
4 – Green-Ampt with Ponding	-	-	unlimited
5 – Green-Ampt with Upper Bound	-	-	2.0m

7.1.4.1 Scenario 1 – No Losses

Using conventional modelling methods, no losses would be applied to the case where upstream inflows are the only source of water. Hydrographs for the 9 plot output locations are presented in Figure 7-8. Note the minimal attenuation due to the low Manning's 'n' value used. The shape of the output hydrograph is very similar to that of the input hydrographs.
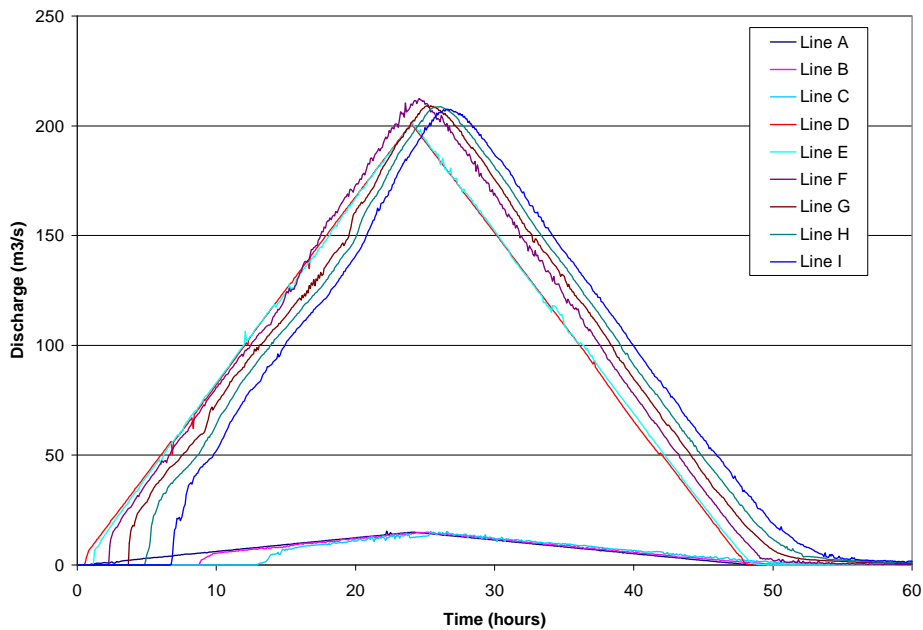
Figure 7-8   Output Hydrographs for Scenario 1

Flood extents are presented in Figure 7-9.
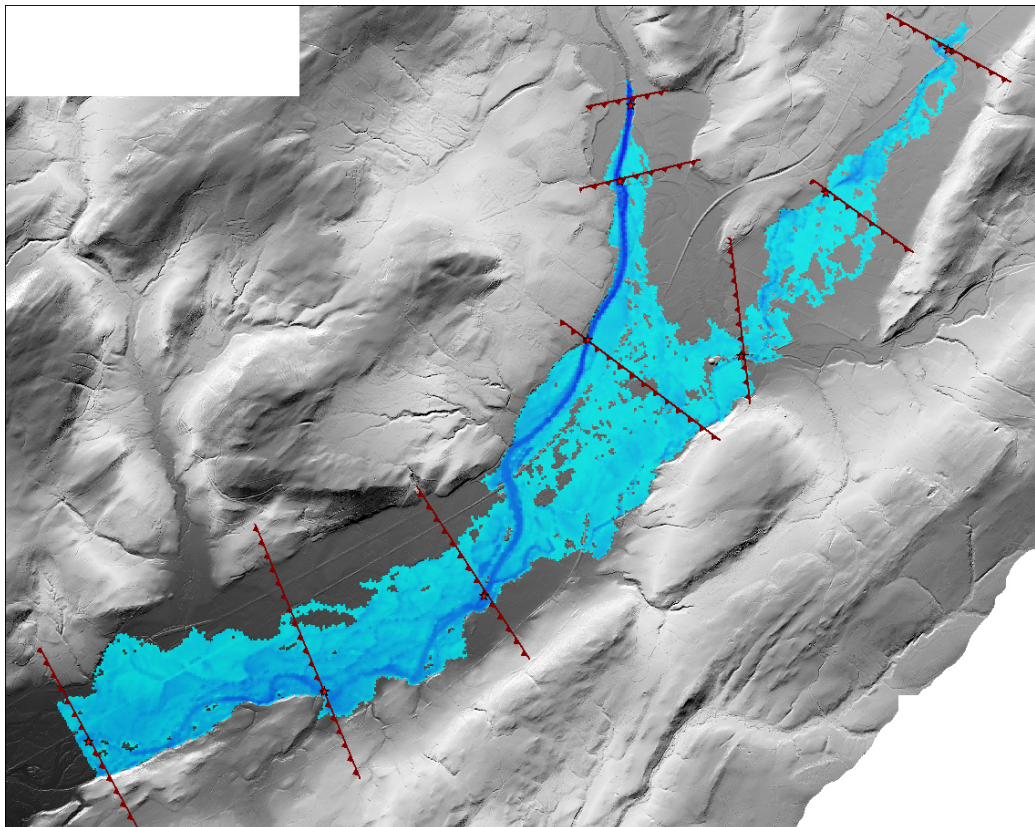
Figure 7-9   Peak Flood Depth (0m to 5m) for Scenario 1

Peak discharge and flood levels at the 9 plot output locations are presented in Table 7-2.

Table 7-2   Plot Output for Scenario 1

Plot Output Location	Peak Discharge (m³/s)	Cumulative Infiltration (mm)	Peak Flood Level (m above datum)
A	15.3	-	75.09
B	15.0	-	70.56
C	15.3	-	65.76
D	200.9	-	71.18
E	202.1	-	69.31
F	212.5	-	65.62
G	209.2	-	58.74
H	208.6	-	55.26
I	207.6	-	50.84

Mass balance for Scenario 1 is presented in Table 7-3. Note that the outflow volume is similar to the inflow volume. The difference represents water remaining on the 2D grid.

Table 7-3   Mass Balance for Scenario 1

Total Inflow	18,576,000m^3
Total Outflow	17,960,101m^3
Infiltrated Volume	0m^3
Percentage of Inflow	0%
Average Depth of Infiltration	0mm

7.1.4.2 Scenario 2 - Surface Losses

Typical initial and continuing loss values of 20mm and 2.5mm/hr respectively have been applied to the model using the surface loss module. Hydrographs for the 9 plot output locations are presented in Figure 7-10.
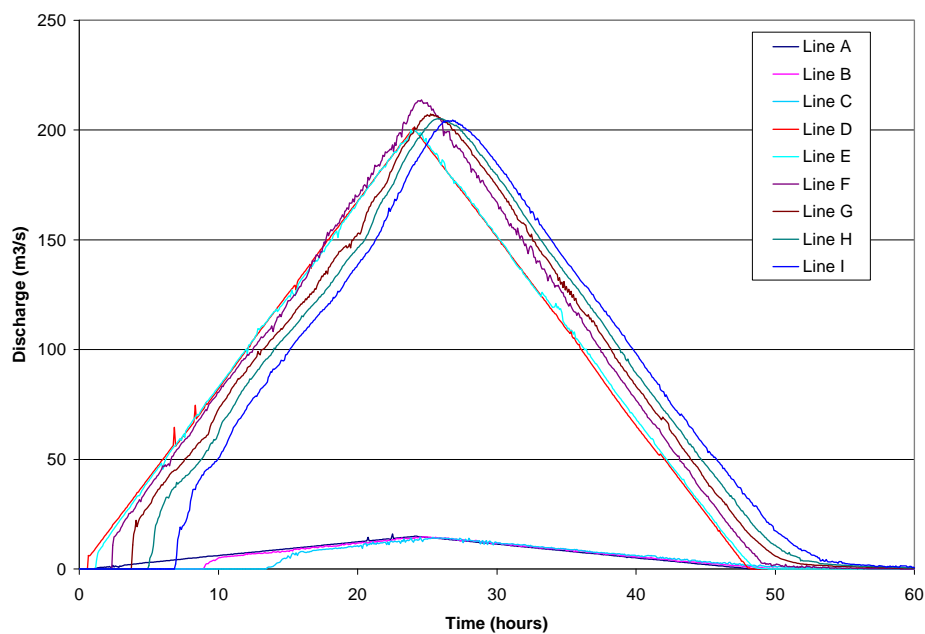
Figure 7-10 Discharge Hydrographs for Scenario 2

The results are barely discernable from those of Scenario 1. Cumulative infiltration for the 9 plot output locations is shown on Figure 7-11.
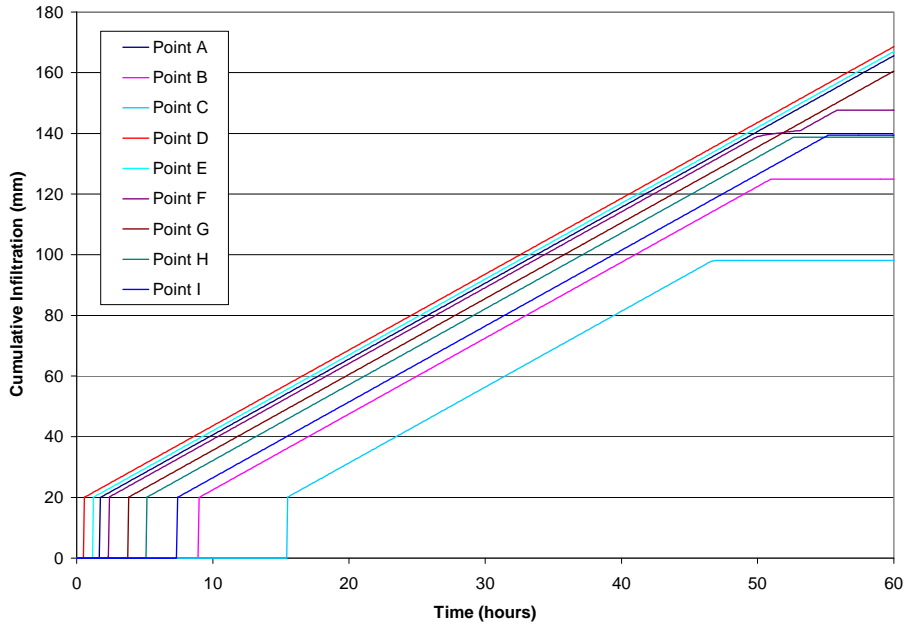
Figure 7-11 Cumulative Infiltration for Scenario 2

Note from Figure 7-11 the initial loss of 20mm, followed by the continuing loss rate of 2.5mm/hr until the surface dries.

Plot output is presented in Table 7-4, with the corresponding output from Scenario 1 included in parenthesis. The peak discharge is shown to decrease marginally, although peak flood levels differ by less than 10mm.

Table 7-4   Plot Output from Scenario 2

Plot Output Location	Peak Discharge (m³/s)	Cumulative Infiltration (mm)	Peak Flood Level (m above datum)
A	16.1 (15.3)	166	75.09 (75.09)
B	14.7 (15.0)	125	70.55 (70.56)
C	14.6 (15.3)	98	65.76 (65.76)
D	200.9 (200.9)	169	71.18 (71.18)
E	200.2 (202.1)	167	69.30 (69.31)
F	213.8 (212.5)	148	65.62 (65.62)
G	207.3 (209.2)	161	58.73 (58.74)
H	205.2 (208.6)	139	55.25 (55.26)
I	204.5 (207.6)	139	50.84 (50.84)

Mass balance is presented in Table 7-5. The average depth of infiltration across the extent of flooded ground is 110mm. Although nearly 472,000m³ of water has been lost to infiltration, it only represents

2.5% of the inflow volume. This fraction would be expected to increase with decreasing flow magnitude.

Table 7-5 Mass Balance for Scenario 2

Total Inflow	18,576,000m³
Total Outflow	17,542,506m³
Infiltrated Volume	471,988m³
Percentage of Inflow	2.5%
Average Depth of Infiltration	110mm

7.1.4.3 Scenario 3 – Green-Ampt Infiltration without Ponding Influence

Scenario 3 represents the Green-Ampt module with typical USDA soil parameters for a sandy soil as presented in Table 5-1. It can be seen from Figure 7-12 that the flood wave is significantly more attenuated than in the previous scenarios.
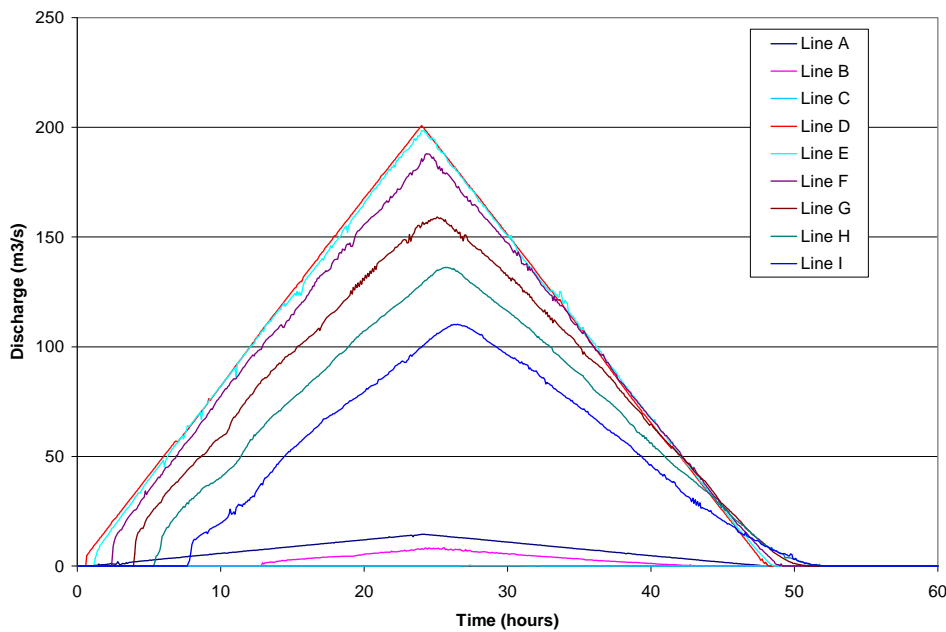
Figure 7-12 Discharge Hydrographs for Scenario 3

Cumulative infiltration is shown on Figure 7-13 at the 9 plot output locations. Due to the scale of the plot, the slopes of the lines appear constant. On closer inspection, it is possible to see the slight initial curvature of the lines. The general slope of the line is governed by the hydraulic conductivity.

Some commentary regarding the excessive cumulative infiltration is made in Scenario 5.
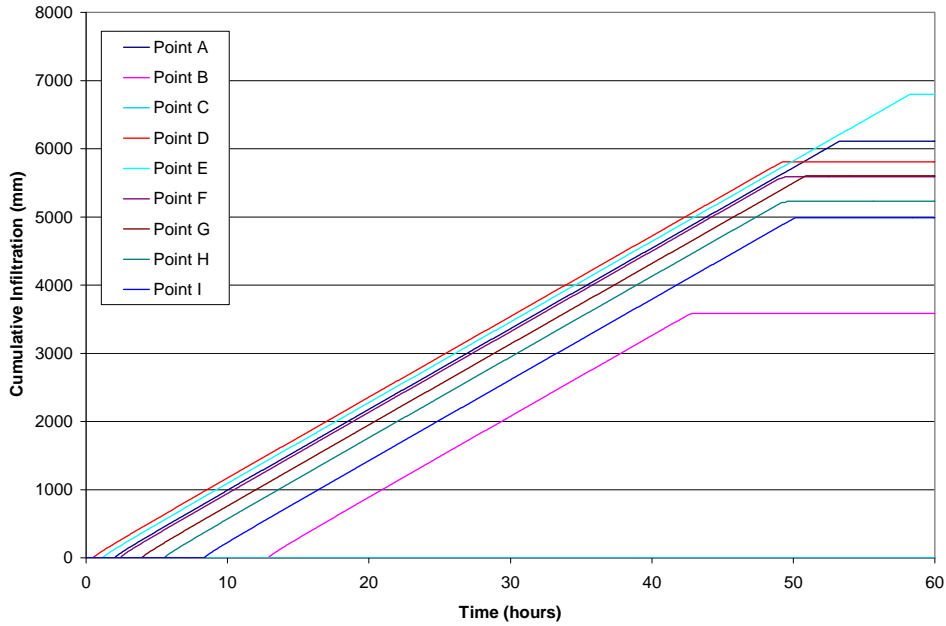
Figure 7-13   Cumulative Infiltration for Scenario 3

Infiltration rate time series for the same locations is shown on Figure 7-14. The infiltration curves are the same, although the initial infiltration rate is shown to differ due to the time series output interval.
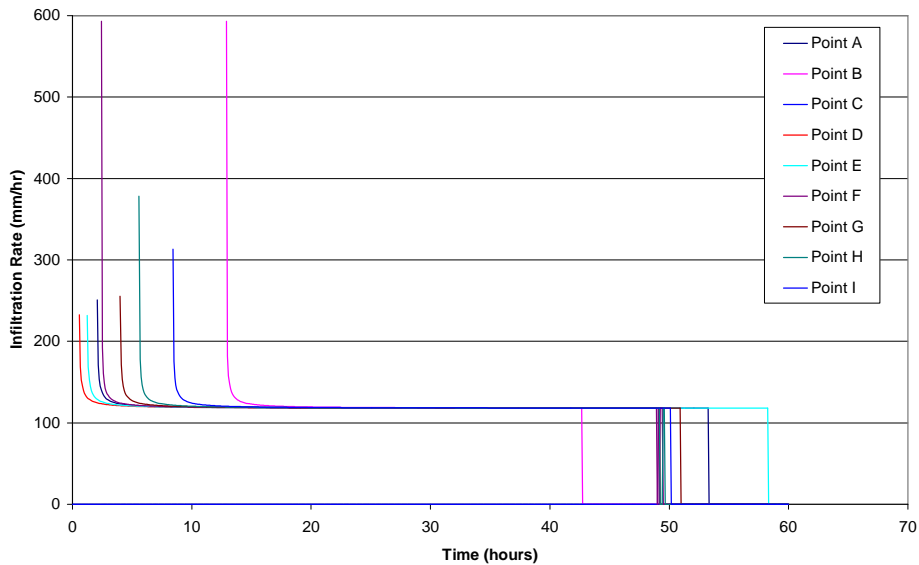
Figure 7-14   Infiltration Rate for Scenario 3

Cumulative infiltration is mapped in Figure 7-15. Note the higher cumulative infiltration within the channel where the surface is flooded for longer. The extent of cumulative infiltration shown is the same as the extent of flooding for this scenario. Note from Figure 7-12 and Figure 7-15 the infiltration of all flow from 'Inflow 02'. This scenario often occurs in desert environments where the runoff seldom reaches the receiving environment.
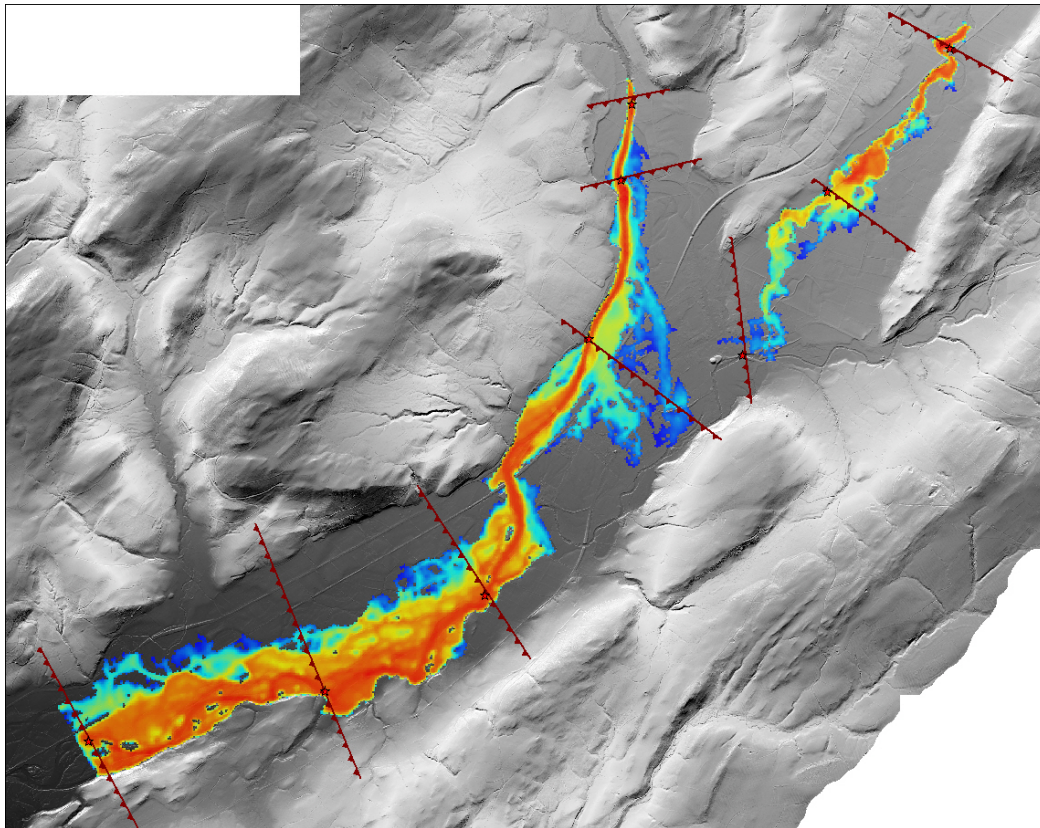
Figure 7-15   Cumulative Infiltration Mapping for Scenario 2

Plot output is presented in Table 7-6, with the corresponding output from Scenario 1 included in parenthesis. At the downstream end of the model, only 50% of the discharge from Scenario 1 is shown to occur. This corresponds to a reduction on peak flood level of 280mm.

Table 7-6   Plot Output from Scenario 3

Plot Output Location	Peak Discharge (m^3/s)	Cumulative Infiltration (mm)	Peak Flood Level (m above datum)
A	14.5 (15.3)	6,110	75.07 (75.09)
B	8.3 (15.0)	3,581	70.45 (70.56)
C	0.3 (15.3)	0	65.68 (65.76)
D	200.8 (200.9)	5,806	71.17 (71.18)
E	198.5 (202.1)	6,801	69.29 (69.31)
F	187.9 (212.5)	5,590	65.57 (65.62)
G	159.2 (209.2)	5,605	58.56 (58.74)
H	136.2 (208.6)	5,233	55.00 (55.26)
I	110.3 (207.6)	4,988	50.56 (50.84)

Mass balance is presented in Table 7-7. The average depth of infiltration across the extent of flooded ground is 3,159mm. The 9,788,796m^3 of infiltrated water equates to 53% of the total inflow.

Table 7-7   Mass Balance from Scenario 3

Total Inflow	18,576,000m^3
Infiltrated Volume	9,788,796m^3
Percentage of Inflow	52.7%
Average Depth of Infiltration	3,159mm

7.1.4.4 Scenario 4 – Green-Ampt Infiltration with Ponding Influence

To demonstrate the influence of ponding on the Green-Ampt scheme, Scenario 3 is repeated with the ponding flag activated in the model. Output hydrographs are presented in Figure 7-16. The results are similar to the no ponding case.
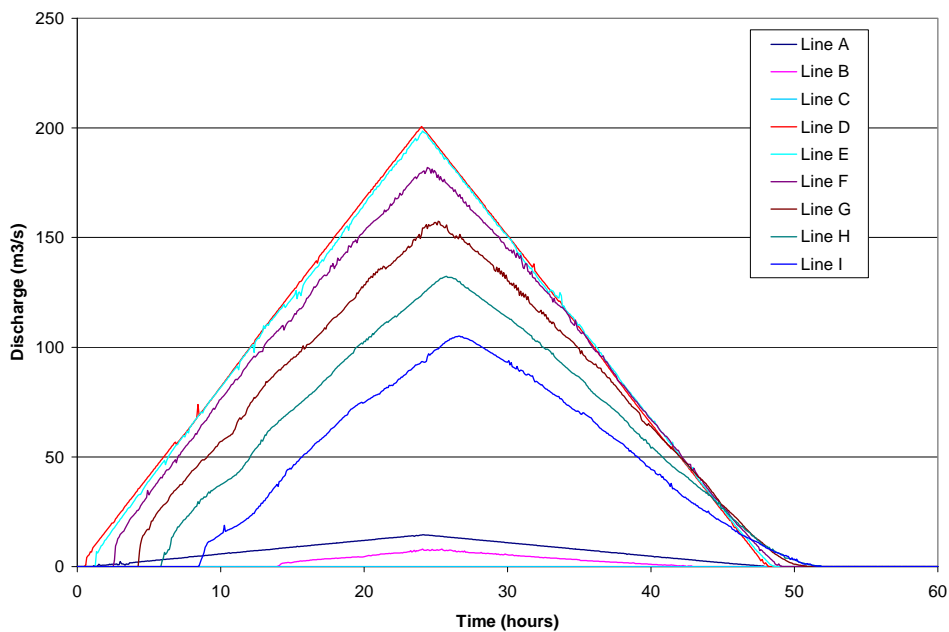
Figure 7-16 Discharge Hydrographs from Scenario 4

The cumulative infiltration presented in Figure 7-17 is greater than that presented in Scenario 3. From Figure 7-17 it is also possible to see the curvature of the lines.
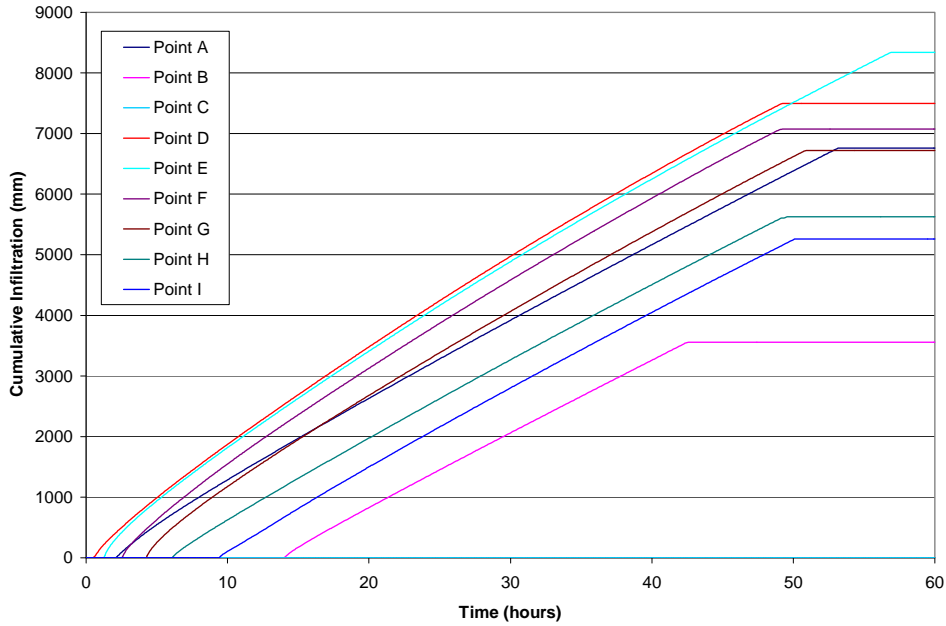
Figure 7-17   Cumulative Infiltration from Scenario 4

Infiltration rate time series for the same locations is shown on Figure 7-18. The infiltration curves differ from each other due to the influence of ponding. Note the recovery shown on some of the curves.
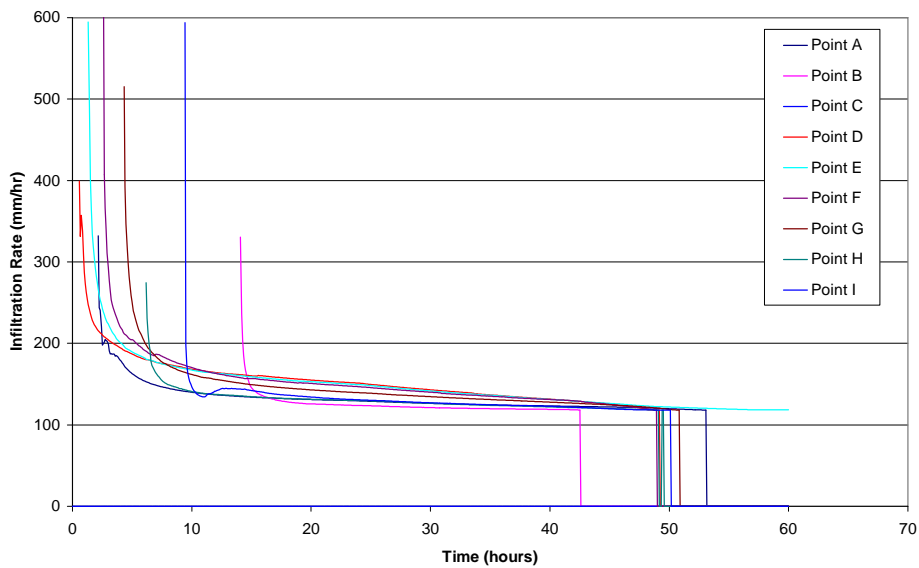
Figure 7-18   Infiltration Rate fromScenario 4

Plot output is presented in Table 7-8, with the corresponding output from the no ponding case included in parenthesis. Peak discharges reduce marginally, although cumulative infiltration increases significantly. Peak flood levels differ by no more than 10mm.

Table 7-8   Plot Output from Scenario 4

Plot Output Location	Peak Discharge (m^3/s)	Cumulative Infiltration (mm)	Peak Flood Level (m above datum)
A	14.4 (14.5)	6,760 (6,110)	75.07 (75.07)
B	8.1 (8.3)	3,554 (3,581)	70.45 (70.45)
C	0 (0.3)	0 (0)	no flooding
D	200.7 (200.8)	7,497 (5,805)	71.17 (71.17)
E	198.6 (198.5)	8,340 (6,801)	69.28 (69.29)
F	182.0 (187.9)	7,072 (5,590)	65.57 (65.57)
G	157.5 (159.2)	6,723 (5,605)	58.54 (58.56)
H	132.3 (136.2)	5,629 (5,233)	54.98 (55.00)
I	105.1 (110.3)	5,261 (4,988)	50.55 (50.56)

Mass balance is presented in Table 7-9. The average depth of infiltration across the extent of flooded ground is 3,483mm, thus a 10% increase from the no ponding case.

Table 7-9   Mass Balance from Scenario 4

Total Inflow	18,576,000m^3
Infiltrated Volume	10,427,762m^3
Percentage of Inflow	56.1%
Average Depth of Infiltration	3,483mm

7.1.4.5 Scenario 5 – Green-Ampt Infiltration with Upper Bound

Such extreme depths to the wetting front are unlikely in most situations, particularly when considering the assumptions of isotropic homogenous soils. Bedrock or perched layers with lower hydraulic conductivity are likely to limit the infiltration volume. Soils with high values of hydraulic conductivity will exhibit lateral groundwater flow. This highlights the importance of applying an upper bound to the cumulative infiltration. Two simplistic methods have been applied as discussed in Section 6:

1. Maximum depth to groundwater table; and

2. Groundwater table elevation.

Investigation of more complex methods is beyond the scope of this study, and is more applicable to groundwater modelling and soil moisture accounting.

Scenario 5 represents a maximum depth to groundwater of 2m. Thus, the maximum cumulative infiltration is 2m multiplied by the soil moisture deficit.

Output hydrographs are presented in Figure 7-19.
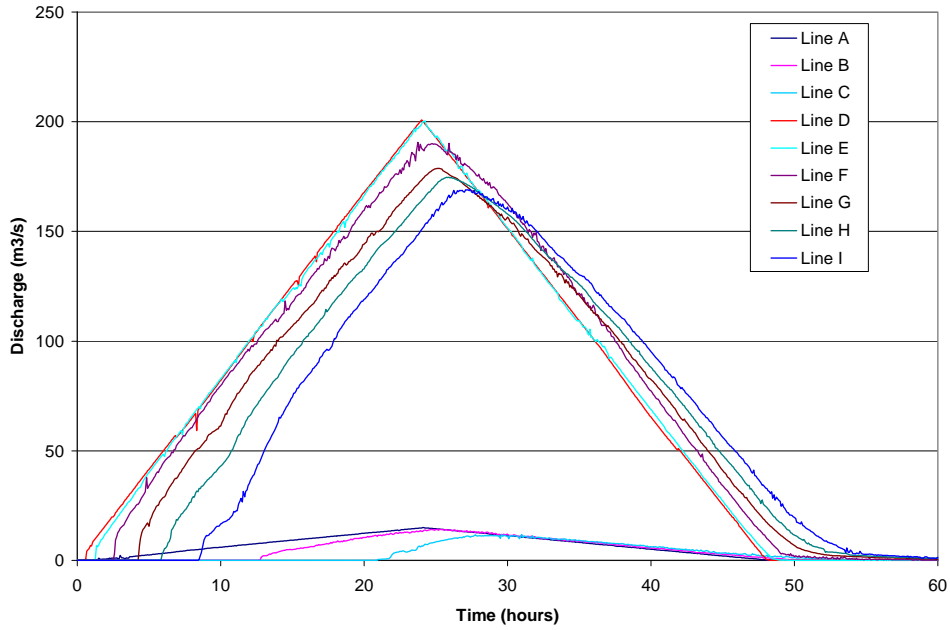
Figure 7-19   Discharge Hydrographs from Scenario 5

The cumulative infiltration is presented in Figure 7-20.   Prior to the soil reaching capacity, the infiltration curves are similar to those presented in Scenario 4.   The minor difference will be associated with the changed hydraulic behaviour in the lower parts of the model, due to the reduced infiltration.
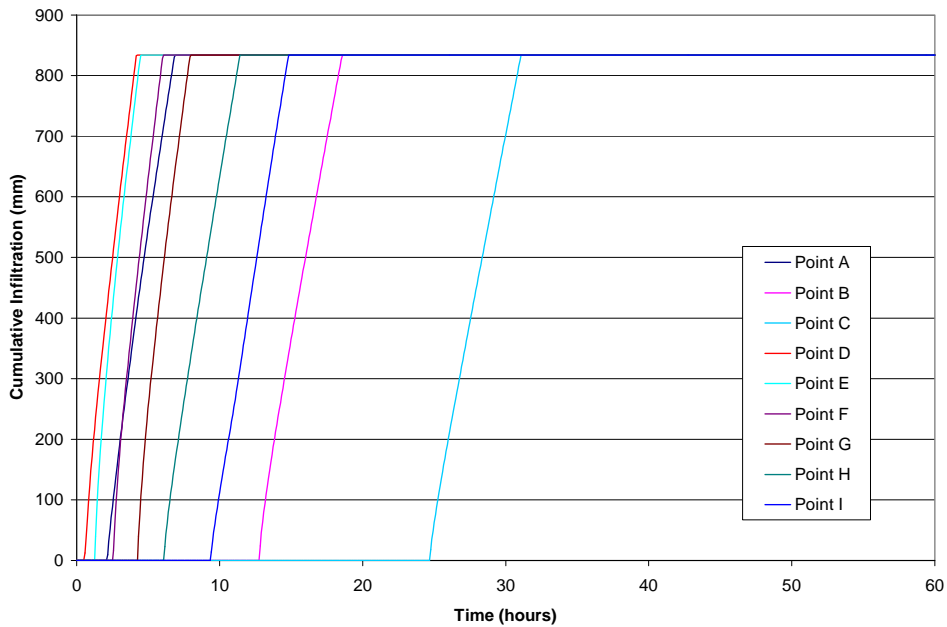
Figure 7-20   Cumulative Infiltration from Scenario 5

Corresponding infiltration rate curves are presented in Figure 7-21.
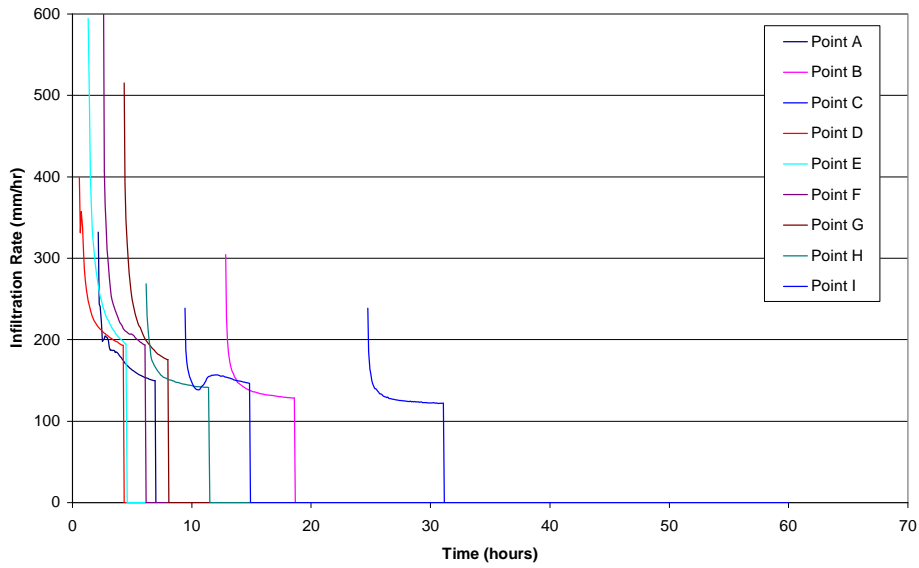
Figure 7-21   Infiltration Rate from Scenario 5

The plot output from Scenario 5 is presented in Table 7-10 and the corresponding mass balance presented in Table 7-11.

Table 7-10   Plot Output from Scenario 5

Plot Output Location	Peak Discharge (m³/s)	Cumulative Infiltration (mm)	Peak Flood Level (m above datum)
A	14.9	834	75.09
B	14.3	834	70.55
C	11.8	834	65.75
D	200.9	834	71.18
E	200.4	834	69.30
F	190.6	834	65.61
G	178.8	834	58.63
H	174.8	834	55.15
I	169.2	834	50.72

Table 7-11   Mass Balance from Scenario 5

Total Inflow	18,576,000m³
Infiltrated Volume	3,197,952m³
Percentage of Inflow	17.2%
Average Depth of Infiltration	813mm

8 CASE STUDIES

8.1 Case Study Summary

Three catchments have been selected to highlight some of the issues associated with loss modelling. The first two (Case Studies 1 and 2) are used to show how the conversion of digital elevation models (DEMs) into 2D grids for modelling can result in 'artificial depressions', which can undesirably influence modelling output. The third catchment (Case Study 3), also used for the depression storage analysis, is then used for application and further testing of the infiltration module.

The case study catchments have been selected for their differing topography, size and landuse as summarised below:

- ➢ **Case Study 1** - Newrybar Swamp, Richmond Valley, NSW

    - o Medium sized rural catchment of approximately 64km^2;

    - o Steep escarpment dropping to a flat swampy floodplain; and

    - o Typically agricultural landuse.

- ➢ **Case Study 3** – Throsby Creek, Newcastle, NSW

    - o Medium sized urban catchment of approximately 39km^2; and

    - o Steep escarpment dropping to a flat urbanised floodplain.

- ➢ **Case Study 3** – Rous River, Tweed Valley, NSW

    - o Medium sized rural catchment of approximately 130km^2;

    - o Gauged catchment with 10 daily and 3 pluviograph rainfall stations and 1 streamflow station, all covering 3 major flood events;

    - o Steep topography ranging from 0m to greater than 1,100m AHD;

    - o Mixture of agricultural and natural forest land cover; and

    - o Various soil types.

8.2 Methodology

8.2.1 DEM and Depression Storage Analysis

Representing complex topography using a grid of square elements presents a range of issues including:

> ➢ Inability to represent sub-grid scale topography;

> ➢ Potential inability to represent continuous flowpaths due to sampling of the DEM; and

> ➢ Potential creation of artificial depressions within the 2D grid.

Refer to Figure 8-1 for a graphical example of how artificial depressions can be created in the 2D grid following the grid sampling process. The flowpath invert follows a diagonal alignment relative to the grid element orientation (top right to bottom left). The 2D flow within the blue grid element will be blocked by the adjacent cells, which are at a higher elevation. In this example, 5.5m depth of water will be trapped in the blue grid cell. Based on an 80m grid element size, that equates to 35,200m^3 of lost water.

Britton and Subasing (2004) undertook a direct rainfall study using the MIKE 21 software. One of the findings of their study was the sensitivity of discharge to artificial depressions within the DEM. They reported improved results using a pit-filling algorithm on the DEM. This is discussed further below.
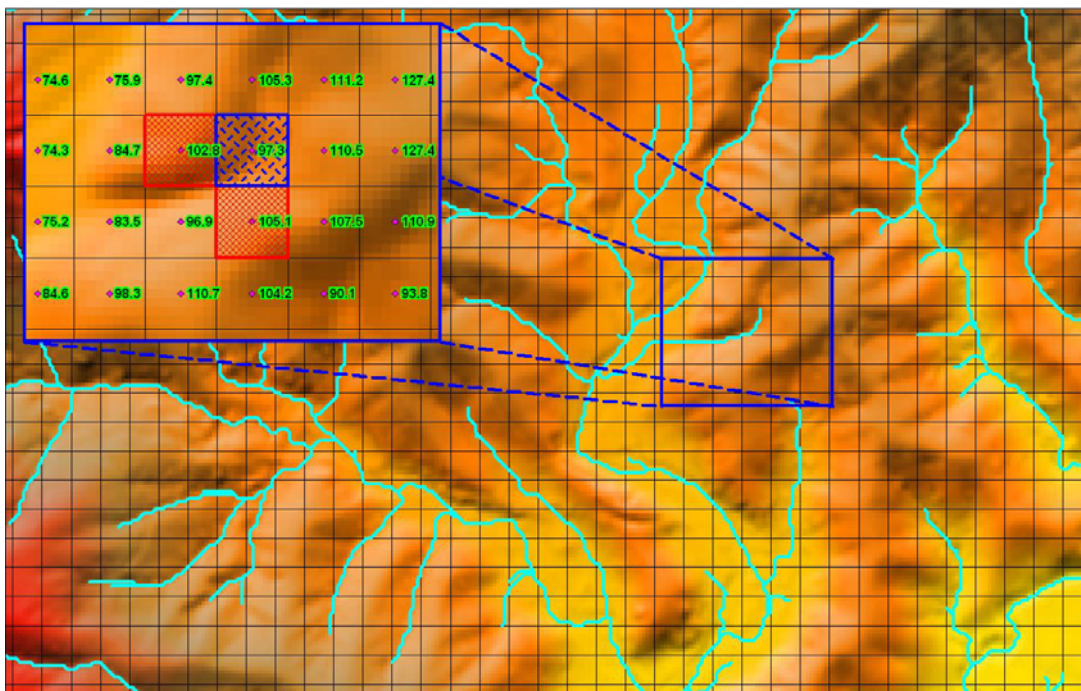
Figure 8-1   Example of Artificial Depression Created in 2D Grid

These previously listed issues are related, and generally their influence decreases with a smaller grid element size. However, practical modelling requires a balance between grid size and simulation run times.

Steeper and more intricate topography presents the greatest challenge to the grid sampling process. To investigate these issues, a depression storage analysis has been undertaken on the DEMs used for each of the case study catchments. A summary of the depression storage analysis findings is included in Section 8.6.1.

The purpose of the analysis is to assess the quantity of water held in depressions across the catchment. This depression storage can be described in two ways:

➤ The volume of water required to fill depressions before runoff will commence; or

➤ The volume of water retained on an impervious catchment once fully drained.

The depression storage analysis will be undertaken on each DEM re-sampled at various resolutions. The methodology used is as follows:

1. Resize original high resolution DEM to the required coarser resolution using Vertical Mapper.

2. Apply 'pit-fill' process to the resized DEM using the Streambuilder add-on for Mapinfo.

3. Subtract 'pit-filled' DEM from the original of the same resolution using Vertical Mapper.

4. Calculate volume of the resultant DEM using Vertical Mapper.

5. 'Sanity' check of results using volumetric output of the resultant DEM.

The volume of the resultant DEM represents the volume of depression storage within that DEM. Dividing the volume by the DEM area gives an average depth over the DEM extent.

8.2.2 Loss Model Parameter Testing

During the model testing presented in Section 7, a flow versus time boundary was applied to the upstream extents of Test Model 2. Thus, no rainfall or point inflows were applied across the modelling domain. For Case Study 3 two methods are compared for application of rainfall to the 2D modelling domain, as discussed in Section 4.2.2:

➤ Surface Area (SA) method; and

➤ Direct Rainfall (DR) method.

The influence of using different infiltration methods is investigated using a gauged rural catchment.

8.3 Case Study 1 – Newrybar Swamp

8.3.1 Catchment Description

Newrybar Swamp lies within the North Creek catchment draining to the Richmond River at Ballina. The catchment ranges in elevation from sea level to over 165m AHD. Over 50% of the 165km^2 catchment is below 5m AHD, thus highlighting the flat nature of the catchment.

Along the western boundary, the steep escarpment of the Alstonville plateau falls steeply to the floodplains of the Newrybar Swamp. The floodplain area is predominantly used for sugar cane farming. Drainage is characterised by a series of farm drains, eventually discharging into North Creek at Ross Lane. From Ross Lane, North Creek flows in a southerly direction parallel to the coastline.

Airborne laser scanning (ALS) survey of the Newrybar Swamp catchment was captured for the NSW Roads and Traffic Authority's Pacific Highway Upgrade program. The DEM was made available for this study. Refer to Figure 8-2 for the digital elevation model (DEM) of the catchment.
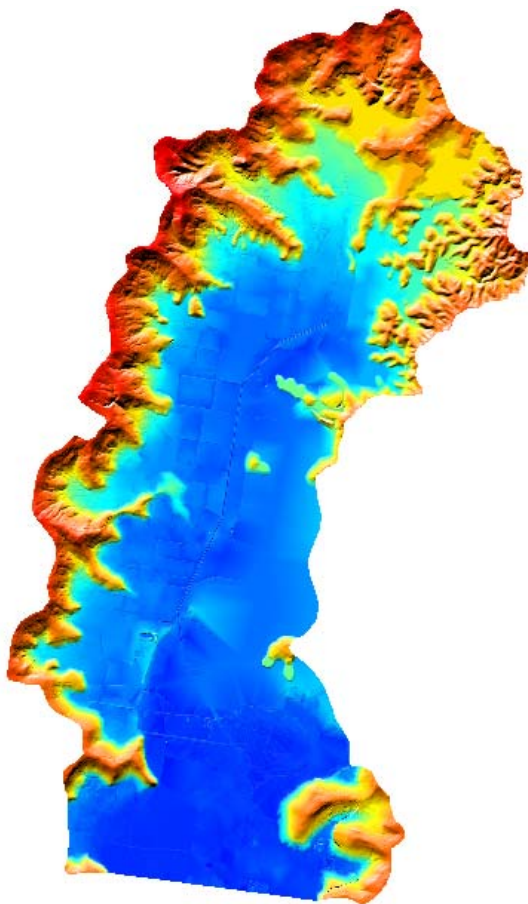
Figure 8-2   Newrybar Swamp Digital Elevation Model

8.3.2 DEM and Depression Storage Analysis

The Newrybar Swamp DEM was re-sampled to produce DEM's with grid elements of 5, 10, 20, 40 and 80 metres. The Streambuilder pit-filling algorithm was performed on each, and the resulting DEM compared against the original with the same element size.

The mean depth of depression storage across each DEM is presented in Table 8-1.

Table 8-1   Depression Storage Results for Newrybar Swamp DEM

Grid Element Size (m)	Mean Depth of Storage Across Catchment (mm)
5	38
10	33
20	35
40	42
80	50

A general trend of increasing depth with decreasing grid resolution is apparent.

8.4 Case Study 2 – Throsby Creek

8.4.1 Catchment Description

The Throsby Creek catchment covers the Newcastle urban area in central NSW. The majority of the catchment is urbanised, covering an area of 38.6km^2. The broad floodplain covering the majority of the catchment is surrounded by a ridge of steep hills. Flooding is an ongoing issue within the catchment.

Photogrammetric survey of the catchment was captured for the Throsby and Cottage Creeks Flood Study for Newcastle City Council. The DEM was made available for this study. Refer to Figure 8-3 for the digital elevation model (DEM) of the catchment.
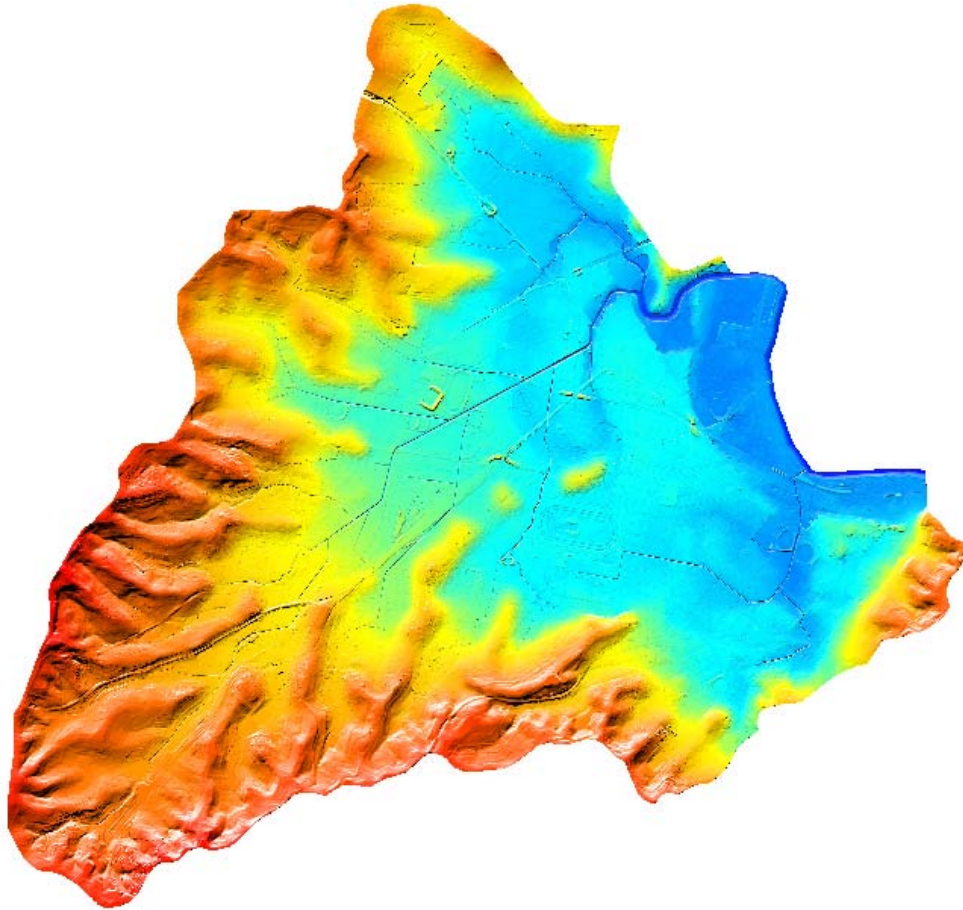
Figure 8-3   Throsby Creek Digital Elevation Model

8.4.2 DEM and Depression Storage Analysis

The depression storage routine was again repeated on the Throsby Creek DEM for grid element sizes of 2.5, 5, 10, 20, 40 and 80 metres. The results of the analysis are presented in Table 8-2.

Table 8-2 Depression Storage Results for Throsby Creek DEM

Grid Element Size (m)	Mean Depth of Storage Across Catchment (mm)
2.5	14
5	14
10	18
20	23
40	26
80	31

The same trend of increasing depth with decreasing grid resolution is apparent as per Case Study 1.

8.5 Case Study 3 – Rous River

8.5.1 Catchment Description and Model Development

The Rous River is one of the major tributaries of the Tweed River in Northern NSW. The Rous River catchment covers approximately 130km^2, measuring approximately 16km from east to west, and 12km from north to south. The catchment is generally steep, although the downstream reaches of the river flow across a wide floodplain. Ground elevation across the catchment ranges from 0m AHD to over 1,100m AHD. Land cover is a mix of natural forest and pasture. Refer to Figure 8-4 for the digital elevation model (DEM) of the catchment.
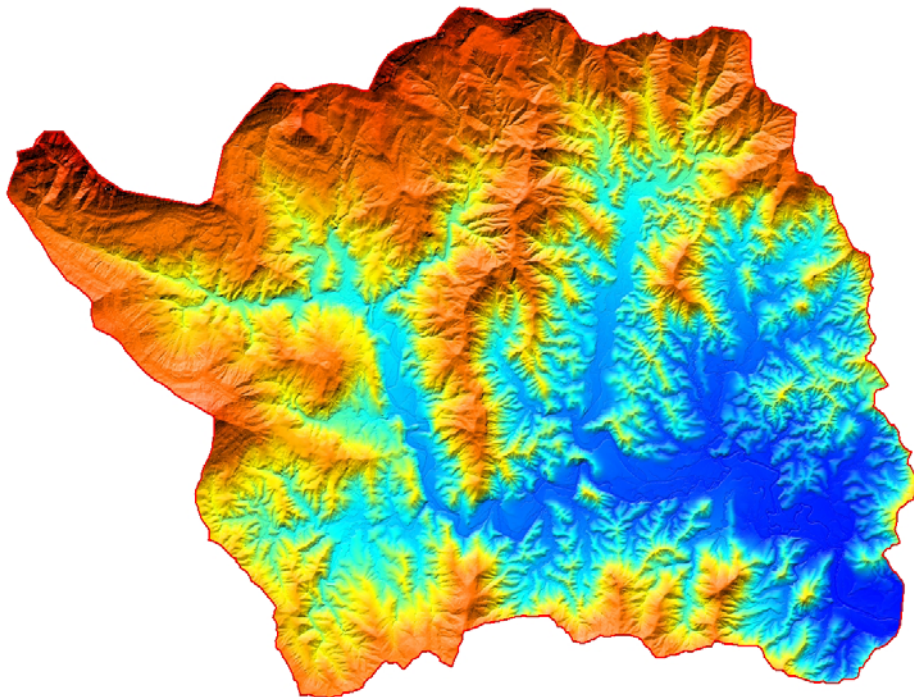
Figure 8-4   Rous River Digital Elevation Model

For Case Study 3, new WBNM and TUFLOW models have been developed using a broadscale approach. An 80m grid cell resolution was selected for the TUFLOW models to minimise computer simulation times. For simplicity, no bridges or major drainage structures have been included in the model. The following models have been developed:

➢ WBNM hydrological model comprising 35 sub-catchments;

➢ TUFLOW Surface Area (SA) model with boundary conditions read from WBNM output; and

➢ TUFLOW Direct Rainfall (DR) model.

Historical streamflow and rainfall data was sourced for three historical flood events; March 1974, March 1978 and May 1980.

Refer to Appendix A for details on the data and model development.

Presented in Table 8-3 is the average rainfall depth across the catchment for each historical event, based on the rainfall isohyets and temporal distributions discussed in Appendix A. Also presented in Table 8-3, are:

> ➢ volumetric flow rates from the Boat Harbour gauge;

> ➢ equivalent average depth of runoff across the catchment based on the volumetric flow;

> ➢ difference between the average rainfall depth and equivalent average depth of runoff, presented as loss; and

> ➢ percentage of the average rainfall depth, estimated as loss.

Table 8-3   Estimated Losses from Historical Events

Event	Average Rainfall Depth (mm)	Flow (m^3)	Estimated		Percentage Loss (%)
			Runoff Depth (mm)	Loss (mm)	
March 1974	720	74,375,671	591	129	17.9
March 1978	497	51,615,428	410	87	17.6
May 1980	589	48,754,604	387	202	34.0

Three key assumptions for these calculations are:

> ➢ Boat Harbour streamflow records and rating curve is accurate;

> ➢ recorded rainfall data is accurate; and

> ➢ rainfall distribution is accurately represented.

Since the accuracy of the data and rainfall distribution has not been verified, no reliable conclusions can be made from these calculations in relation to catchment losses. Therefore, these calculations are purely presented for interest only.

8.5.2 DEM and Depression Storage Analysis

The depression storage routine was repeated on the Rous River DEM for grid element sizes of 5, 10, 20, 40 and 80 metres. The results of the analysis are presented in Table 8-4.

Table 8-4 Depression Storage Results for Rous River DEM

| Grid Element Size (m)	Mean Depth of Storage Across Catchment (mm)
5	10
10	7
20	11
40	27
80	106

The similar trend to the Newrybar Swamp and Throsby Creek DEMs is apparent, with increasing mean depth of storage across the catchment for the larger grid elements. The significant mean depth increase between the 40m and 80m DEMs can be attributed to the steepness of the catchment.

Further discussion of the pit-filling options is provided below.

8.5.3 Loss Method Testing

The following loss methods have been tested as presented in the subsequent sections:

- ➢ **Scenario 1**: No losses – Prior to pit-filling of the DEM;

- ➢ **Scenario 2**: No losses – Pit-filling of the DEM using Streambuilder;

- ➢ **Scenario 3**: No losses – Advanced pit-filling using routine developed for this study;

- ➢ **Scenario 4**: Rainfall excess continuing losses (CL);

- ➢ **Scenario 5**: Continuing surface losses (CSL);

- ➢ **Scenario 6**: Green-Ampt with unlimited infiltration – Loamy soil;

- ➢ **Scenario 7**: Green-Ampt with unlimited infiltration – Silty clay soil;

- ➢ **Scenario 8**: Green-Ampt with no ponding influence – Loamy soil; and

- ➢ **Scenario 9**: Green-Ampt with limited infiltration – Loamy soil.

Note that Scenarios 4 through to 9 all incorporate the advanced pit-filling routine presented in Scenario 3.

8.5.3.1 Scenario 1 – No Losses Pre-Pit Filling

The first scenario uses a 2D grid with cell sides and centres interrogated directly from the source DEM. Thus, no attempt has been made to remove artificial depressions generated as part of the DEM sampling process. Additionally, no initial or continuing losses have been applied.

For each of the three historical events, both the SA and DR methods have been simulated.

Presented in Figure 8-5 is the depth of water remaining on the 2D grid following completion of the 1974 event surface area simulation.
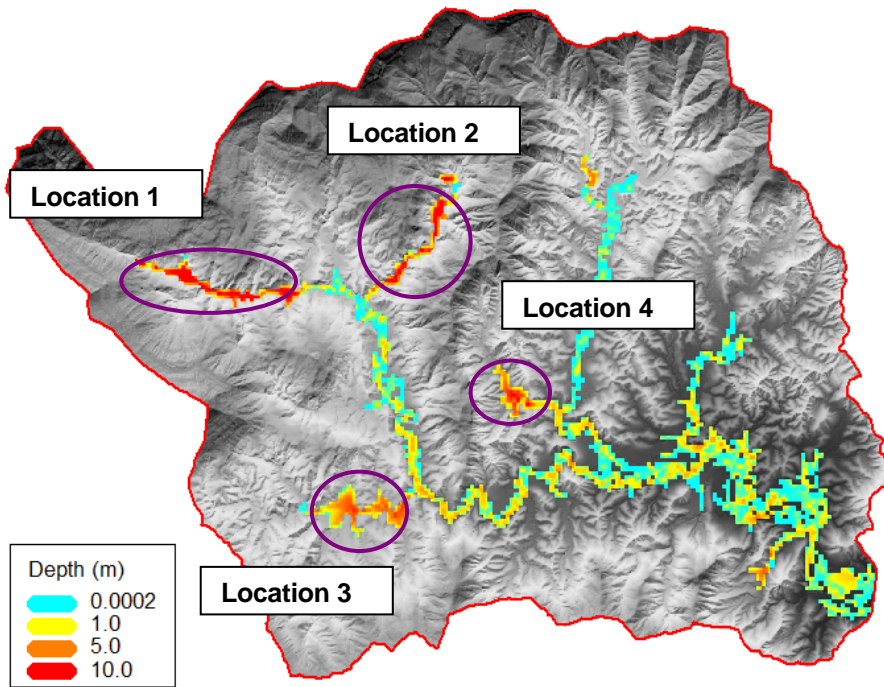
Figure 8-5   Water Remaining on Catchment after 1974 Surface Area Simulation

From Figure 8-5 we can see four areas where the depth of ponded water remaining on the grid exceeds 10m. On closer inspection of the north-western area (labelled 'Location 1' on Figure 8-5), we can see the cause of the ponding being due to the grid sampling process. Refer to Figure 8-6. At the constriction, the two grid cells with elevations of 118.9m and 114.1m are higher than the upstream grid cells, which are as low as 97.9m. Thus, a depth of water up to 16.2m depth is trapped behind this constriction, unable to be routed through the downstream catchment.
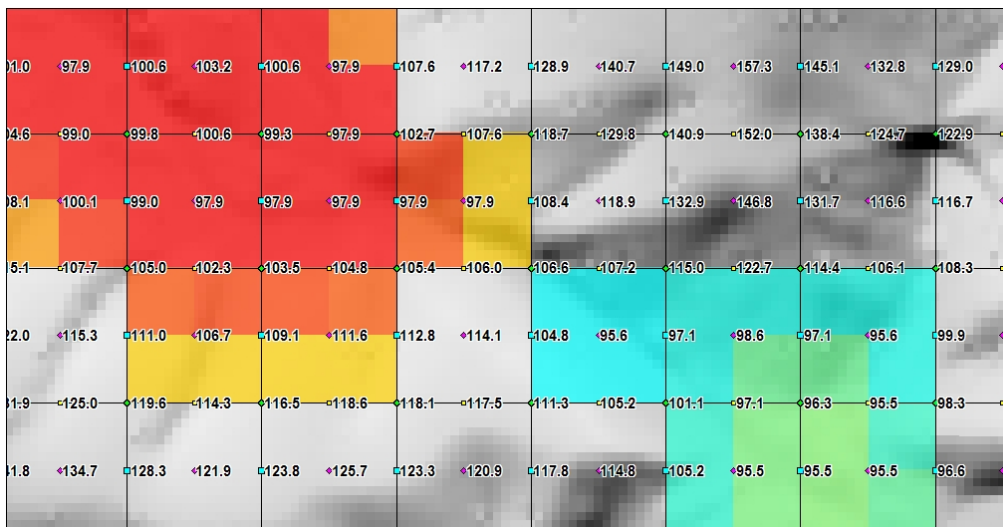
Figure 8-6   Artificial Depression Storage Creation

Presented in Figure 8-7 is the depth of water remaining on the 2D grid following completion of the 1974 direct rainfall simulation. The 'speckled' appearance is a result of the numerous depressions as discussed above. Clearly, mapping of this nature has limited value.
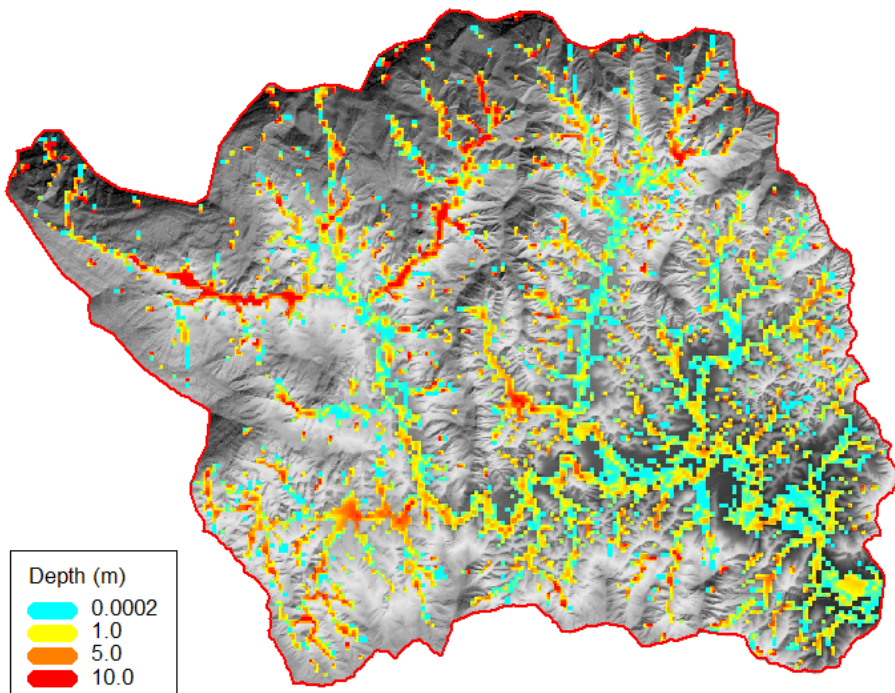
Figure 8-7 Water Remaining on Catchment after 1974 Direct Rainfall Simulation

Presented in Figure 8-8, Figure 8-9 and Figure 8-10 are the outflow hydrographs for the different models at the Boat Harbour stream flow gauge. The recorded data is also included for comparison.
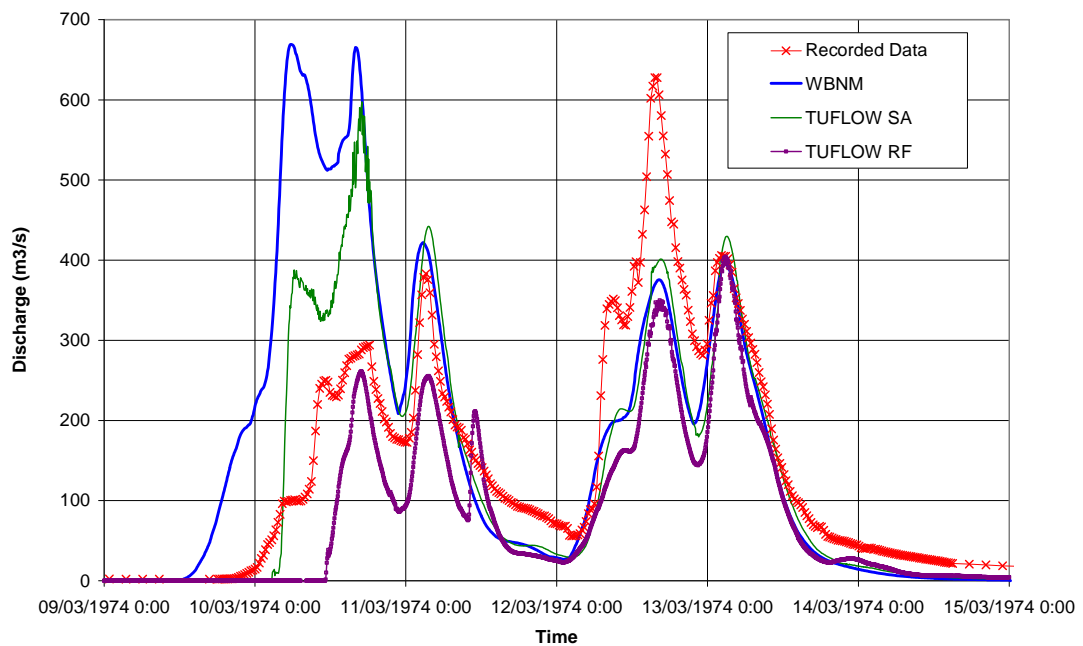
Figure 8-8 1974 Event Results for Scenario 1
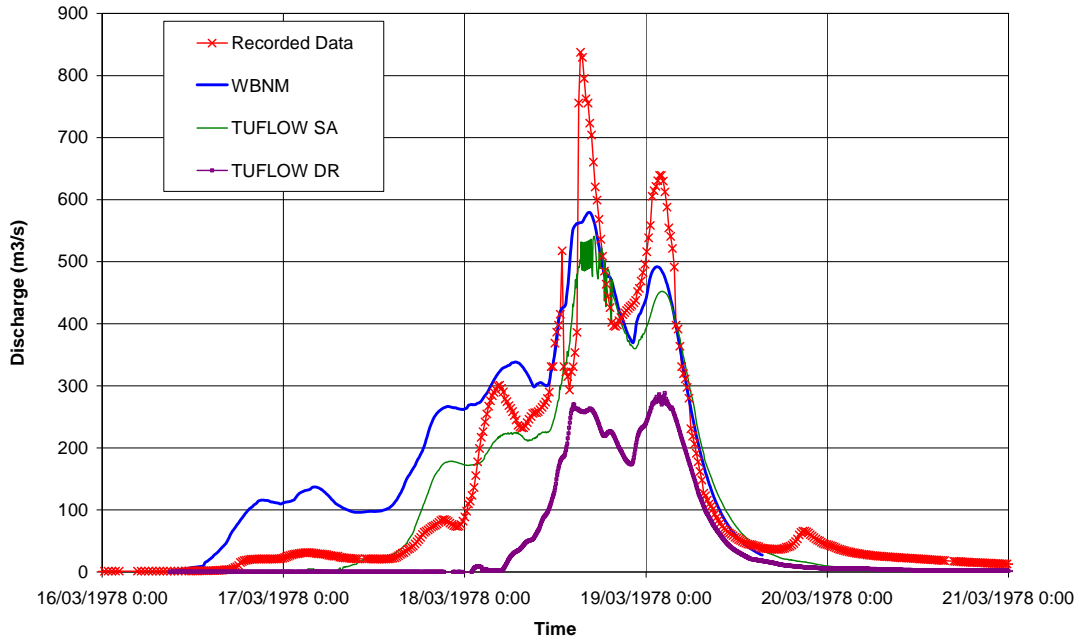
Figure 8-9   1978 Event Results for Scenario 2
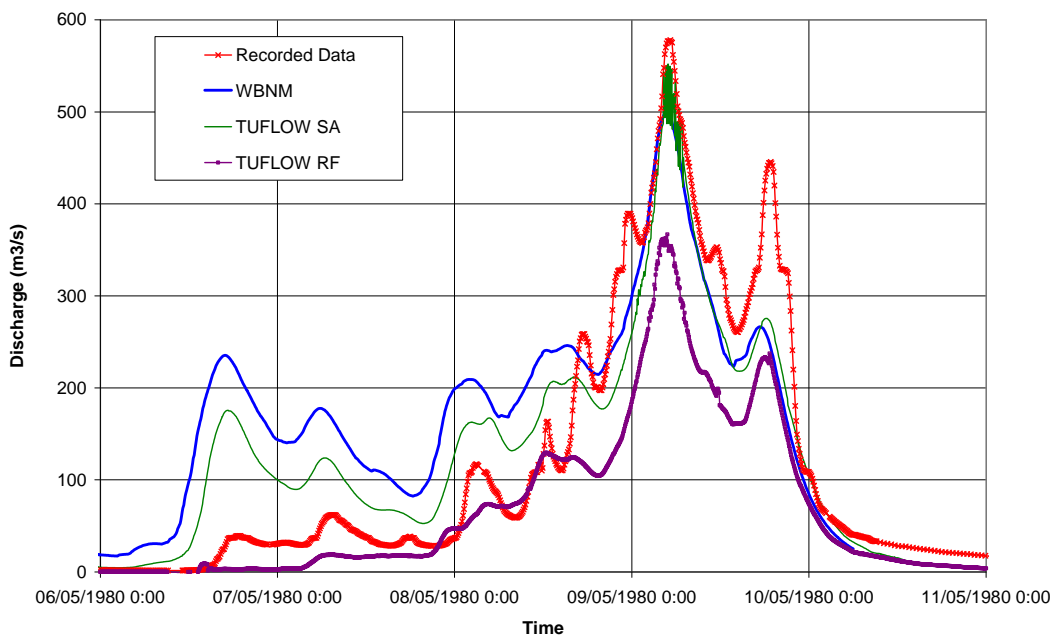
Figure 8-10   1980 Event Results for Scenario 2

The first observation to provide comment on is the comparison of the recorded flow to the modelled flow. Calibration of the model is not an objective of this model, and as such, no attempt has been made to match the recorded data. The limited rainfall data, broadscale modelling approaches, and lack of losses applied account for much of the difference.

A second key observation is the similar timing of the flood peaks between the different modelling methods. However, the direct rainfall model results exhibit a delay before runoff commences. This is

due to the DEM having numerous depressions, which are filled prior to runoff commencing. This will be further examined during Scenarios 2 and 3.

A final observation is the similarity between the surface area method and the WBNM results. The initial deviation is also due to the depressions in the DEM, although reduced due to the reduced flow area.

Figure 8-8 is reproduced as Figure 8-11 omitting the WBNM and recorded data. This plot shows that once the storage requirements of the depressions have been filled, the two methods return similar results. This similarity is not repeated for the 1978 and 1980 results since the total volume of water is less than the 1974 results.
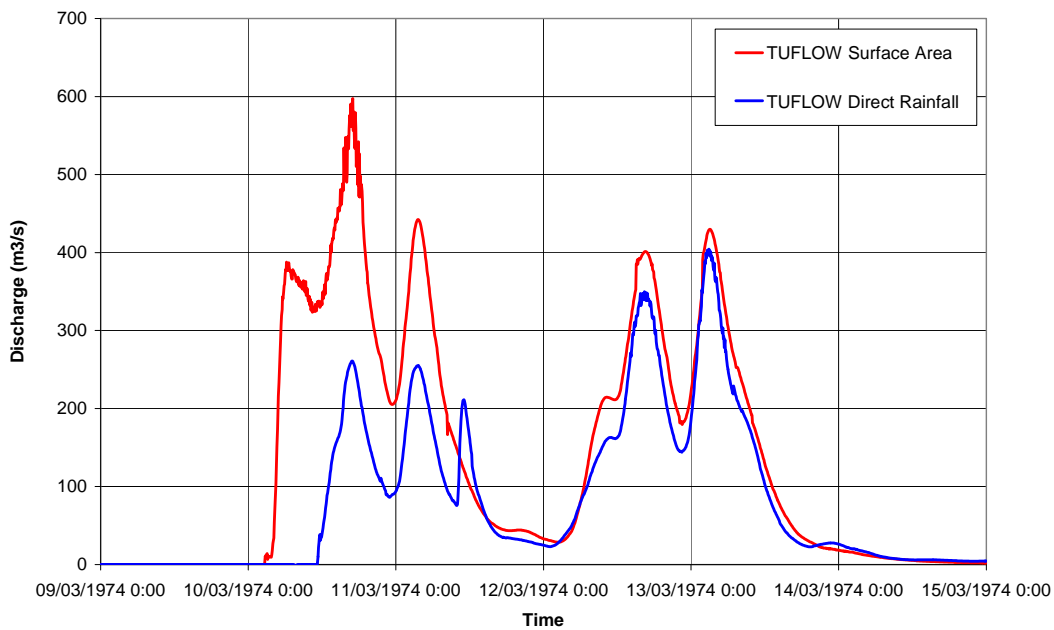
Figure 8-11   1974 Event Comparison between SA and DR Methods

The mass balance for the six Scenario 1 simulations is presented in Table 8-5.

Table 8-5   Mass Balance from Scenario 1

Event	Rainfall Method	Inflow (m³)	Volume Remaining (m³)	Percentage Remaining (%)
1974	Surface Area	91,362,670	**17,682,868**	19.3
	Direct Rainfall	90,821,779	**46,502,628**	51.2
1978	Surface Area	64,600,553	**17,739,333**	27.5
	Direct Rainfall	64,329,255	**44,425,980**	69.0
1980	Surface Area	76,206,012	**17,922,866**	23.5
	Direct Rainfall	75,754,060	**44,603,085**	58.9

From the mass balance it is clear to see from the volume of water remaining in the model following completion of the simulation is similar for each event. Thus, the three surface area simulations have approximately 18,000ML of water remaining (red text in Table 8-5). Similarly, the three direct rainfall simulations have approximately 45,000ML of water remaining (blue text in Table 8-5). This indicates water trapped within the depressions of the 2D grid

8.5.3.2 Scenario 2 – No Losses Post-Pit Filling

Using the Steambuilder routine for Mapinfo, the DEM was processed using the pit-filling algorithm. The pit-filling algorithm processes the DEM so that one of the eight neighbours of a grid cell has a lower elevation than the cell itself. This results in a DEM with continual flowpaths, and no depressions. Although this approach is considered to reduce the incidence of depressions in the 2D grid, a major limitation is recognised. The algorithm operates in both horizontal and vertical directions, as well as diagonally. However, the 2D hydraulic modelling only uses the horizontal and vertical directions. Therefore, the 'pit-filled' DEM will still result to some depressions when used for hydraulic modelling. The example depression highlighted in Figure 8-6 will remain unchanged in this simulation.

Again, both the SA and DR methods have been simulated for the three events.

Presented in Figure 8-12 is the depth of water remaining on the 2D grid following completion of the 1974 event surface area simulation.
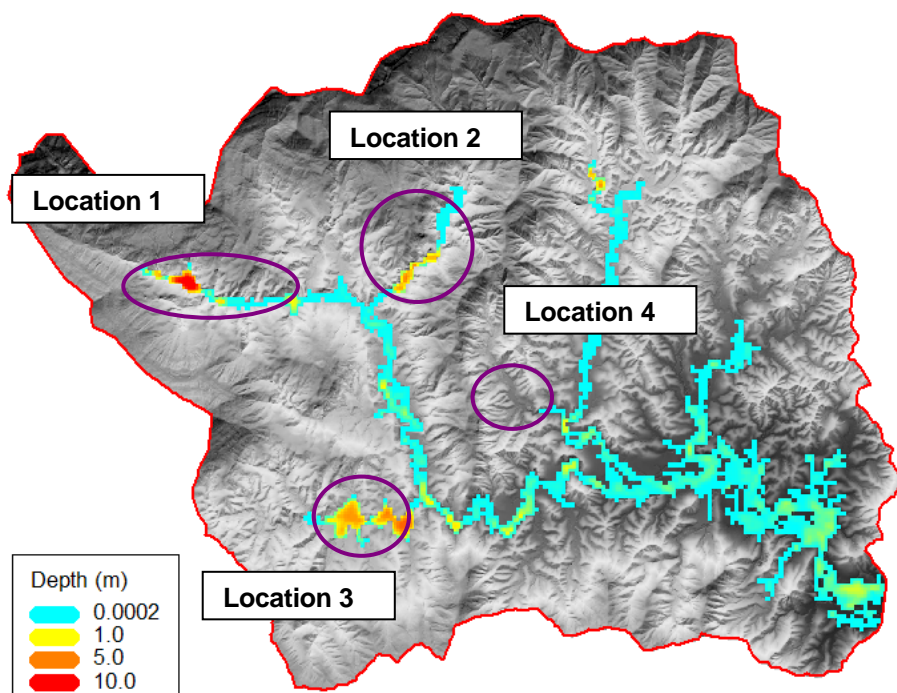
Figure 8-12 Water Remaining on Catchment after 1974 Surface Area Simulation

The mapping is similar to that of Scenario 1, although the main flowpath is more continuous. The ponded areas at Locations 1 and 2 are still apparent. However, the ponded area at Location 3 has been corrected.

Presented in Figure 8-13 is the depth of water remaining on the 2D grid following completion of the 1974 event direct rainfall simulation. A reduction in the 'speckled' appearance of the mapping highlights the improvement in the modelling.
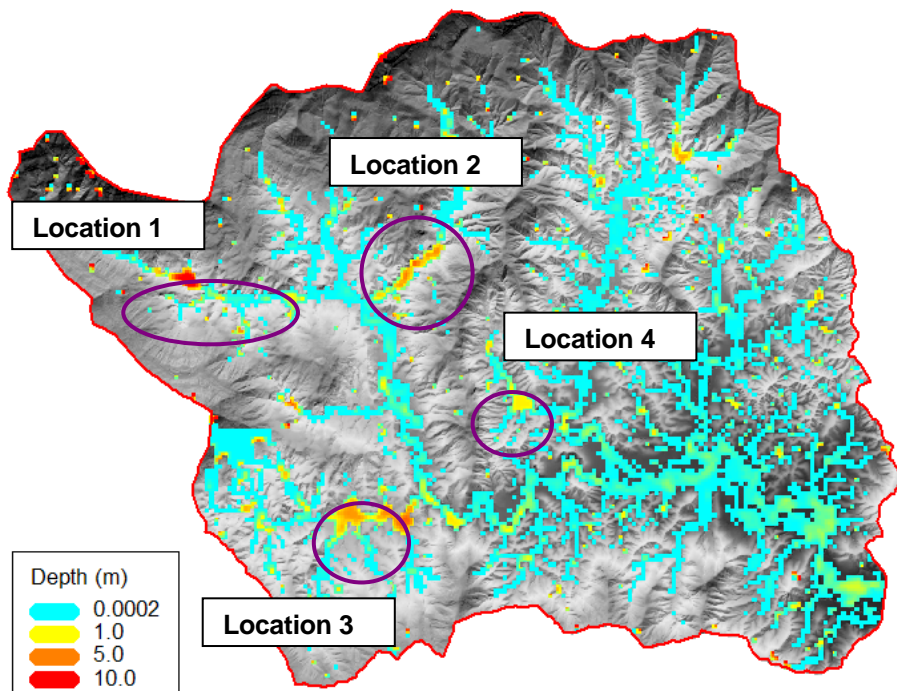
Figure 8-13   Water Remaining on Catchment after 1974 Direct Rainfall Simulation

The mass balance for the six Scenario 2 simulations is presented in Table 8-6.

Table 8-6   Mass Balance from Scenario 2

Event	Rainfall Method	Inflow (m^3)	Volume Remaining (m^3)	Percentage Remaining (%)
1974	Surface Area	91,362,670	**7,272,086**	8.0
	Direct Rainfall	90,821,779	**29,130,269**	32.1
1978	Surface Area	64,600,553	**7,267,525**	11.2
	Direct Rainfall	64,329,255	**27,895,848**	43.4
1980	Surface Area	76,206,012	**7,738,542**	10.1
	Direct Rainfall	75,554,060	**28,677,209**	37.9

As per Scenario 1, the volume of water remaining on the 2D grid is similar for the three SA simulations, and again similar for the three DR simulations, independent of the inflow volume (red and blue text from Table 8-6). This indicates water trapped within the depressions of the 2D grid;

The percentage of inflow volume remaining on the grid ranges from 8.0% to 11.2% for the SA approach, and between 32.1% and 43.4% for the DR approach. The larger 'wet' area associated with the DR approach accounts for the higher percentages.

Close inspection of the mapping shows the broader extents of water remaining on the 2D grid. This is a product of the pit-filling process, and subsequent flattening of upstream grid cells, resulting in longer time of inundation at shallow depths.

8.5.3.3 Scenario 3 – No Losses – Advanced-Pit Filling

In recognising the limitations of standard pit-filling routines, an advanced pit filling algorithm has been developed for this study. The algorithm processes the 2D grid used as input into the hydraulic model, to eliminate the incidence of depressions. Only the four adjacent grid cells in the horizontal and vertical directions are adjusted, to enable water to freely flow from any cell to the model outlet.

Use of this approach has the potential to significantly alter the detail of the DEM, thus, it should be used with caution. For broadscale direct rainfall modelling, its use is shown to improve the modelling results.

Once again for this scenario, both the SA and DR methods have been simulated for the three events.

Presented in Figure 8-14 is the depth of water remaining on the 2D grid following completion of the 1974 event surface area simulation.
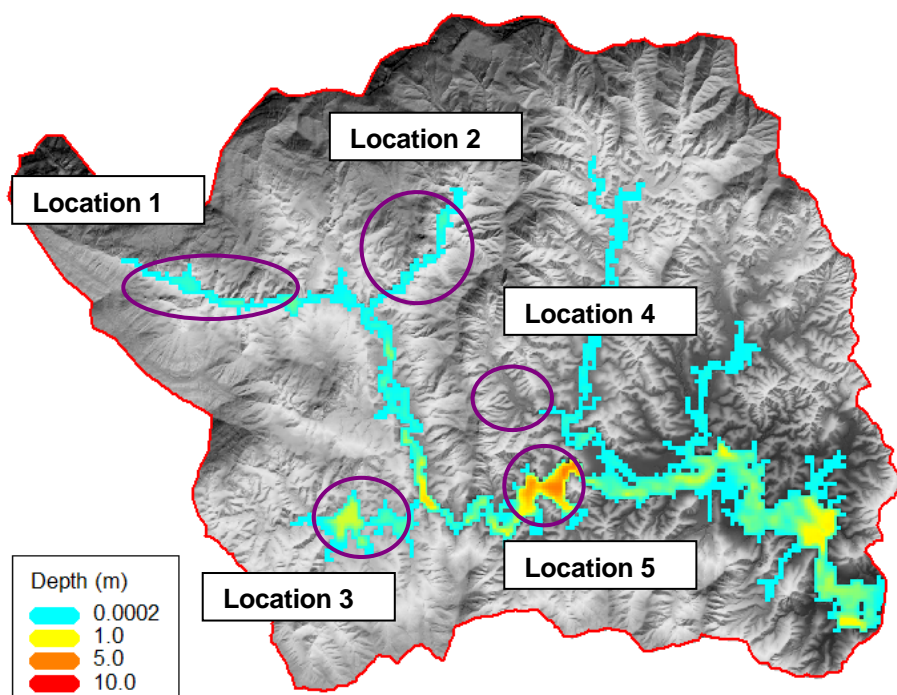
Figure 8-14 Water Remaining on Catchment after 1974 Surface Area Simulation

We can see that the previously ponded areas at Locations 1, 2 and 4 have now been resolved, although there is still ponding at Location 3. There is also additional ponding at Location 5. This

ponding is largely due to the constriction in the flowpath, rather than being due to a 'trapped' depression. Should the simulation be run for long enough, this area will eventually drain.

Presented in Figure 8-15 is the depth of water remaining on the 2D grid following completion of the 1974 event direct rainfall simulation. The mapping is more continuous than previously shown.
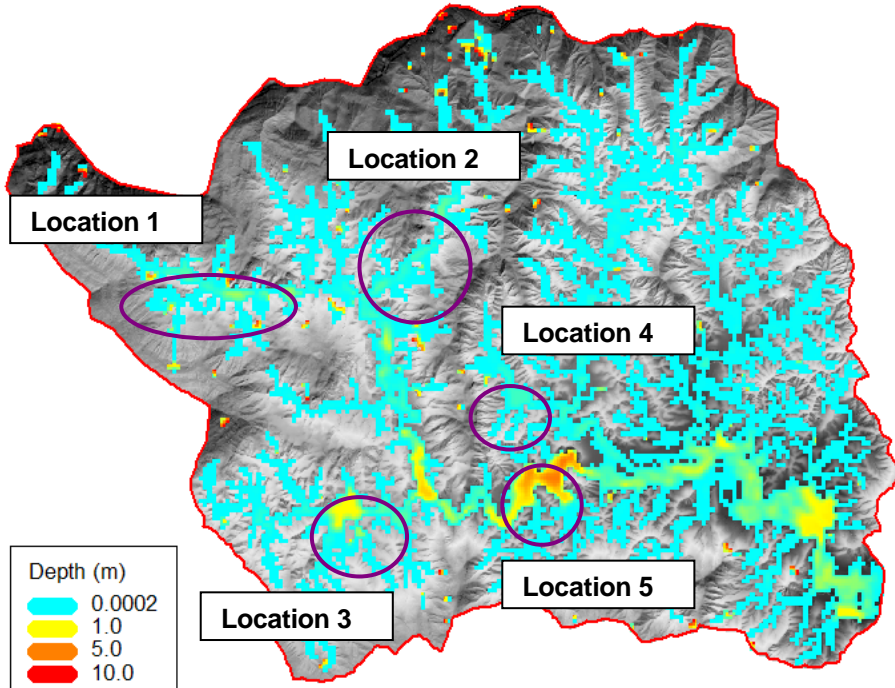
Figure 8-15 Water Remaining on Catchment after 1974 Direct Rainfall Simulation

The mass balance for the six Scenario 3 simulations is presented in Table 8-7.

Table 8-7   Mass Balance from Scenario 3

Event	Rainfall Method	Inflow (m³)	Volume Remaining (m³)	Percentage Remaining (%)
1974	Surface Area	91,362,670	4,269,307	4.7
	Direct Rainfall	90,821,779	4,771,299	5.2
1978	Surface Area	64,600,553	975,170	1.5
	Direct Rainfall	64,329,255	1,551,616	2.4
1980	Surface Area	76,206,012	6,379,556	8.4
	Direct Rainfall	75,754,060	7,865,861	10.4

In Scenarios 1 and 2, the volume of water remaining on the 2D grid following completion of the simulation was comparable for each of the three events modelled. Since the artificial depressions have been removed for Scenario 3, the same trend is no longer present. Rather, the volume of water remaining on the 2D grid is of similar magnitude for the SA and DR methods, varying on an event basis.

Presented in Table 8-8 is the volume of water remaining on the 2D grid for each scenario, presented as the average depth of water across the 2D model domain. As we would expect, the average depth decreases between Scenarios 1 and 2, and Scenarios 2 and 3, due to the pit-filling algorithms used.

Table 8-8   Comparison of Pit-Filling Methods

Event	Rainfall Method	Average Depth of Water Remaining on Grid (mm)		
		Scenario 1	Scenario 2	Scenario 3
1974	Surface Area	137	56	33
	Direct Rainfall	359	225	37
1978	Surface Area	137	56	8
	Direct Rainfall	343	215	12
1980	Surface Area	138	60	49
	Direct Rainfall	344	221	61

From these results, we can conclude that use of the advanced pit-filling algorithm will significantly improve the topographical representation in the model.

Similar to Scenario 2, review of the mapping shows a broader extent of water remaining on the 2D grid. Again, this is a product of the pit-filling process, and is more pronounced with a larger number of cells being raised during the pit-filling process.

The outflow hydrographs from Scenarios 1, 2 and 3 at the Boat Harbour gauge for the 1974 event surface area simulations are compared in Figure 8-16.
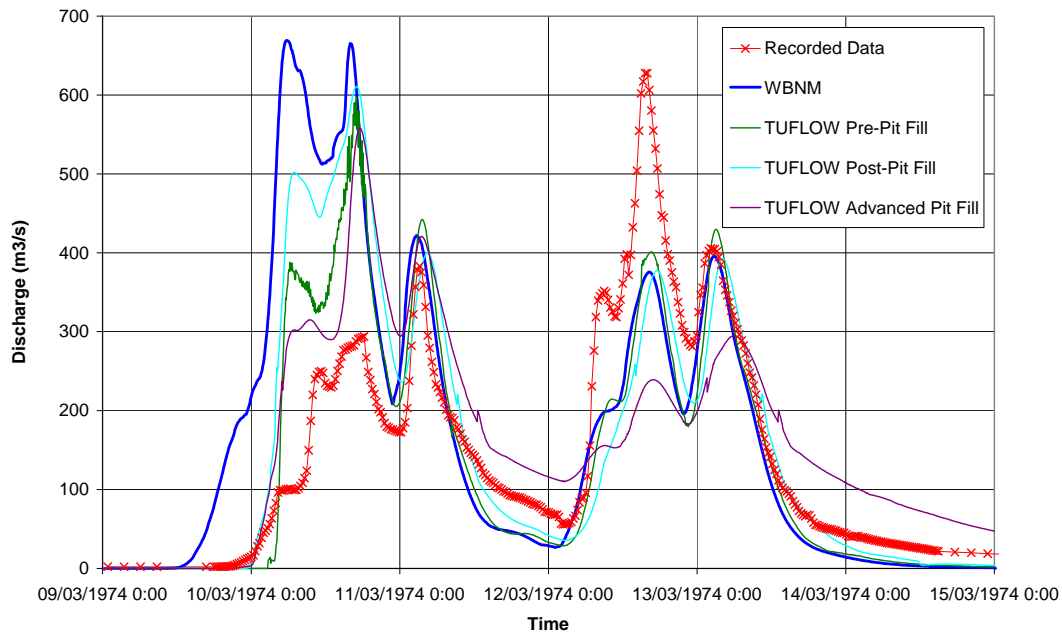
Figure 8-16   1974 Event Surface Area Simulation Comparison

The outflow hydrograph for the advanced pit-filling option indicates greater attenuation than the previous methods. This trend is also apparent in the direct rainfall results presented in Figure 8-17.
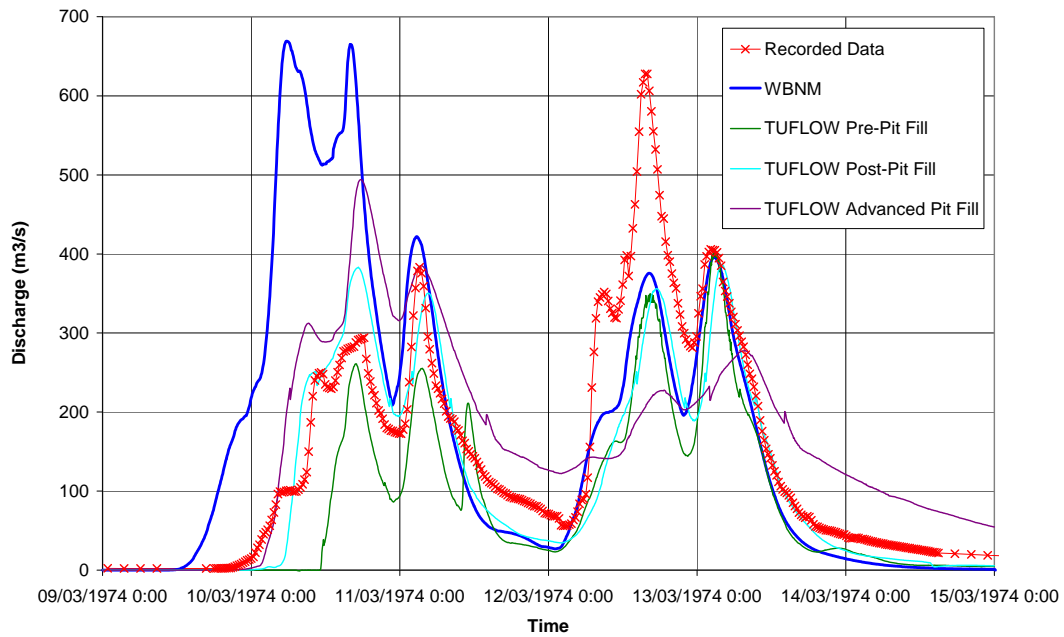
Figure 8-17 1974 Event Direct Rainfall Simulation Comparison

When using the DR approach, the advanced pit-filling shows significant improvement in the early stages. Of interest from these results is the comparison between the surface area and direct rainfall results, as shown in Figure 8-18. A similar trend is shown for the 1978 and 1980 results.
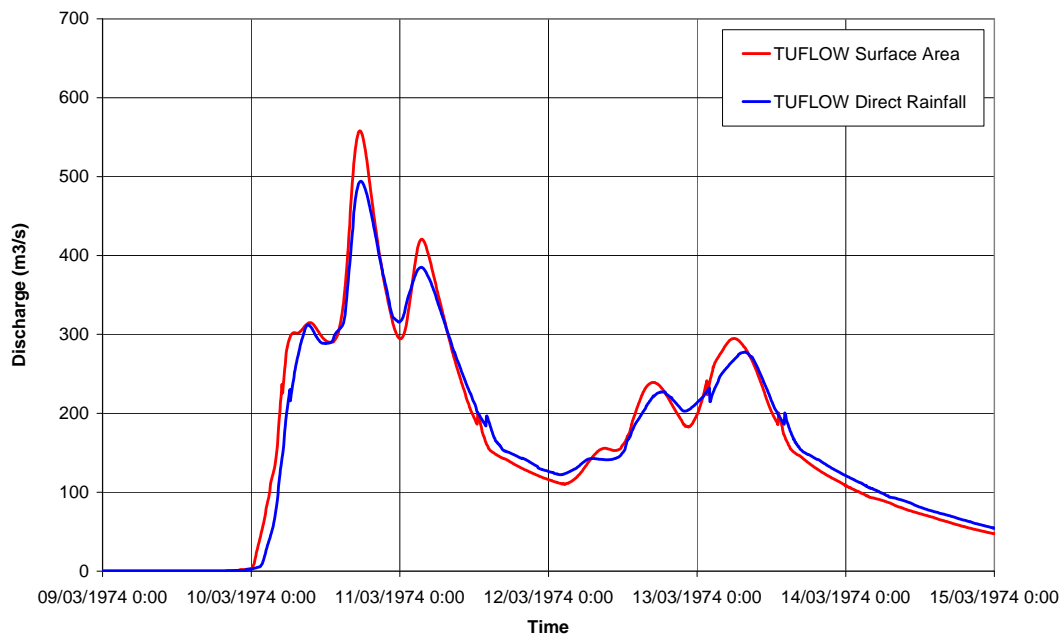
Figure 8-18 1974 Event Comparison between SA and DR Methods

8.5.3.4 Scenario 4 – Rainfall Excess Continuing Losses (CL)

Using the advanced pit-filled model from Scenario 4, a continuing loss of 2.5mm/hr was applied to the rainfall input. Both the SA and DR methods have been simulated for the three events. The mass balance for the six Scenario 4 simulations is presented in Table 8-9.

Table 8-9   Mass Balance from Scenario 4

Event	Rainfall Method	Inflow (m³)	Volume Infiltrated (m³)	Percentage Losses (%)	Average Depth of Losses (mm)
1974	Surface Area	91,362,670	20,058,640	22.0	155
	Direct Rainfall	90,821,779	20,807,483	22.9	160
1978	Surface Area	64,600,553	15,747,862	24.4	122
	Direct Rainfall	64,329,255	16,159,203	25.1	125
1980	Surface Area	78,206,204	23,354,382	29.9	180
	Direct Rainfall	75,754,060	23,513,550	31.0	182

The minor differences between the average depth of losses for the SA and DR approaches is due to differences in model input. Since the losses are applied to the rainfall, the same losses can be expected from each method.

The key observation from this Scenario is the percentage of rainfall that is removed as a continuing loss being between 22% and 31% across the different events. Addition of an initial loss would increase this fraction further.

The results of the surface area simulations for Scenarios 3 and 4 (no losses against losses) are compared in Figure 8-19.
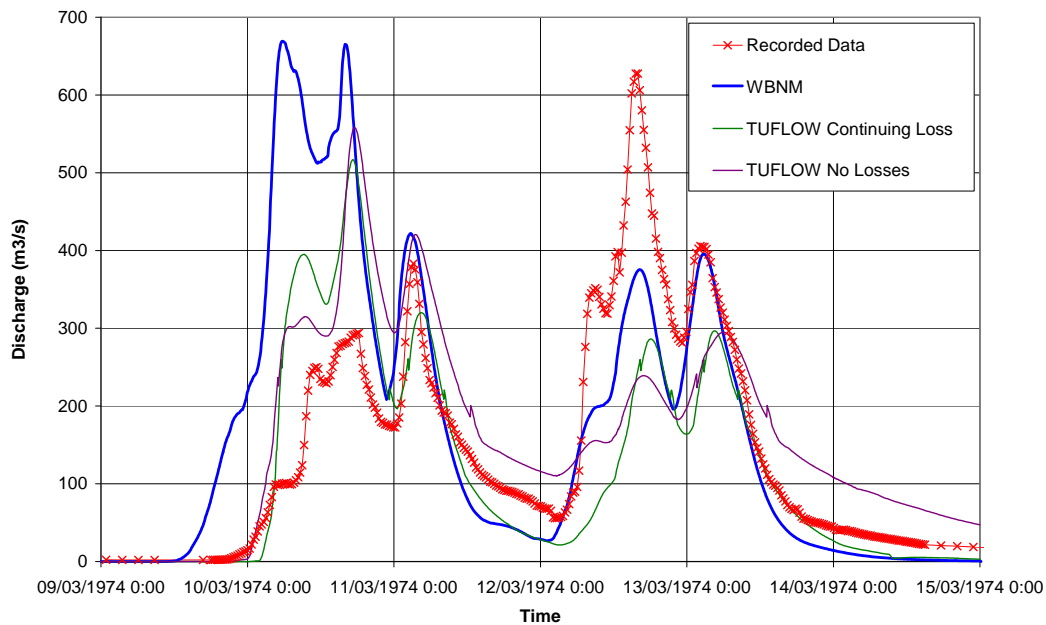
Figure 8-19 1974 Event Surface Area Simulation Comparison

The results of the direct rainfall simulations for Scenarios 3 and 4 (no losses against losses) are also compared in Figure 8-20.
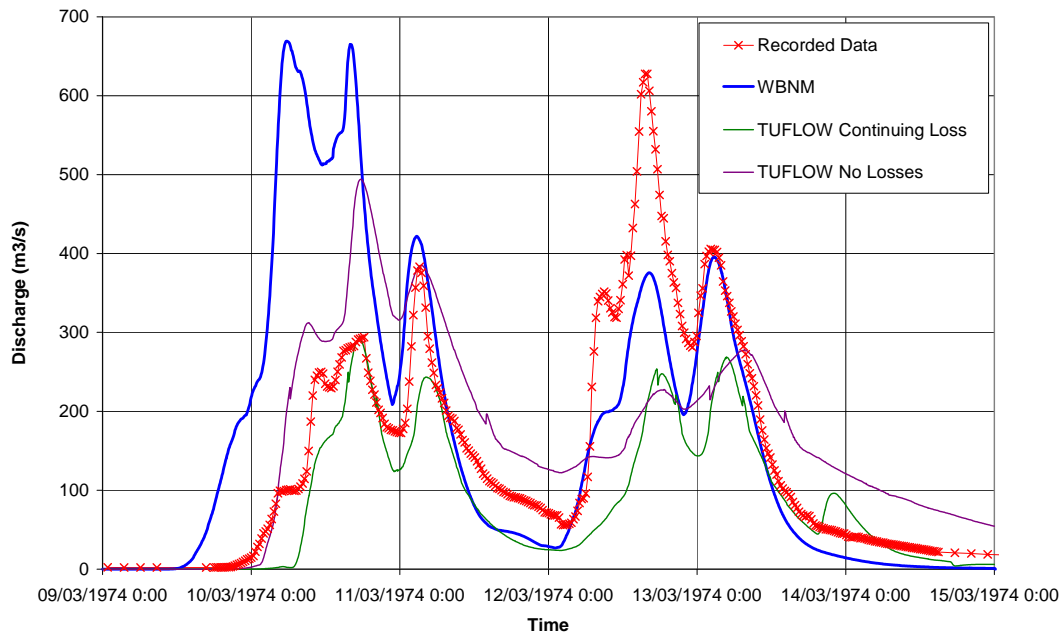
Figure 8-20   1974 Event Direct Rainfall Simulation Comparison

8.5.3.5 Scenario 5 – Continuing Surface Losses (CSL)

Using the advanced pit-filled model from Scenario 4, a continuing loss of 2.5mm/hr was applied, this time to the ground surface. Both the SA and DR methods have been simulated for the three events. The mass balance for the six Scenario 5 simulations is presented in Table 8-10.

Table 8-10   Mass Balance from Scenario 5

Event	Rainfall Method	Inflow (m^3)	Volume Infiltrated (m^3)	Percentage Losses (%)	Average Depth of Losses (mm)
1974	Surface Area	91,362,670	21,621,194	23.7	167
	Direct Rainfall	90,821,779	29,938,573	33.0	231
1978	Surface Area	64,600,553	17,594,387	27.2	136
	Direct Rainfall	64,329,255	21,780,038	33.9	168
1980	Surface Area	76,206,204	24,572,183	32.2	190
	Direct Rainfall	75,754,060	33,133,958	43.7	256

As expected, the volume of losses is higher than the previous scenario. A comparison between the CL and CSL method average infiltration depths is presented in Table 8-11.

Table 8-11   Comparison of Losses for CL and CSL Methods

Event	Rainfall Method	Average Loss CL Method (mm)	Average Loss CSL Method (mm)	Increase (%)
1974	Surface Area	155	167	7.7
	Direct Rainfall	160	231	44.4
1978	Surface Area	122	136	11.5
	Direct Rainfall	125	168	34.4
1980	Surface Area	180	190	5.6
	Direct Rainfall	182	256	40.6

Losses are shown to increase by up to 11.5% for the surface area simulations and up to 44.4% for the direct rainfall simulations.

8.5.3.6 *Scenario 6 - Unlimited Green-Ampt Infiltration – Loam Soil*

Green-Ampt parameters representing a loam soil were adopted for Scenario 6, as recommended by Rawls et al (1993). This soil type is applied for the entire catchment, thus, no attempt has been made to represent soil types based on available soil mapping. Only the DR approach is modelled for this scenario since the Green-Ampt infiltration cannot be applied separately to the hydrological model.

The mass balance for the three Scenario 6 simulations is presented in Table 8-12.

Table 8-12 Mass Balance from Scenario 6

Event	Rainfall Method	Inflow (m^3)	Volume Infiltrated (m^3)	Percentage Losses (%)	Average Depth of Losses (mm)
1974	Direct Rainfall	90,821,779	43,554,766	48.0	336
1978	Direct Rainfall	64,329,261	34,475,717	53.6	226
1980	Direct Rainfall	75,754,060	46,351,247	61.2	358

The results show between 48% and 61% of water has been infiltrated. This equates to depths between 226mm and 358mm across the three events. Considering a soil porosity of 0.4, the depth to wetting front would be less than 1.0m for all events. This depth of infiltration is considered high, although plausible.

8.5.3.7 *Scenario 7 – Unlimited Green-Ampt Infiltration – Silty Clay Soil*

Green-Ampt parameters representing a silty-clay were adopted for Scenario 7, as recommended by Rawls et al (1993). The mass balance for the three Scenario 6 simulations is presented in Table 8-13.

Table 8-13   Mass Balance from Scenario 7

Event	Rainfall Method	Inflow (m³)	Volume Infiltrated (m³)	Percentage Losses (%)	Average Depth of Losses (mm)
1974	Direct Rainfall	90,821,779	8,400,840	9.2	65
1978	Direct Rainfall	64,329,261	7,134,028	11.1	55
1980	Direct Rainfall	75,754,060	9,336,398	12.3	72

Comparing these Scenario 7 (Silty Clay) results to the Scenario 6 (Loam) results, it is clear to see that the soil type has a significant influence on the infiltration. Refer to Figure 8-21 for a comparison between the 1974 event hydrographs at the Boat Harbour gauge. Peak flood levels along parts of the floodplain are up to 1m lower when using the silty clay parameters. The influence is generally more pronounced where floodwaters are deep, typically upstream of natural constrictions.
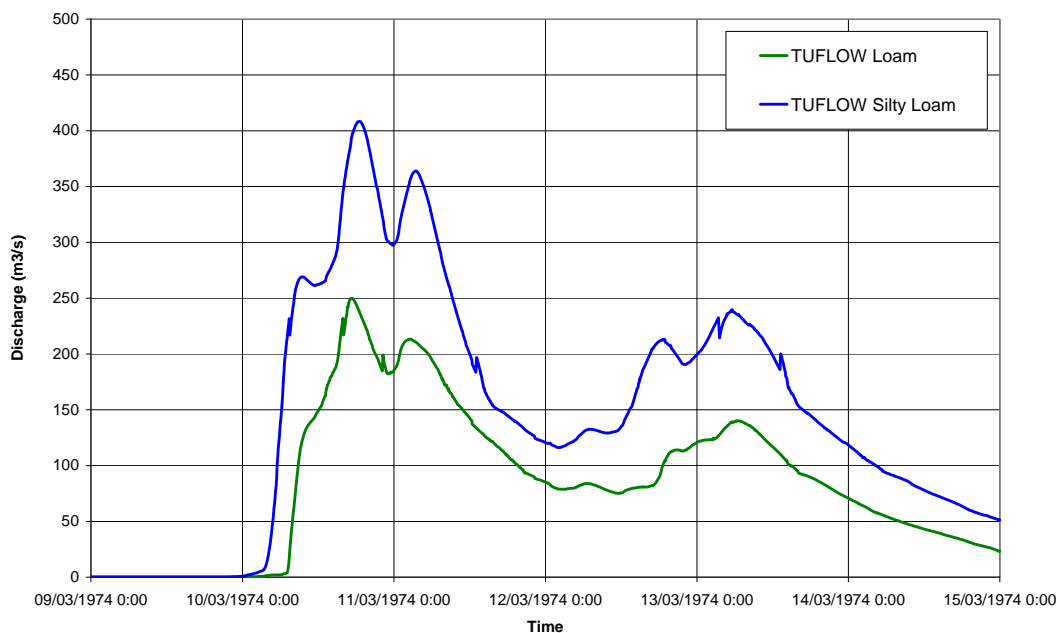
Figure 8-21   1974 Event Comparison between Loam and Silty Clay

8.5.3.8 Scenario 8 – Green-Ampt Infiltration – No Ponding Influence

Using the loam soil type from Scenario 6 as a base, Scenario 8 is used to investigate how much of an influence ponding has on the Green-Ampt infiltration. A switch has been built into the infiltration module to enable to ponding term to be inactivated.

The mass balance for the three Scenario 8 simulations is presented in Table 8-14.

Table 8-14   Mass Balance from Scenario 8

Event	Rainfall Method	Inflow (m^3)	Volume Infiltrated (m^3)	Percentage Losses (%)	Average Depth of Losses (mm)
1974	Direct Rainfall	90,821,779	41,013,929	45.2	317
1978	Direct Rainfall	64,320,399	32,885,138	51.1	254
1980	Direct Rainfall	75,754,060	45,030,163	59.4	348

From these results, it is apparent that the ponding depth does not have a significant influence on the overall mass balance of the model. This can be explained by considering two different areas:

➢ Floodplain areas where depth is high are likely to experience significantly increased infiltration when accounting for ponding depth on the infiltration process; and

➢ The remaining catchment areas where sheet flow is dominant are likely to experience far less of an influence of ponding depth.

Since the floodplain area only accounts for a small fraction of the overall catchment area for this case study, the mass balance does not show a significant influence. However, should a catchment with a larger proportion of floodplain be modelled (such as Newrybar Swamp from Case Study 1), the ponding influence will have a far greater influence on the overall mass balance.

8.5.3.9 Scenario 9 – Limited Green-Ampt Infiltration

Again, the loam soil type from Scenario 6 has been used as a base for this scenario in which, the volume of water that can be infiltrated is limited by two criteria:

➢ Groundwater level of 0m AHD. Thus, once the soil profile between 0m and the ground surface has been saturated, no further infiltration is possible. This will limit the infiltration in the lower floodplain; and

➢ Maximum depth to groundwater equal to 2m. Thus, infiltration depth is limited to the soil porosity multiplied by 2m. This will also only affect areas of high infiltration (>0.8m with 0.4 porosity), such as the floodplains.

The mass balance for the three Scenario 9 simulations is presented in Table 8-15.

Table 8-15   Mass Balance from Scenario 9

Event	Rainfall Method	Inflow (m^3)	Volume Infiltrated (m^3)	Percentage Losses (%)	Average Depth of Losses (mm)
1974	Direct Rainfall	90,821,779	39,908,168	43.9	308
1978	Direct Rainfall	64,292,118	32,561,183	50.6	251
1980	Direct Rainfall	75,754,060	42,698,075	56.4	330

The results show minimal difference from the unlimited Scenario 6 results. Again, this is due to the minimal floodplain area where the depth of infiltration is large. It is expected that the results would be noticeably different should a shallower depth to groundwater be applied.

8.6 Case Study Conclusions

8.6.1 Depression Storage

A comparison between the depression storage analysis results from the three case studies is presented in Table 8-16. From the results, there is a clear trend for increasing mean storage depth with use of a coarser DEM. Although only three DEMs have been analysed for this study, it is apparent that depressions do exist within DEMs, regardless of the quality of the data. This may be due to error in the survey and digital representation of the surface, or physical manmade or natural depressions within the catchment. In reality, major depressions are usually either lakes or ponds, or are likely to be connected to sub-surface drainage.

Table 8-16   Depression Storage Results for Rous River DEM

Grid Element Size (m)	Mean Depth of Storage Across Catchment (mm)		
	Newrybar Swamp	**Throsby Creek**	**Rous River**
2.5	-	14	-
5	38	14	10
10	33	18	7
20	35	23	11
40	42	26	27
80	50	31	106

Referring to the hypothesis discussed in Section 1.3.2, the following points are noted:

➢ An insufficient number of catchments have been analysed to demonstrate that the influence of depression storage will be more pronounced in:

   o **urban environments** where the depressions represented in the DEM are likely to be directly connected to a sub-surface drainage system; and

   o **steep catchments** where the two-dimensional grid representation and sampling process generates artificial depressions within the model.

➢ Pre-processing the digital elevation data to remove the artificial depressions minimises the water lost to depression storage and improves the continuity of water flow.

8.6.2 Loss Method Testing

The testing has shown that different methods used for representing losses can have a substantial affect on the modelling results, i.e. volumetric output, flow rates, timing, and flood levels. The following points summarise the key observations in relation to the case study catchment. It is noted that the results are likely to differ when considering alternate catchments and events:

- ➢ Extraction of continuing losses at the ground surface, rather than from the input rainfall, are shown to increase the total volume of infiltrated water by:

    - o up to 11.5% when using the surface area method; and

    - o up to 44.4% when using the direct rainfall method.

- ➢ Use of the direct rainfall approach has resulting in four times the volume of losses compared with the surface area approach.

- ➢ The volume of infiltrated water associated with the surface area method will increase for catchments with larger proportion of floodplain area.

- ➢ Representation of different soil types when using the Green-Ampt infiltration is shown to have a significant influence on model results.

- ➢ The influence of ponding depth can increase the infiltration rate significantly. Floodplain areas where deep water is present will have higher infiltration than the steeper areas of the catchment where shallow sheetflow is common. Therefore, the influence of ponding on the infiltration process will be amplified on catchments with a larger proportion of floodplain area.

- ➢ The depth of infiltration can be limited, although knowledge of groundwater or bedrock depth is required.

9 CONCLUSIONS

9.1 Study Outcomes

9.1.1 TUFLOW Infiltration Module

For this assessment, an infiltration module has been developed for the TUFLOW hydrodynamic modelling software. The infiltration module has the following options:

> ➢ Application of initial and continuing losses to the ground surface, rather than the rainfall input;

> ➢ Application of the Green-Ampt infiltration model (with or without ponding influence);

> ➢ Spatial variability of soil types across the two-dimensional (2D) grid;

> ➢ Input of groundwater depth and / or elevation;

> ➢ Point time series output of infiltration rate and cumulative infiltration;

> ➢ Mapping output of infiltration rate and cumulative infiltration; and

> ➢ Animations of infiltration rate and cumulative infiltration.

9.1.2 Topographic Representation

Two-dimensional finite difference hydrodynamic modelling is typically based on a grid of square elements or cells. Each cell contains a lumped value representing catchment characteristics, such as elevation and surface roughness as a minimum. Thus, the overall modelling domain is defined in a distributed manner with model resolution determined by the grid cell size.

Within the 2D model, water can flow between a grid cell and the four surrounding cells, limited by factors such as cell elevation and water depth. Thus water cannot directly flow from a cell to any of the four diagonal cells. Elevation is commonly assigned to a cell using raster based digital elevation models (DEM), often with a higher resolution than the 2D grid. In situations where a flowpath crosses a series of cells in a diagonal direction, the flow of water between the cells is restricted by the higher elevation of the neighbouring cells. The overall result is a 2D grid with a series of artificial depressions (or pits), which water can flow into, but not out of.

To reduce the incidence of artificial depressions, a commercially available pit-filling algorithm was applied to the DEMs from three case study catchments. The algorithm ensures at least one of the surrounding eight cells has a lower elevation. The resolution of the DEM was varied, and the volume of the depressions calculated. The clear trend from the analysis was for an increase in volume with a coarser DEM. The depth of depression storage, averaged over the catchment area was between 10mm and 40mm for a 5m grid resolution, and between 50mm and 110mm for an 80m grid resolution.

Inspection of the DEM and comparison of the hydraulic modelling results using the pre and post pit-filled DEMs, showed a significant decrease in depression storage loss, when using the processed

DEM. However, use of the commercial pit-filling process still allowed some pits to remain when considering water is not able to flow in a diagonal direction. An advanced pit filling algorithm was developed and applied to the DEM, compatible with the 2D flow of water across the grid. The subsequent inspection of the DEM and hydraulic analysis showed complete removal of the depression storage loss.

9.1.3 Surface Area or Direct Rainfall Modelling

Two methods for application of the rainfall to the 2D grid have been assessed:

> ➢ **Surface Area–** the rainfall hyetograph, or routed hydrograph, for each sub-catchment is applied directly to the 2D grid; and

> ➢ **Direct Rainfall –** the rainfall hyetograph for each sub-catchment is applied uniformly across every grid cell.

The higher number of 'wet' cells associated with the direct rainfall approach resulted in a larger proportion of losses when using the pre pit-filled DEMs. Comparison between the results of the two modelling approaches showed significant difference using the pre pit–filled DEMs. Comparison between the results of the two modelling approaches, when using the processed DEM showed good agreement.

Direct rainfall modelling has the advantages of removing the need for a separate hydrological model whilst improving the representation of catchment storage. Whilst the advantages of the latter have not been demonstrated using the case study catchment, particular catchments are likely to be better suited to direct rainfall simulation. The considerable data requirements and increased simulation times of direct rainfall modelling should also be noted.

9.1.4 Rainfall Excess or Surface Loss

Extraction of losses has been assessed using two approaches:

> ➢ **Rainfall Excess** representing the traditional approach whereby losses are extracted from the rainfall hyetograph prior to application of the rainfall to the ground surface; and

> ➢ **Surface Loss** where losses are extracted from the ground surface opposed to the rainfall hyetograph. This option allows rainfall losses to continue across all wetted cells, regardless of rainfall.

The volume of losses using the rainfall excess approach is essentially the same when using either the surface area or direct rainfall methods. Application of the surface loss approach resulted in a volumetric loss increase of up to 11.5% for the surface area simulations and up to 44.4% for the direct rainfall simulations.

9.1.5 Initial Loss / Continuing Loss or Green-Ampt Infiltration

Representation of infiltration has been assessed using the following models:

> **Initial Loss / Continuing Loss** (rainfall excess and as surface loss options);

> **Green-Ampt with Ponding Influence** (surface loss only); and

> **Green-Ampt without Ponding Influence** (surface loss only).

Use of the physically based Green-Ampt infiltration model showed a significant difference in modelling output when considering different soil types.

The depth of surface ponding has been shown to have a significant influence on the infiltration rate. As expected, the analysis has shown that floodplain areas are more susceptible to the influence of ponding, where depths are greater. Therefore, catchments with a higher proportion of floodplain area are likely to experience higher infiltration volumes.

Given the poor knowledge of event rainfall distribution, lack of soil data and uncertainties associated with the input data, model calibration was not feasible. It is, therefore, not possible to draw any conclusive proof that a more advanced infiltration algorithm gives more reliable output than using the rainfall excess concept.

9.2 Implications

The concepts investigated during the study have highlighted the importance for the practitioner to be informed about the potential implications of adopting one process over another. The following recommendations are offered to the practitioner for enhanced confidence in modelling output:

> Representation of elevation using a 2D grid of square elements must be checked to ensure undesirable artificial depressions are not present. This is particularly important for direct rainfall modelling.

> Application of a pit-filling process to the DEM should be considered. The pit-filling algorithm should enable drainage in the horizontal and vertical directions, consistent with the hydraulic modelling approach. To ensure transfer of the pit-filled DEM to the 2D grid:

> o the raster DEM should be resized so that the resolution equals the 2D grid element size; and

> o the raster DEM pixels should align with the 2D grid cells.

> Use of the surface loss approach should be considered due to its sound physical basis.

Due to the minimal testing undertaken, use of the Green-Ampt infiltration model for direct rainfall modelling should only be used with caution. At the time of writing, there is insufficient data to suggest that use of the model will improve modelling output. Rather, the additional process parameters and variables introduced using the model provide a greater opportunity for the occurrence of compensatory errors.

9.3 Further Research

The preceding study has identified the need for further research into the field of losses associated with 2D flood modelling applications. Some of the key areas of interest are:

➢ Investigation of spatial variability of soil type. Of interest is how the flood behaviour is changed due to the representation of different soil types, and whether a lumped approach to soil distribution is appropriate. Of key interest is whether the additional input data and modelling detail has a benefit to modelling output.

➢ Application of distributed rainfall patterns, such as radar data. This has the potential to improve the model calibration, enabling a more detailed assessment of infiltration throughout the flooding period.

➢ The influence that different modelling approaches have upon design flood behaviour.

10 ACKNOWLEDGEMENTS

11 References

Abbot, J, C, Bathurst, J, A, Cunge, J, A, O'Connell & Rasmussen, J, 1986, 'An introduction to the European hydrological system – systeme hydrologique Europeen, "she", 2 structure of a physically-based, distributed modeling system', *Journal of Hydrology*, vol 87, pp 61-77.

Beven, K, 2004, 'Robert E. Horton's perceptual model of infiltration processes', *Hydrological Processes*, vol 18, 3447-3460.

Britton, M & Wijersiri, S, 2007, 'Integrated MIKE21 modeling of Catchments – An alternative to traditional hydrological modeling techniques'

Caddis, B,M, Jempson, M, A, Ball, J,E & Syme, W,J, 2008, 'Incorporating hydrology into 2D hydraulic models – the direct rainfall approach', Engineers Australia 9th Conference on Hydraulics in Water Engineering, Darwin Convention Centre, Australia, 23-26 September 2008.

Chen, L & Young, M, 2005, 'Green-AMPT infiltration model for sloping surfaces ', *Water Resources Research*, vol 42, pp 1-9.

Chow, V, T, Maidment, D, R & Mays, L, W 1988, *Applied hydrology*, McGraw Hill, United States of America.

Chu, S, T, 1987, 'Generalised Mein-Larson infiltration model, *Journal of Irrigation and Drainage Engineering*, vol 113, no 2.

Clark, K, 2008, 'Suitability of 2D Hydraulic model for rainfall runoff routing', Kristen Clark, *Bachelor of Engineering Thesis 2008.*

Clark, K.M, Ball, J, E &, Babister, M, K, 2008, 'Can fixed grid 2D hydraulic models be used as hydrologic models?' Water Down Under Conference, Adelaide 2008.

Chi, S, T, 1978 'Infiltration during an unsteady rain', *Water Resources Research*, vol 14, no 3, 461-466.

Delft Hydraulics, 2004, 'Technical reference rainfall-runoff', *Sobek Technical Reference Manual*,

Gowdish, I & Munoz-Carpena, R, 2009, 'An improved Green-Ampt infiltration and redistribution method for uneven multistorm series', *Vadose Zone Journal*, vol 8, no 2, May 2009.

Green, H & Ampt, G, A, 1911, 'Studies on soil physics part 1: The flow of air and water through soils', *Journal of Agricultural Science*, vol 4, pp 1 – 24.

Haverkamp, R, Parlange, J. Y, Starr, J.I, Schmitz, G & Fuentes, 1990, 'Infiltration under ponded conditions: 3. Predictive equation based on physical parameters', *Soil Science*, vol. 149, no 5, pp 292-300.

Hill, P, Mein, R & Siriwardena, L, 1998, 'How much rainfall becomes run-off? Loss modeling for flood estimation', *Cooperative Research Centre for Catchment Hydrology*, Industry Report, pp 1-23.

Institution of Engineers Australia, 2001, 'Australian rainfall and runoff', Institute of Engineers, Barton, ACT.

Julien, P, Y, Saghafian, B & Ogden, F, L, 1995, 'Raster-based hydrologic modeling of spatially-varied surface runoff', *Water Resources Bulletin*, vol 31, no 3, 523-535.

Maidment, D, R 1992, *Handbook of Hydrology*, McGraw Hill, United States of America.

Mein, R, G & Larson, C, L, 1973, 'Modeling infiltration during a steady rain', *Water Resources Research*, vol 9, no 2, pp 384-393.

Nandakumar, N, Mein, R, G & Siriwardena, L, 1994, 'Loss modeling for flood estimation – a reviews', *Cooperative Research Centre for Catchment Hydrology*, Industry Report 94/4, pp 1-43.

Ogden, F, 1998, 'A brief description of the hydrologic model of CASC2D', University of Connecticut, viewed 26 February 2007, http://horton.engr.uconn.edu/ogden/case2d/casc2_desc.htm

Parlange, J, Y, Haverkamp, R & Touma, J, 1985, 'Infiltration under ponded conditions: 1 optimal analytical solution and comparison with experimental observations'*, Soil Science*, vol. 139, no 4, pp 305-311.

Philip, J, R, 1992, 'Falling-head ponded infiltration with evaporation', *Journal of Hydrology*, 138, 591-598.

Philip, J, R, 1993, 'Variable-head ponded infiltration under constant or variable rainfall', *Water Resources Research*, vol 29, no 7, pp 2155-2165.

Philip, J, R, 1994, 'Falling-head ponded infiltration with evaporation – Reply', *Journal of Hydrology*, vol 162, 215-221.

Phillip, J, r, 2006, 'The theory of infiltration: 1. The infiltration equation and its solution', *Soil Science*, vol 171, 34-46.

Ravi, V & Williams, J, R, 1998, 'Estimation of infiltration rate in the vadose zone: compilation of simple mathematical models volume 1', www.epa.gov/ada/csmos/niflmod.html

Rawls, W, J, Brakesiek & Miller, N, 1983, 'Green-Ampt infiltration parameters from soils data', *Journal of Hydraulic Engineering*, vol 109, 62-71.

Salvucci, G.D, & Entekhabi, D, 1994, 'Explicit expressions for Green-Ampt (delta function diffusivity) infiltration rate and cumulative storage', *Water Resources Research*, vol 39, no 9, pp 2661-2663.

Sign, V, P & Woolhiser, D 2002, 'Mathematical modeling of watershed hydrology', *Journal of Hydrologic Engineering*, July/ August 2002.

US Army Corps of Engineers, 1994, 'Engineering and design – flood runoff analysis

US Environmental Protection Agency*,* 2007, 'Ground water and ecosystems restoration research – Infiltration models descriptions*, http://www.epa.gov/cgi-bin/epaprintinly.cgi*

Willliams, J, R, Ouyang, Y, Chen, J, S & Ravi, V, 1998, 'Estimation of infiltration rate in vadose zone: application of selected mathematical models volume 2, www.epa.gov/ada/csmos/niflmod.html

APPENDIX A: ROUS RIVER FLOOD MODEL DEVELOPMENT

A1 Overview

The Rous River is one of the major tributaries of the Tweed River in Northern NSW. The Rous River catchment covers approximately 130km^2, measuring approximately 16km from east to west, and 12km from north to south. The catchment is generally steep, although the downstream reaches of the river flow across a wide floodplain. Ground elevation across the catchment ranges from 0m AHD to over 1,100m AHD. Land cover is a mix of natural forest and pasture.

For Case Study 3, new WBNM and TUFLOW models have been developed using a broadscale approach. An 80m grid cell resolution was selected for the TUFLOW models to minimise computer simulation times. For simplicity, no bridges or major drainage structures have been included in the model. The following models have been developed:

➢ WBNM hydrological model comprising 35 sub-catchments;

➢ TUFLOW Surface Area (SA) model with boundary conditions read from WBNM output; and

➢ TUFLOW Direct Rainfall (DR) model.

Historical streamflow and rainfall data was sourced for three historical flood events; March 1974, March 1978 and May 1980. A summary of each event is presented in Table 8-3.

A2 Topographic Data

Airborne laser scanning (ALS) survey data was captured for the entire catchment as part of the Tweed River Flood Study for Tweed Shire Council. Refer to Figure 11-1 for the digital elevation model of the catchment.
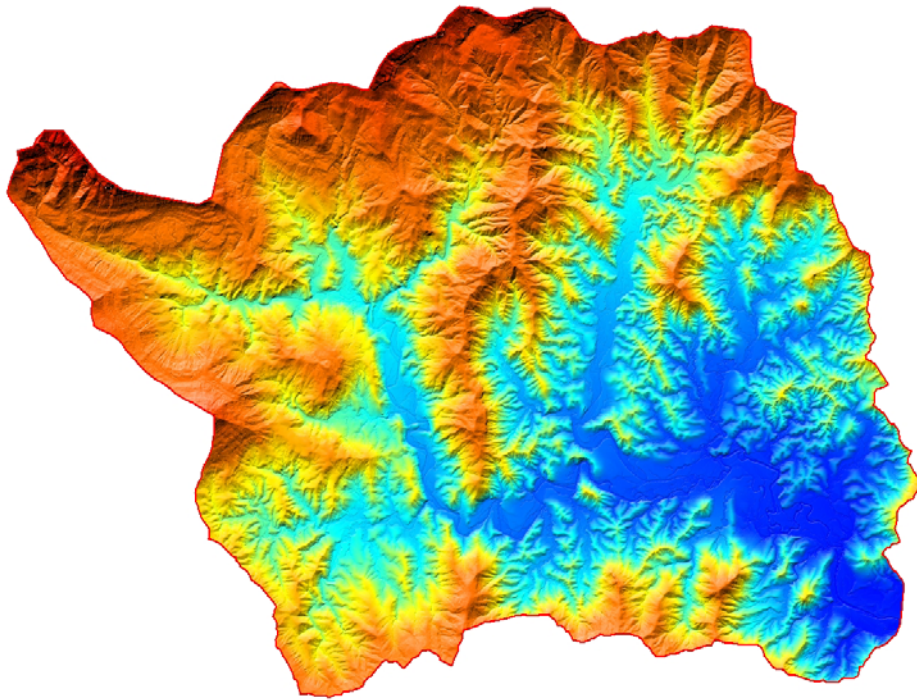
Figure 11-1   Rous River Catchment Digital Elevation Model

A3 Hydrologic Data

Rainfall records for three historical events were sourced from the Bureau of Meteorology. The data included three pluviograph recordings at six minute intervals for each event, and nine daily rainfall stations as shown in Figure 11-2. Refer to Figure 11-3 for the cumulative rainfall for the 1974 event. The significant difference in the temporal distribution highlights the problems associated with achieving a good model calibration.

The following procedure was used for representation of the rainfall in the models:

1. Rainfall isohyets were produced for the three events.

2. The average total rainfall depth within each sub-catchment was calculated.

3. A Thiessen distribution was used to assign temporal patterns to each sub-catchment.

4. Rainfall for each sub-catchment was applied based on the relevant temporal pattern and average rainfall depth.

Streamflow records for the three events were sourced from the NSW Department of Water and Energy for the Boat Harbour gauge at the catchment outlet as shown in Figure 11-2.
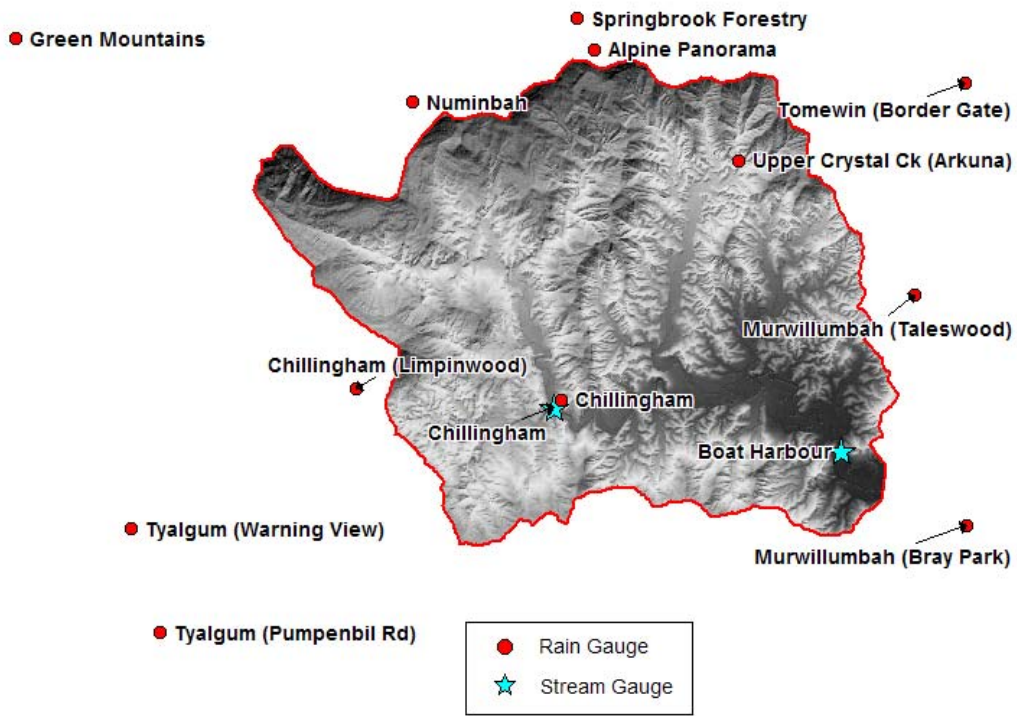
Figure 11-2   Rainfall and Streamflow Locations
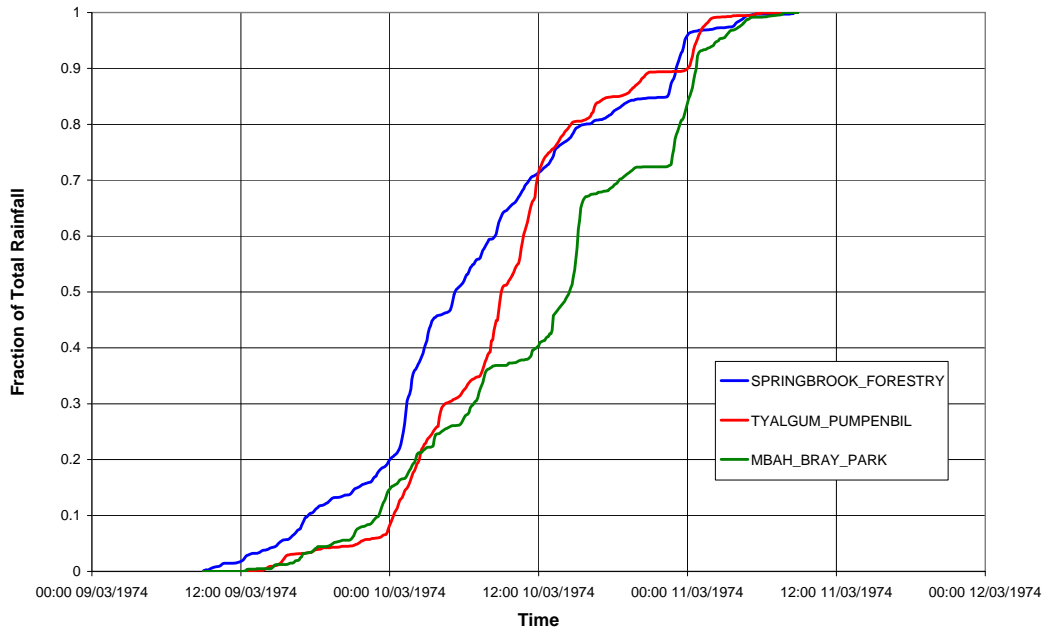

Figure 11-3   March 1974 Normalised Cumulative Rainfall

A4 Catchment Hydrology

The catchment has been divided into 35 sub-catchments as shown on Figure 11-4. The WBNM model layout is also shown. A catchment lag parameter of 1.8 was applied to all sub-catchments.
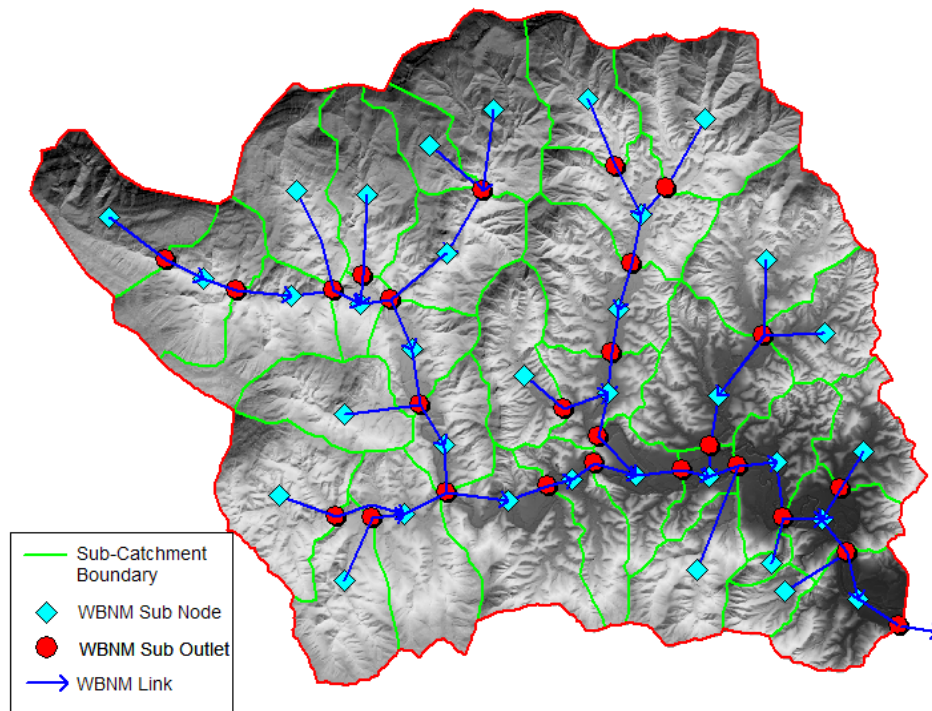

Figure 11-4   WBNM Hydrologic Model Layout

A5 Hydraulic Model Development

To maintain manageable simulation times, an 80m 2D grid resolution has been used. Grid cell elevation in TUFLOW is represented by 'z-points'. Each grid cell has four z-points as follows:

- ➢ Zc (cell centre) – this z-point is located at the centre of the 2D grid cell. Each grid cell has a flat base with elevation equal to the Zc value. The Zc is used to calculate storage;

- ➢ Zu and Zh (cell sides) – these z-points represent the elevation of the cell side, thus, control the flow of water between adjacent grid cells; and

- ➢ Zh (cell corners) – z-point is not used for hydraulic calculations.

Z-point elevations have been assigned based on the point elevation of the DEM at the z-point location (point inspection). Prior to the point inspection process, the DEM was re-sized to have a cell resolution of 80m. Z-points were aligned with the DEM raster grid cells. This approach ensured that

the DEM raster cell elevations from the pit-filling procedure were consistent with the z-point elevations.

A discharge-head boundary was automatically calculated by TUFLOW for the downstream boundary using a water gradient of 1%.

Refer to Figure 11-5 for TUFLOW model layout showing, 2D model extents, sub-catchment boundaries used for rainfall input, plot output locations and the downstream boundary location.
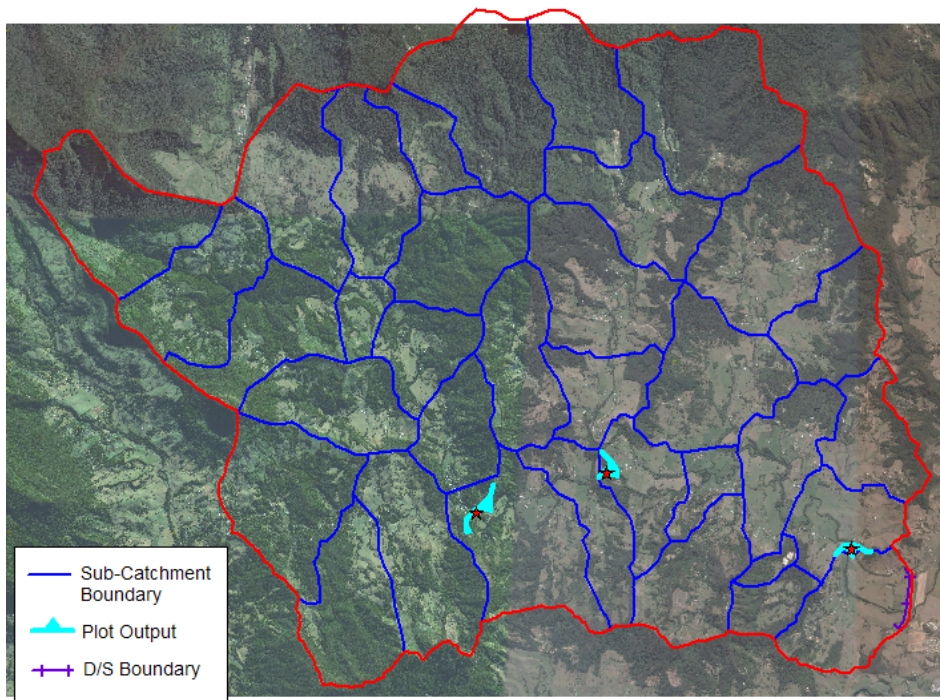
Figure 11-5 TUFLOW Hydraulic Model Layout

Surface roughness was determined based on available aerial photography.